

8-2022

Sex Differences in Cancer Cachexia and a Novel Mitochondrial Target for Cancer-Induced Muscle Wasting

Seongkyun Lim
University of Arkansas, Fayetteville

Follow this and additional works at: <https://scholarworks.uark.edu/etd>



Part of the [Biomechanics Commons](#), [Cancer Biology Commons](#), and the [Motor Control Commons](#)

Citation

Lim, S. (2022). Sex Differences in Cancer Cachexia and a Novel Mitochondrial Target for Cancer-Induced Muscle Wasting. *Graduate Theses and Dissertations* Retrieved from <https://scholarworks.uark.edu/etd/4577>

This Dissertation is brought to you for free and open access by ScholarWorks@UARK. It has been accepted for inclusion in Graduate Theses and Dissertations by an authorized administrator of ScholarWorks@UARK. For more information, please contact scholar@uark.edu, uarepos@uark.edu.

Sex Differences in Cancer Cachexia and a Novel Mitochondrial Target for Cancer-Induced
Muscle Wasting

A dissertation submitted in partial fulfillment
of the requirements for the degree of
Doctor of Philosophy in Health, Sport, and Exercise Science

by

Seongkyun Lim
Baekseok University
Bachelor of Business, 2011
Kyunghee University
Master of Physical Education, 2014
East Carolina University
Master of Science in
Kinesiology, 2018

August 2022
University of Arkansas

This dissertation is approved for recommendation to the Graduate Council:

Nicholas P. Greene, PhD
Dissertation Director

Tyrone A. Washington, PhD
Committee Member

Michael P. Wiggs, PhD
Committee Member

Kevin A. Murach, PhD
Committee Member

Christopher E. Nelson, PhD
Committee Member

Abstract

Cancer cachexia (CC) is a devastating wasting syndrome characterized by marked weight loss including skeletal muscle atrophy that affects approximately 80% of cancer patients. Current therapeutic treatments including pharmacological and nutritional intervention are insufficient to prevent or reverse it. Prior studies demonstrated lower muscle mass, impaired muscle function, and mitochondrial health in the development of CC. Specifically, mitochondrial fusion protein, Optic atrophy 1 (OPA1) which plays a significant role in skeletal muscle health, is suppressed in the development of CC. Furthermore, most pre-clinical CC studies were mainly focused on males although there are distinct phenotypical differences in skeletal muscle between males and females. Therefore, these studies were set to investigate two independent research questions (Chapter 3 & 4). The purpose of this dissertation project was to investigate skeletal muscle alterations during the development of CC in female tumor-bearing mice (Chapter 3) and determine the efficacy of OPA1 as a therapeutic target for cancer-induced muscle atrophy (Chapter 4). To accomplish this research plan, I completed a series of studies using both cell culture and animal models of CC. For the Chapter 3 experiments, 60 female mice were given either an IP injection of PBS or Lewis Lung Carcinoma (LLC) injection and the tumors were allowed to grow for 1, 2, 3, or 4-wk to assess the time course of cachectic development. We found a dichotomous effect on tumor mass between 3- and 4-wk animals where approximately half of mice between the two groups exhibited low tumor (LT) mass (<1.2 g) while the other half developed higher tumor (HT) mass (>2 g). Furthermore, HT mice revealed greater protein degradation, impaired muscle contractility, and mitochondrial degeneration. These alterations are relatively modest when compared to male data from previous studies. For the Chapter 4 experiments, I utilized both pharmacological (*in vitro* & *in vivo*) and genetic overexpression of OPA1 (OPA1 TG) in LLC-conditioned media (LCM) and LLC-induced CC. 72 hours of LCM intervention induced smaller myotubes, which was normalized by BGP-15 treatment and this effect appeared to be driven by

suppressed inflammatory cytokine and autophagic-lysosomal pathway (ALP) activity at the mRNA level. 4-wk of LLC implantation was sufficient to induce cachectic phenotype while this effect was normalized in OPA1 overexpression in tumor-bearing mice. In conclusion, my dissertation data suggests both biological sex as an important variable and OPA1 as a novel therapeutic target for cancer-induced muscle wasting.

Acknowledgements

I would like to thank many people who both involved in my dissertation work and supported me throughout my journey of dissertation including my advisor, Cachexia Research Laboratory members, Exercise Muscle Biology Laboratory members, Molecular Muscle Mass Regulation Laboratory members, dissertation committee members, faculties and student at Exercise Science Research Center, CLAF animal care staffs, experimental mouse donators, and my family members. I am truly thankful for their support and contribution to my dissertation journey.

First and foremost, I am extremely thankful to my supervisor, Dr. Nicholas Greene, for his invaluable supervision and continuous support during my PhD. The major reason that I was able to successfully complete my dissertation project was because of his invaluable guidance. I feel that I am very fortunate to work with such an excellent mentor and also a very nice person for the last ~4 years.

I have been grateful to work with such great lab members also known as “lab family.” We are not just only lab mates, but also good friends each other. They are excellent coworkers in the lab because all of them are genuinely intelligent and nice. I have learned a lot from each of our lab members (Fran Morena, Regina Cabrera, and Roula Tsitkanou). This also includes other trainees (Eleanor Schrems, Landen Saling, and Sabin Khadgi) from Dr. Tyrone Washington and Kevin Murch laboratory and former lab members including (Megan Rosa-Caldwell, Will Deaver, Wesley Haynie, Lisa Jansen, Kirsten Dunlap, and others). These prior and current lab members extensively helped with the experiments and animal works leading up to this project completion.

Special thanks to my dissertation committee members. Drs. Tyrone Washington, Kevin Murach, Christopher Nelson, and Michael Wiggs. I really appreciate your invaluable advice and comments for my dissertation work. All the comments I have received from them were extremely helped, leading to improve the quality of my dissertation.

I also thank many faculties and students at the exercise science research center, especially former director Dr. Michelle Gray, former administrative assistants Shari Witherspoon and Jennifer Shipley, and current administrative assistants Liliana Evans, Joe Hamilton, and Anaid Espinosa for their administrative supports.

I would like to thank former and current animal care staffs and CLAF managers who took a diligent care of my experimental mice for up to 4 years. Without their efforts, I could not successfully complete my dissertation projects.

Lastly, special thanks to experimental animal providers, Drs. Lucas Scorrano (U of Padova) and Thomas Sanderson (U of Michigan). I really appreciate their generous donation of experimental animals (OPA1 TG mice). These animals became a big part of my dissertation work.

Dedication

I am thankful to my family for supporting and motivating me throughout my journey of dissertation. Thereby, I dedicate this dissertation to my family, especially my Mom (Sun-Soon Whang), Dad (Chang-Sik Lim), sister (Mi-Jung Lim), and niece (So-Dam Kim). They have been always supported and believed in me for a successful PhD and academic career. Especially, my Mom and Dad supported and trusted my decision when I left South Korea and started graduate studies in the United States. The fundamental reason that I am at this point is because of their unconditional support. Thank you and I love you Mom and Dad!

Table of Contents

I.	Review of Literature.....	1
	A. Introduction.....	1
	B. Cancer Cachexia	2
	C. Pre-Clinical Models to Study Cancer Cachexia	3
	D. Sex Differences in Cancer Cachexia.....	5
	E. Skeletal Muscle Contractile Properties in Cancer Cachexia	7
	F. Protein Turnover in Cancer Cachexia	9
	G. Role of Mitochondrial in Cancer Cachexia	13
	H. Conclusions.....	18
	I. References	20
II.	Proposal.....	35
	A. Specific Aims	35
	B. Research strategy.....	38
	C. Approach	40
	D. Aim 1	42
	E. Aim 2.....	47
	F. Proposed timeline of dissertation projects.....	52
	G. References	53
III.	Manuscript from Specific Aim I (LLC Female).....	57
	A. Graphical Abstract	57
	B. Abstract	58
	C. Introduction.....	60
	D. Methods.....	62
	E. Results	71
	F. Discussion	76
	G. References	96
IV.	Manuscript from Specific Aim II (OPA1 TG).....	101

	A. Abstract	101
	B. Introduction.....	103
	C. Methods.....	105
	D. Results	114
	E. Discussion	120
V.	Conclusions.....	136
	A. Chapter 3.....	136
	B. Chapter 4.....	136
	C. Overall conclusion	136
	D. Limitations and Delimitations	138
	E. Final Thoughts.....	140
	F. References	141
VI.	Appendices.....	146
	A. AUP/IBC Approval Letters	146
	B. Protocols	150

List of Tables

I.	Chapter II	35
	A. Table 1. Summary of alterations in development of LLC-induced muscle atrophy.....	39
	B. Table 2. Proposed timeline for the dissertation project.....	52
II.	Chapter III	57
	C. Table 1. Characteristics of female LLC study	84

List of Figures

I.	Chapter I (Literature Review).....	1
	A. Figure 1. Autophagy-lysosomal pathway.	10
	B. Figure 2. Mitochondrial quality control system	14
	C. Figure 3. OPA1-HSP70-BGP-15 axis.....	17
	D. Figure 4. Opa1 target (BGP-15) prevents CC in vitro.	17
	E. Figure 5. Experimental design for OPA1 target in CC	18
II.	Chapter II (Proposal)	35
	A. Figure 1. Animal experimental design for Aim 1.....	43
	B. Figure 2. Changes in OPA1 protein content during development of LLC-induced CC.....	47
	C. Figure 3. OPA1 target (BGP-15) prevents CC <i>in vitro</i>	48
	D. Figure 4. Experimental design for Aim 2.	49
III.	Chapter III (Female LLC study).....	57
	A. Figure 1. Oxidative phenotype	85
	B. Figure 2. Skeletal muscle contractility	86
	C. Figure 3. Protein synthesis	87
	D. Figure 4. Protein degradation & Inflammation	88
	E. Figure 5. Myogenic & cell proliferation factors.....	89
	F. Figure 6. Mitochondrial function & Network.....	90
	G. Figure 7. Mitochondrial quality control.....	91
	H. Supplemental Figure 1. Oxidative phenotype.....	92
	I. Supplemental Figure 2. Oxidative phenotype.....	93
	J. Supplemental Figure 3. Oxidative phenotype.....	94

	K. Supplemental Figure 4. Oxidative phenotype.....	95
IV.	Chapter IV (OPA1 study).....	101
	A. Figure 1. Protein anabolism for BGP-15 <i>in vitro</i> experiments.....	126
	B. Figure 2. Protein degradation & Inflammation.....	127
	C. Figure 3. Mitochondrial quality control.....	128
	D. Figure 4. Myogenic & cell cycling regulator.....	129
	E. Figure 5. Tissue weights for BGP-15 <i>in vivo</i> experiments.....	130
	F. Figure 6. Muscle contractility.....	131
	G. Figure 7. Mitochondrial network health.....	132
	H. Figure 8. Tissue weights for OPA1 TG experiments.....	133
	I. Figure 9. Muscle contractility.....	134
	J. Figure 10. Mitochondrial network health & Function.....	135

List of Published Papers

1. Seongkyun Lim, J. William Deaver, Megan E. Rosa-Caldwell, Wesley A. Haynie, Francielly Morena da Silva, Ana Cabrera Ayuso, Eleanor R. Schrems, Landen W. Saling, Lisa T. Jansen, Kirsten R. Dunlap, Michael P. Wiggs, Tyrone A. Washington, Nicholas P. Greene. **"Development of metabolic and contractile alterations in development of cancer cachexia in female tumor-bearing mice."** Journal of Applied Physiology (2021) Nov; 11. PMID: 34762526. DOI: 10.1152/jappphysiol.00660.2021.

Chapter number: 3

The status of publication: Published (January 5th, 2022)

CHAPTER I: REVIEW OF LITERATURE

Seongkyun Lim & Nicholas P. Greene

A. INTRODUCTION

Cancer Cachexia (CC) results in an involuntary weight loss of lean body mass, which leads to reduced mobility, quality of life, and increases mortality(1). Approximately one-quarter of all cancer-related death is due to CC (2, 3). Nutritional intervention has not been successful and overall, to date there are currently no effective treatments to reverse or prevent CC (4). Although preclinical CC studies are limited to mimic the nature of human cancer, they have provided potential therapeutic strategies to improve cancer outcomes (5-9). Most pre-clinical studies of CC are mainly focused on males and cachectic signatures during the development of CC in females are still lacking. Prior evidence indicates distinct biological sex differences in skeletal muscle phenotype, and skeletal muscle responses in males and females to various myopathies are distinct, including disuse-induced muscle atrophy (10, 11). Therefore, a critical need remains to understand phenotypical and molecular alterations in the skeletal muscle across biological sex during the development of CC.

Mitochondrial health and function have long been implicated with various human diseases including CC (12-15). Impaired mitochondrial function and quality have been reported from various clinical (16, 17) and preclinical CC studies (12, 18). Previous evidence from our laboratory demonstrated mitochondrial degeneration including lower mitochondrial fusion protein content precedes cancer-induced muscle wasting (12). However, it is unknown if early targeting of mitochondrial fusion prevents cachectic phenotypes and improves cancer outcomes. Additional supportive investigations on targeting mitochondrial fusion are needed to elucidate mitochondrial regulations during the development of CC. The purpose of the current dissertation literature

review is to discuss skeletal muscle alterations during the development of CC across biological sex using preclinical animal models and the role of mitochondria in CC.

B. Cancer Cachexia

i. Recent cancer statistics

Cancer has been a leading cause of death in many countries of the world, responsible for approximately 10 million deaths in 2020 (19). Specifically, the World Health Organization (WHO) has recently (2020) reported that cancer was the first or second leading cause of death before the age of 70 years in 112 of 183 countries globally. Furthermore, the global cancer incidence rate is expected to be increased by ~47% in 2040 (28.4 million cases) from 2020 (19.3 million cases) (19). In addition, the majority of cancer patients experience many symptoms including unintended weight loss, anorexia, and fatigue, which affect their mortality and quality of life (1).

ii. Cancer Cachexia: Mechanism of Muscle Wasting

Cancer cachexia (CC), cancer-induced muscle loss, is a multifactorial syndrome characterized by a progressive loss of skeletal muscle mass, which can affect up to 80% of cancer patients depending on the type of cancer (2, 20). CC is clinically defined as 5% of bodyweight loss over a 6-month period, or weight loss > 2% in individuals already showing depletion (body mass index <20 kg/m²) or low skeletal muscle mass (sarcopenia) (3). CC is the primary cause of death for 22-30% of cancer patients (2, 20), with incidence predicted to grow in years to come (21). CC is often irreversible once weight loss begins to occur; therefore, using weight loss as diagnostic criteria is therapeutically superlative, requiring the need to identify a pre-cachectic signature both for diagnostic and prevention/mitigation purposes.

All cancers can present with cachexia and common cancers such as those of the pancreas, lung, and liver are responsible for approximately half of all cancer-related deaths worldwide (22). Cancers more commonly associated with cachexia are often diagnosed at an advanced stage (cachectic state) and have direct effects on digestion (23), at which point the condition is mostly irreversible back to pre-cachectic state. Baseline assessments of pre-cachexia (early stage of CC without marked weight loss; i.e., $\leq 5\%$) (3) or mass loss history are critical for predicting CC trajectory (24). To predict if CC will occur in patients, there is a desperate need for a defined pre-cachectic signature, which would allow for the development and implementation of preventative therapeutic strategies to decrease the cancer-induced mortality rate.

Many clinical studies have taken place to identify characteristics of CC across several diverse types of cancers in humans. However, results of clinical studies often show varying outcomes compared to pre-clinical models. While pre-clinical models have consistently shown that muscle proteolysis (breakdown process) occurs with CC, the results from clinical studies are much more variable (25). One source of variation could be that in pre-clinical models of experimental conditions such as tumor size are tightly controlled for, while in clinical studies the progression of cancer is often not controlled for. Our group has recently reviewed common pre-clinical models of CC (26), notably, current efforts are ongoing to develop pre-clinical models of CC to more accurately recapitulate human CC.

C. Pre-Clinical Rodent Models to Study Cancer Cachexia

i. Pre-Clinical Rodent Models of Cancer Cachexia

Pre-clinical models are limited to perfectly mimic the heterogeneity of human cancer, research findings from studies utilizing pre-clinical animal models of CC have provided potential therapeutic strategies to improve cancer outcomes (5-9). There are two types of commonly used

pre-clinical animal CC models including tumor allograft and genetically mutated CC models. Tumor allograft-induced tumor-bearing mouse is mainly driven via subcutaneous tumor cell injection into the flank of a mouse wherein the tumors grow relatively fast and develops a cachectic phenotype within a few wks following the tumor injection in most cases (12, 27). Currently, several tumor allograft rodent models to study CC have been used including Lewis Lung Carcinoma (LLC; lung cancer model) (28), Colon-26 (C26; colorectal cancer model) (29), MAC16 (colon cancer model) (30, 31), Yoshida AH-ascites (AH-130; hepatic cancer model) (32), RXF (renal cancer model) (33), and Walker-256 (breast cancer model) (34). On the other hand, one of the most widely used genetic (transgenic) CC animal models is Adenomatous Polyposis Coli ($Apc^{Min/+}$; colorectal cancer model) (35-37). Mutation of the $Apc^{Min/+}$ gene represents a large percentage of human colon cancer cases and genetic mutation of $Apc^{Min/+}$ in rodents will spontaneously develop intestinal adenomas and it has become an excellent pre-clinical model to mimic human colorectal cancer (35-37). In addition, Talbert et al (38) recently introduced a new genetically modified animal model of CC. In this study, they engineered a mouse model of pancreatic ductal adenocarcinoma (PDA) via breeding $Kras^{LSL-G12D/+}$, $PTEN^{+/f}$ mice to $Ptf1a^{ER-Cre/+}$, $PTEN^{+/f}$ mice and this animal model is similar to PDA patients including progressive loss of skeletal muscle and adipose mass as well as similar gene ontology in response to tumor development.

Among different pre-clinical rodent CC models, this review will concentrate on the LLC-induced tumor-bearing mouse model in this current project. Lung cancer remains the leading cause of cancer-related death in 2020 and one of the most commonly diagnosed cancers in human (19). The LLC cell line was first developed in 1980 (28) and has been widely used since the 1990s. Upon the LLC tumor allograft, it generally takes up to 4 wks to fully develop the tumor sufficiently to induce cachectic phenotype (12, 27). At a 4-wk time point, the tumor sizes typically

average ~2.5 grams (12, 27) which may limit direct application of these models to human cachexia due to its large tumor size (~10% of body weight is attributable to tumor mass).

As a preventative purpose, understanding pre-cachectic signatures are imperative to prevent cancer-induced muscle wasting and other cachectic phenotypes. However, clinical cancer studies have not been successful to effectively investigate the pre-cachectic signatures. Since most cancer patients are diagnosed with cancer when they are already experiencing cachectic phenotypes such as weight loss, at which point is difficult to treat to reverse. One of the benefits of using pre-clinal animal models is that researchers can observe physiological or molecular changes during the initial stages of tumor development. Our laboratory has committed to study pre-cachectic signatures utilizing pre-clinical animal models of CC, and we found some novel evidence. We found that mitochondrial degeneration such as impaired ROS emission and mitochondrial dynamics preceded cancer-induced cachectic phenotype in LLC tumor-bearing male mice (12). However, studies investigating pre-cachectic signatures are still sparse, making it difficult to develop therapeutic treatments to prevent cancer-induced muscle wasting during early-stage cancer.

D. Sex Differences in Cancer Cachexia

i. Phenotypical differences between sexes in various myopathies

Skeletal muscle mass takes up to 40% of total body mass and is maintained via a homeostatic balance between protein synthesis and protein degradation, whereby an increase in protein degradation to synthesis ratio results in muscle loss (39). Loss of muscle mass is closely associated with various muscle pathologies(40) as well as lower quality of life (41) and higher mortality (42, 43). Although muscle loss is a common symptom for many muscle pathologies

including cancer (27), the mechanisms contributing to muscle wasting vary depending on the types of pathologies. For example, muscle atrophy is associated with inflammatory action of the tumor-host interactions in cancer (38, 44), while this interaction is absent during other pathologies such as disuse-induced muscle wasting. In addition, recent evidence suggests there are distinct phenotypical differences in development of muscle atrophy between males and females (45). Females tend to rely more on oxidative metabolism and have greater relative content of type 1 (oxidative/slow-twitch) muscle fibers compared to males, who have more type 2 fibers (glycolytic/fast-twitch) compared to females (46-48). Disuse-induced muscle atrophy extensively occurs in type 1 oxidative muscle fibers, while inflammation-induced muscle wasting occurs preferentially in type 2 glycolytic muscle fibers (12, 49, 50). Thus, females appear to be more vulnerable to disuse-induced muscle wasting (51-53), while males are more sensitive to cancer-induced muscle wasting (12, 49, 50). Nevertheless, the role of biological sex in different forms of muscle pathologies including CC remains understudied. This relative dearth of information likely contributes to the current lack in effective therapeutic strategies.

ii. Sex differences in Cancer Cachexia

Biological sex has been recently reported as an important factor in terms of cancer incidence and mortality (54). Although both male and female cancer patients exhibit cachexia, the development of CC may differ between sexes (45). A recent study shows cancer incidence is 20% higher in males than females and the male-to-female incidence ratio was distinctly different in many primary malignant tumor developments such as liver, bladder, oral cavity, esophageal, and thyroid cancer in the US (55). The mortality rate in malignant cancers is ~30% higher in males compared to females in various age groups (56, 57). Moreover, cancer-induced cachexia generally occurs in 40-50% of female patients and 40-60% of male patients over 60 years of age

(58, 59) and the overall prevalence of severe muscle loss criteria among cancer patients was much higher in males (61%) than females (31%) (60). Although CC occurs in both male and female populations, mechanisms that drive muscle loss differ between sexes (45, 61). Females are less sensitive to inflammation-mediated activation of the ubiquitin-proteasome system and subsequent muscle protein breakdown, common in CC, as compared to males (50, 62, 63). In addition, the Carson group demonstrated while male *Apc^{min/+}* mice exhibit a high IL-6 dependency for cancer development, female mice demonstrate a relative IL-6 independency (15, 64). Differences in the inflammation and protein breakdown pathways observed in prior works show distinct variations in cancer-induced muscle degradation mechanisms that occur between sexes in mice (45, 61). Although above-mentioned data indicate the biological sex difference in muscle phenotype and inflammation-induced muscle pathologies, most pre-clinical studies of CC are mainly focused on males. Therefore, more studies are needed to delineate the ambiguous roles of biological sex during the development and progression of CC. Considering differences in CC susceptibility by biological sex, explorations of mechanistic differences in CC between biological sexes may provide valuable insight to therapeutic approaches to prevent or attenuate this condition.

E. Skeletal Muscle Contractile Properties in Cancer Cachexia

i. Muscle contractility & Extracellular Matrix (ECM)

In addition to muscle loss, reduced muscle strength is an important indicator of the survival rate among patients with advanced cancer (65). One of the major features of skeletal muscle is the ability to produce force and the intrinsic mechanism is controlled by contractile properties such as fiber type, motor unit, ATPase activity, calcium homeostasis (14, 66), and neuromuscular connection (67). However, prior evidence notes that multiple deficits in muscle contractility (force

production and fatigability) and contractile properties have been identified in tumor-bearing cachectic mice (68-70) and advanced cancer patients (65) as well as primary cells derived from cancer patients (71). Notably, increased muscle fatigability was present in weight stable *Apc^{Min/+}* mice (69), suggesting increased muscle fatigability in pre-cachexia may serve as an early functional marker for CC. The capacity to produce muscle force has become an excellent indicator of survival rate among patients or rodents with advanced cancer as these patients and animals often show diminished force production and elevated fatigability (65, 69, 72). In fact, VanderVeen et al (2018) (69) demonstrated that *Apc^{Min/+}* mice, a genetic mouse model of colorectal cancer, showed increased inflammation, which was accompanied by decreased muscle tissue weight, muscle fatigability, and force production. In addition, C26 adenocarcinoma-induced cancer cachectic mice revealed a decrease in specific force and myofiber cross-sectional area (CSA), and a muscle fiber type shift towards a more glycolytic phenotype (70).

Furthermore, muscle force production is closely associated with the integrity of ECM in that muscle force generated by the actomyosin cross-bridge mechanism transmits the force to external tendons via the ECM (73). However, prior evidence showed disrupted ECM structure in *Apc^{Min/+}* mice via accumulating non-contractile tissues such as connective tissue deposition (74). Additionally, the matrix metalloproteinase (MMP) family of extracellular proteinases play an important role in regulating the integrity of ECM via digesting essential ECM components such as collagens, thereby interrupting the interaction between cells at the basement membrane and cell-to-cell signaling, creating space for cancer cells to move forward and new blood vessels to form to favor cancer cells, resulting in metastatic colonization (75). MMPs including MMP-2, -3, and -9 are identified to alter ECM architecture in skeletal muscle and a recent report reveals that these MMPs were elevated as cancer develops, thereby increasing collagen deposition (76). However, the regulation of ECM in CC has not been completely understood and additional investigations are required.

F. Protein Turnover in Cancer Cachexia

i. Protein Degradation in CC

The major feature of CC is the net loss of skeletal muscle protein, which occurs when protein degradation exceeds protein synthesis (77, 78). Prior evidence shows that pre-clinical rodent models of CC exhibit elevated protein degradation while protein synthesis is suppressed (79-82). Two major protein degradation processes, the ubiquitin proteasome system (UPS) and the autophagy-lysosomal pathway (ALP) are often activated during muscle wasting conditions including CC (78). These protein degradation systems are regulated via a transcription-dependent pathway including activation of transcription factor FOXO, which are negatively controlled by IRS/AKT pathway and NF- κ B (78, 83, 84). In the UPS, ubiquitin is conjugated to target proteins that are tagged and recognized through E3-E2 ubiquitin ligases, which are then degraded via the ATP-dependent 26S proteasome(85). Two major atrophy-related genes, atrogin-1 (also known as MAFbx) (86, 87) and MuRF1 (muscle RING finger protein 1) (86) and both atrogenes encode E3 ubiquitin ligases, which initiate ubiquitination of target protein substrates (88-90), thereby upregulating muscle atrophy. It should be noted that other atrophy-associated genes have been recently described such as Growth arrest and DNA damage inducible alpha (GADD45a) and Ubiquitin C (UBC) (91-93). These markers are elevated in various models of atrophy including CC, disuse, and denervation-induced muscle wasting (81, 94, 95). Recent evidence from our group also showed that elevated mRNA content of Atrogin-1 and MuRF1 and protein content of ubiquitin were found in the skeletal muscle of Lewis Lung Carcinoma (LLC)-induced tumor-bearing male mice 4 wks following tumor implantation (cachectic state) (81). A ~40% lowered fractional synthesis rate (FSR) of mixed proteins was observed in muscle tissues in tumor-bearing mice as well (81). Similar findings using the *Apc*^{Min/+} mouse (colon cancer model) have been previously reported by the Carson group (36, 80), where significant reduction of muscle protein synthesis and elevated E3 ligases are observed during the progression of CC. Interestingly, these

lower E3 ligase activities were observed in both male and female animal models of muscle atrophy including disuse (10) and CC (96), suggesting E3 ligases are a universal biomarker for many different forms of muscle atrophy in both sexes.

Autophagy is a natural and conserved cellular homeostatic degradation and recycling system that removes dysfunctional, unnecessary, long-lived proteins, or other organelles through a lysosome-dependent mechanism (97). In the ALP, Beclin, LC3, and p62 play a critical role in membrane formation, cargo transport, and selective removal of unnecessary organelles. During the ALP, cytoplasmic components are targeted and isolated from the cell within a double-membrane vesicle (autophagosome), which fuses with a lysosome, bringing its specialty process of waste management and disposal; and eventually, becomes an autolysosome that are degraded and recycled (98, 99) (**Figure 1**).

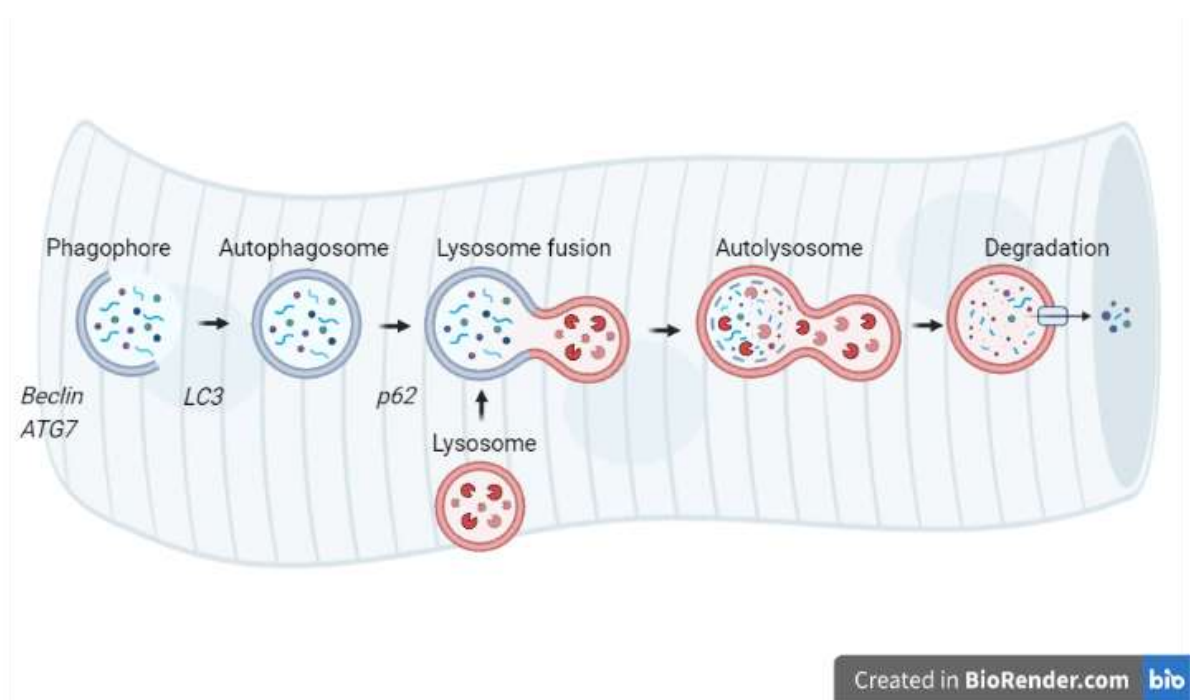


Figure 1. Autophagy-Lysosomal Pathways.

ii. Protein Synthesis in CC

Muscle protein synthesis is one of the two major components when it comes to net protein balance while its role in CC has not been clearly understood. A reduced protein synthesis per se can be responsible for the mechanism of atrophy (78). While our data (81, 82) and other works (79, 80) clearly demonstrate reduced protein anabolism in pre-clinical animal models of CC, understanding of the suppression of anabolic signaling remains incomplete (79, 100). The primary cellular signaling pathway of muscle growth known as Akt/mTOR signaling is an essential part of muscle protein synthesis (101, 102). It has been known that insulin and insulin-like growth factor (IGF-1) initiate the protein synthesis (muscle hypertrophy) pathway by inducing phosphorylation of Phosphoinositide 3-kinase (PI3K) and Protein kinase B (AKT), which leads to activation of mammalian target of rapamycin (mTOR), whose downstream targets include, Ribosomal protein S6 kinase beta-1 (p70S6K) and Eukaryotic translation initiation factor 4E (eIF4E)-binding protein 1 (4E-BP1) (101). Previous evidence demonstrated that both 4E-BP1 and p70S6K were downregulated in tumor-bearing mice (80), leading to lower muscle protein synthesis in the cachectic state (80, 81). Downstream signaling of the mTOR promotes mRNA translation initiation, thereby leading to generation of newly synthesized protein and increasing muscle mass (103), and mTOR activation can be directly suppressed via its own inhibitors, DEP domain-containing mTOR-interacting protein (DEPTOR) (104) and regulated in development and DNA damage response 1 (REDD1) (105). Recent evidence demonstrated the expression of REDD1 has been upregulated in different forms of CC (6). In addition, our recent work also found elevated DEPTOR protein content concomitant with reduced FSR of muscle protein in LLC-induced cachectic male mice (81), indicating mTOR inhibition via DEPTOR/REDD1 as an essential hub for regulation of muscle protein anabolism in CC. Ribosome biogenesis has emerged as one of the main mechanisms regulating muscle hypertrophy (106), which is also implicated in different forms of muscle atrophy (107, 108) although the precise role of ribosome biogenesis in CC has not been explored.

iii. MAPKs in CC

Mitogen-activated protein kinase (MAPKs) are involved in many different cellular regulations including cell proliferation, differentiation, mitosis, and apoptosis (109). To activate MAPKs, it requires multiple phosphorylation events in their activation loops including ERK, JNK, and p38 kinases (110). MAPKs are key regulators of both anabolic and catabolic signaling within skeletal muscle (111, 112) and prior studies have suggested MAPKs are potent regulators of cancer-induced muscle wasting (81, 113, 114). Sin et al (114) reported cancer-induced p38 β MAPK stimulated C/EBP β acetylation, which is a key regulator to induce muscle wasting. Others (113) also noted p38 MAPK links oxidative stress to autophagy-related gene expression in cancer-induced muscle wasting. In addition, Li et al (115) revealed TNF- α acts via p38 to increase atrogin-1/MAFbx mRNA level in skeletal muscle. This prior evidence is in line with our recent CC study, where cachectic tumor-bearing male mice exhibited greater protein contents of ERK and p38 MAPKs (81), suggesting MAPKs appear to be a central mediator of cancer-induced muscle wasting although underlying mechanisms regarding cancer-induced muscle wasting are required to be further elucidated.

iv. Skeletal Muscle Regeneration in CC

An alternative factor that may contribute to muscle wasting in CC is altered skeletal muscle regeneration (116). A detailed review on muscle regeneration during cancer cachexia has been published elsewhere (117). Skeletal muscle has an efficient homeostatic capacity to regenerate itself in response to injury and it can be hypothesized that skeletal muscle undergoes a regeneration process in response to muscle wasting during CC. Accordingly, it is plausible that cancer-induced muscle wasting is in part due to impaired muscle regeneration capacity

dependently or independently of cellular signaling of protein synthesis. Interestingly, our group has observed downregulated myogenic and cell cycle-associated markers including Cyclin D1, Pax7, MyoD, and Myogenin at the early stages of cancer in tumor-bearing mice prior to cachectic phenotypes and remained suppressed until marked weight loss occurs (81), indicating cancer-induced muscle atrophy might be partially contributed via impairment of the muscle regeneration processes during early-stage cancer. Other work has shown that skeletal muscle regeneration is impaired in tumor-bearing mice (118). Collectively, prior studies demonstrated pronounced protein degradation, synthesis, MAPKs, muscle regeneration, and other factors associated with muscle degeneration during CC although its individual contribution has not been well understood.

G. Role of Mitochondria in Cancer Cachexia

i. Mitochondrial alterations during the development and progression of CC

Mitochondrial health and function have long been implicated with various human diseases including CC (12-14). Prior studies have reported that mitochondrial quality control (MQC), consisting of mitochondrial biogenesis, dynamics (fusion and fission) and autophagy (mitophagy) (119, 120), is the basis for maintaining the integrity and stability of mitochondrial structure and function, and is an important defense mechanism for cells to survive mitochondrial damage (121). Mitochondrial dynamics consists of two distinct mechanisms; mitochondrial fusion and fission, the balance between these two will determine mitochondrial network health (122). Mitochondrial fusion occurs when two or more mitochondria fuse/join together, forming constantly changing tubular organelles, and leading to mitochondrial elongation (122). Mitochondrial fusion mediators differ between the inner and outer membranes of the mitochondria. Indeed, mitofusin (MFN1/2) protein mediate fusion of outer mitochondrial membrane (OMM), while proteins including Optic atrophy 1 (OPA1) mediates fusion between inner mitochondrial membrane (IMM) (122). On the

contrary, mitochondrial fission proteins including Dynamic-1-like protein (DRP1) and mitochondrial fission 1 protein (FIS1) control the final part of mitochondrial fission, pinching off the membrane between two forming daughter mitochondria. Several DRP1-binding proteins including mitochondrial fission factor (MFF)(123), binding DRP1 to induces mitochondrial fission and FIS1, recruiting DRP1 to sites of fission (124). Damaged (fragmented) mitochondria are separated by mitochondrial fission system and eliminated via autophagic lysosomal sequestration, a process known as mitophagy (125). An appropriate balance between mitochondrial fusion and fission allows for mitochondrial reorganization during biogenesis, which is induced via various physiological responses including cellular stress or environmental stimuli such as aerobic exercise (126-128). These physiological responses activate peroxisome proliferator-activated receptor gamma coactivator 1-alpha (PGC-1a) and its downstream including TFAM and NRF2, thereby regulating mitochondrial biogenesis (126, 129-131) (**Figure 2**).

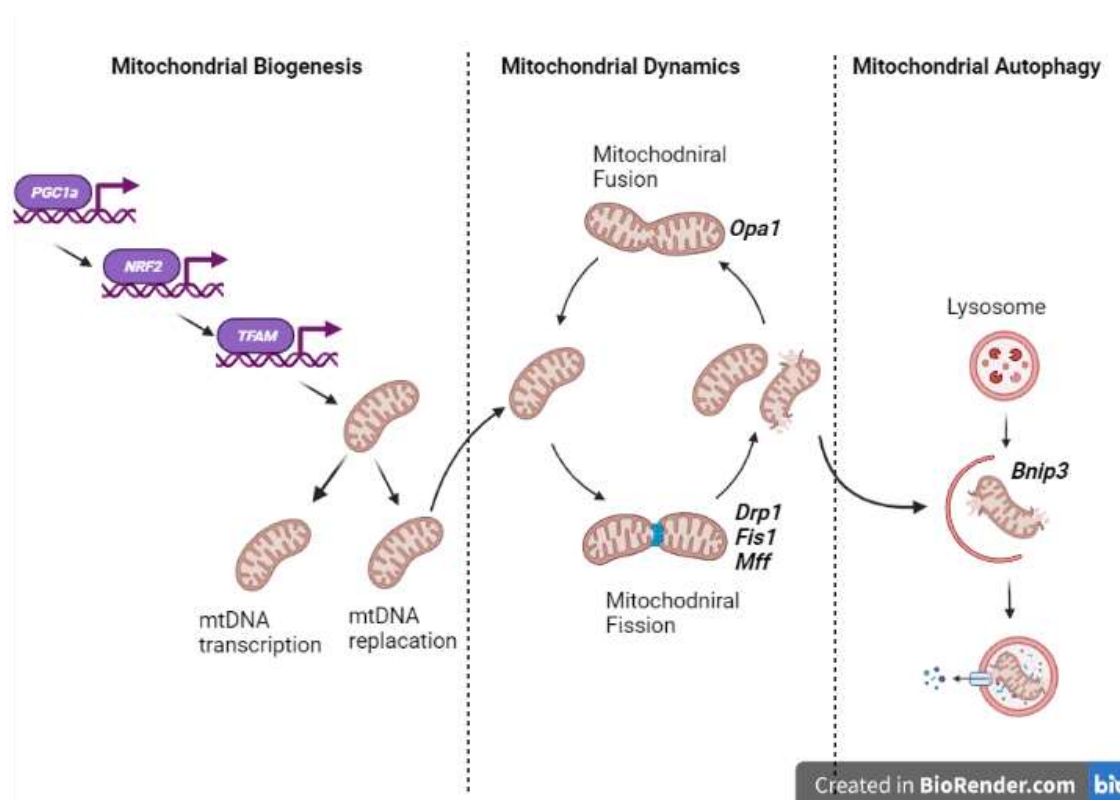


Figure 2. Mitochondrial quality control system.

Dysregulation of muscle MQC from cancer-induced cachectic mice has been shown on multiple occasions (12, 44); however, mitochondrial changes that occur during the development of CC are underexplored. Previous studies have reported that both *in vivo* and *in vitro* models of CC lead to impaired mitochondrial function including reduced respiratory capacity, ATP production, and elevated reactive oxygen species (ROS) emission (18, 82, 132, 133). Furthermore, elevated ROS emission has been implicated with impaired MQC (119, 120). Our recent findings reveal elevated mitochondrial ROS emission and mitochondrial oxidative stress precedes the development of CC in tumor-bearing male mice (12). In this study, elevated ROS occurs concomitantly with reduced content of mitochondrial fusion regulatory proteins (OPA1) during the pre-cachectic stage in tumor-bearing animals. In addition, markers for mitophagy (BNIP3) and FIS1 were upregulated, and mitochondrial respiratory control ratio was impaired during the cachectic phase (12). Similar results were reported by others that reduced mitochondrial fusion, biogenesis, elevated mitochondrial fission, ROS emission, and protein markers associated with autophagosome formation in both cachectic mice (18) and cancer patients (134). Chronic elevation of mitochondrial ROS generation can increase rates of protein degradation via activation of the ubiquitin proteasome-mediated protein breakdown process, leading to muscle wasting (135). Although mitochondrial dysfunction is well studied in male tumor-bearing mice (12, 18), it is still unclear/understudied whether the mitochondrial dysfunction would occur in female counterparts. However, basal mitochondrial function and content are higher in females (136) and female animals showed protective effects on mitochondrial health in different forms of muscle atrophies such as disuse-induced (11). Based on the aforementioned information, it is speculated that female tumor-bearing mice may protect against cancer-induced muscle mitochondrial dysfunction compared to their male counterparts, thereby undergoing less severe cachectic phenotypes. Taken together, our group showed alterations in mitochondrial health and function during the early development of CC in tumor-bearing male mice and currently, it is unknown if early targeting of H₂O₂ and mitochondrial fusion may prevent mitochondrial

degeneration observed during CC in both sexes. Hence, additional supportive investigations on targeting hydrogen peroxide (H₂O₂) and mitochondrial fusion are needed to elucidate mitochondrial regulations during the development of CC.

ii. Mitochondrial Fusion Protein “OPA1” as a Potential Therapeutic Target for Cancer-Induced Muscle Wasting

OPA1 is a mitochondrially targeted GTPase that regulates mitochondrial fusion and cristae structure in the inner mitochondrial membrane as well as contributes to ATP synthesis and apoptosis (137-139). OPA1 localizes to the inner mitochondrial membrane, where it mediates mitochondrial fusion in cooperation with MFN1/2 and other proteins to remodel cristae structure (138, 140). Stabilization of mitochondrial by OPA1 protects against mitochondrial dysfunction, ROS production, and other mitochondrial degenerations (141). Mutations of this gene have been associated with severe mitochondrial dysfunction, apoptosis, dominant optic atrophy (leading to a loss in vision), impairment in muscle contraction, and related dysfunctions (137, 142-144), many of which are hallmarks of cancer (145, 146). Emerging evidence indicates OPA1 might be a key molecular target for cancer biology and resistance to therapy. In fact, OPA1 was identified as one of a few novel prognosis-associated genes in several cancers (147, 148). In addition, prior evidence revealed mitochondrial dysfunction associated OPA1 cleavage contributes to muscle degenerations such as reductions in myosin heavy chain protein (149) and Pax7 (a muscle stem cell marker) (150), both of which are essential components regarding muscle growth. Prior evidence demonstrated OPA1 participates in heat stress-induced cellular protection against apoptotic stimuli and enhances the expression of heat shock protein (HSP) (151). In addition, prior studies utilizing BGP-15 (HSP72 chaperone co-inducer, has recently been reported to promote OPA1 protein content (152)) revealed that daily oral treatment of BGP-15 in rodents resulted in increased mitochondrial number, oxidative capacity, and decreased insulin resistance

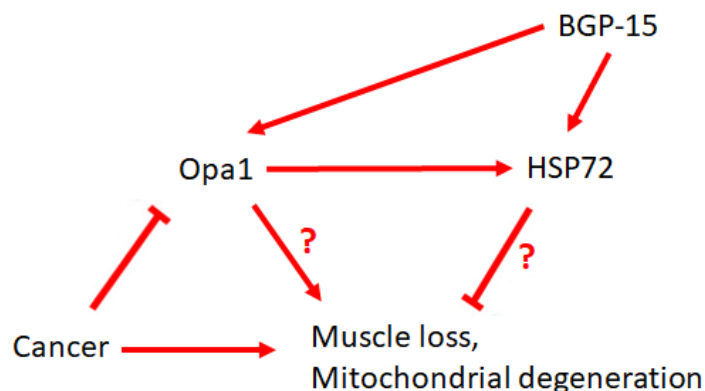


Figure 3. OPA1-HSP70-BGP-15 axis as a potential target to attenuate cancer-induced muscle degeneration

(153). However, whether mitochondrial fusion regulatory proteins play an imperative role in cancer-induced muscle wasting remains elusive (**Figure 3**).

Recently, our laboratory investigated molecular alterations during the development of CC utilizing tumor-bearing male mice in a time-course experimental design (1 through 4 wks). In this study, we found ~50% down-regulated OPA1 protein during the early development of CC (1 wk), which remained lower until cachectic phenotypes occur (between 3- and 4-wk) (12). Furthermore, my preliminary data showed a reduction in myotube diameter via LCM (Lewis lung carcinoma-conditioned media) was attenuated with LCM + BGP-15 intervention (**Figure 4**), suggesting BGP-15 might be an important therapeutic target for cancer-induced muscle wasting. These findings led me to pursue either pharmacological (utilizing BGP-15 treatment in rodents) or genetic overexpression

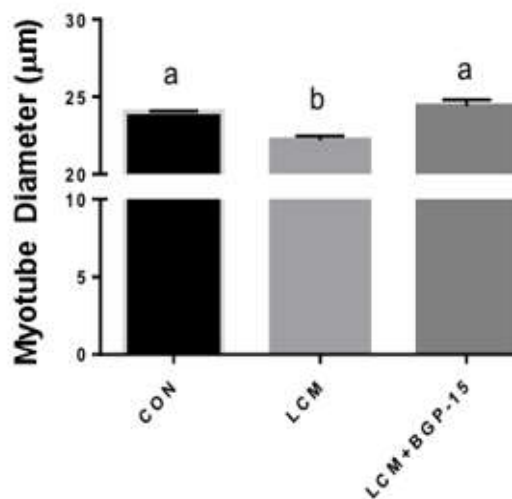


Figure 4. Opa1 target (BGP-15) prevents CC in vitro. BGP-15 -known to induce Opa1. BGP-15 prevents an ~10% loss in myotube diameter by LLC conditioned media (LCM) in C2C12 myotubes. Different letters indicate statistical significance ($p < 0.05$).

of OPA1 (OPA1 transgenic animal model) to determine whether it plays a pivotal role in cancer-induced muscle wasting in rodents. (Figure 5).

Therefore, **the purpose of my dissertation** is to investigate skeletal muscle alterations during the development of CC in female tumor-bearing mice and determine the efficacy of OPA1 as a therapeutic target for cancer-induced muscle atrophy (Figure 5). Therefore, the **CENTRAL HYPOTHESES of this work are: Aim 1)** Impaired muscle contractility, mitochondrial health, and altered protein turnover will present in the skeletal muscle of female tumor-bearing mice and **Aim 2)** Impaired muscular health in response to LLC implantation will be ameliorated via AAV-mediated OPA1 (mitochondrial fusion-associated) gene transfer.

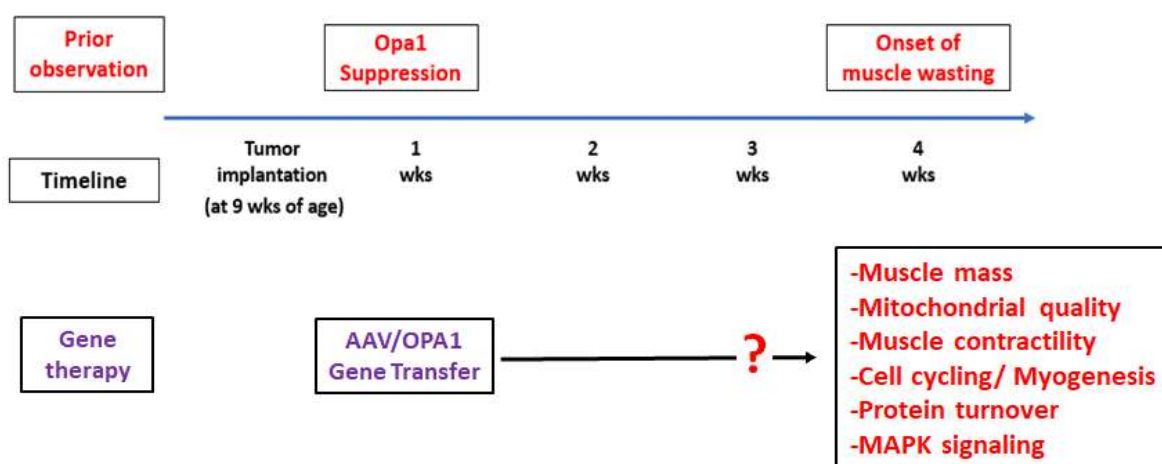


Figure 5. Experimental design for OPA1-dependent pharmacological and genetic designs to target cancer-induced muscle degeneration.

H. CONCLUSION

Progressive muscle loss is a hallmark for devastating conditions among cancer patients, which reduces mobility and increases mortality. Most cancer patients are diagnosed with cancer when cachectic phenotypes occur such as marked weight loss. Therefore, early diagnosis with appropriate treatment is critical to improving cancer outcomes. Although understanding

mechanisms of the early development of CC is crucial, most CC studies have mainly focused on later or advanced stages of cancer. Another gap in CC research is regarding biological sex. Although distinct phenotypical differences in skeletal muscle under normal or various myopathies have been observed between sexes, most preclinical CC studies have been mainly focused on males. These gaps in CC research make it difficult to suggest or provide effective therapeutic strategies, hence future studies are warranted to investigate the development of CC and suggested considering biological sex as an important variable. Therefore, the purpose of this dissertation is to investigate skeletal muscle alterations during the development of CC in female tumor-bearing mice and determine the efficacy of OPA1 as a therapeutic target for cancer-induced muscle atrophy. Many potential biomarkers have been suggested while mechanistic efficacy using these biomarkers has not been successful. Recently, we found downregulated OPA1 in the early development of CC. We hypothesize that targeting OPA1 with a timing of onset of concurrent alterations to endogenous targets during the early development of CC will reveal the importance of specific timing-derived treatment to prevent CC.

I. REFERENCES

1. **Nayak MG, George A, Vidyasagar MS, Mathew S, Nayak S, Nayak BS, Shashidhara YN, and Kamath A.** Quality of life among cancer patients. *Indian journal of palliative care* 23: 445, 2017.
2. **Fearon KCH, Glass DJ, and Guttridge DC.** Cancer cachexia: mediators, signaling, and metabolic pathways. *Cell metabolism* 16: 153-166, 2012.
3. **Fearon K, Strasser F, Anker SD, Bosaeus I, Bruera E, Fainsinger RL, Jatoi A, Loprinzi C, MacDonald N, and Mantovani G.** Definition and classification of cancer cachexia: an international consensus. *The lancet oncology* 12: 489-495, 2011.
4. **Fearon K, Arends J, and Baracos V.** Understanding the mechanisms and treatment options in cancer cachexia. *Nature reviews Clinical oncology* 10: 90-99, 2013.
5. **Ballarò R, Lopalco P, Audrito V, Beltrà M, Pin F, Angelini R, Costelli P, Corcelli A, Bonetto A, and Szeto HH.** Targeting mitochondria by SS-31 ameliorates the whole body energy status in cancer-and chemotherapy-induced cachexia. *Cancers* 13: 850, 2021.
6. **Niu M, Li L, Su Z, Wei L, Pu W, Zhao C, Ding Y, Wazir J, Cao W, and Song S.** An integrative transcriptome study reveals Ddit4/Redd1 as a key regulator of cancer cachexia in rodent models. *Cell Death & Disease* 12: 1-12, 2021.
7. **Lim S, Dunlap KR, Rosa-Caldwell ME, Haynie WS, Jansen LT, Washington TA, and Greene NP.** Comparative plasma proteomics in muscle atrophy during cancer-cachexia and disuse: The search for atrokines. *Physiological Reports* 8: e14608, 2020.
8. **Rosa-Caldwell ME, Brown JL, Lee DE, Wiggs MP, Perry Jr RA, Haynie WS, Caldwell AR, Washington TA, Lo W-J, and Greene NP.** Hepatic alterations during the development and progression of cancer cachexia. *Applied Physiology, Nutrition, and Metabolism* 2019.
9. **White JP, Puppa MJ, Gao S, Sato S, Welle SL, and Carson JA.** Muscle mTORC1 suppression by IL-6 during cancer cachexia: a role for AMPK. *American Journal of Physiology-Endocrinology and Metabolism* 304: E1042-E1052, 2013.
10. **Rosa-Caldwell ME, Lim S, Haynie WA, Brown JL, Deaver JW, Morena Da Silva F, Jansen LT, Lee DE, Wiggs MP, and Washington TA.** Female mice may have exacerbated catabolic signalling response compared to male mice during development and progression of disuse atrophy. *Journal of Cachexia, Sarcopenia and Muscle* 2021.

11. **Rosa-Caldwell ME, Lim S, Haynie WS, Brown JL, Lee DE, Dunlap KR, Jansen LT, Washington TA, Wiggs MP, and Greene NP.** Mitochondrial aberrations during the progression of disuse atrophy differentially affect male and female mice. *Journal of Cachexia, Sarcopenia and Muscle* 2021.
12. **Brown JL, Rosa-Caldwell ME, Lee DE, Blackwell TA, Brown LA, Perry RA, Haynie WS, Hardee JP, Carson JA, and Wiggs MP.** Mitochondrial degeneration precedes the development of muscle atrophy in progression of cancer cachexia in tumour-bearing mice. *Journal of cachexia, sarcopenia and muscle* 8: 926-938, 2017.
13. **Argilés JM, López-Soriano FJ, and Busquets S.** Muscle wasting in cancer: the role of mitochondria. *Current Opinion in Clinical Nutrition & Metabolic Care* 18: 221-225, 2015.
14. **Wallace DC.** Mitochondrial genetic medicine. *Nat Genet* 50: 1642-1649, 2018.
15. **White JP, Baltgalvis KA, Puppa MJ, Sato S, Baynes JW, and Carson JA.** Muscle oxidative capacity during IL-6-dependent cancer cachexia. *American Journal of Physiology-Regulatory, Integrative and Comparative Physiology* 300: R201-R211, 2011.
16. **Puente-Maestu L, Pérez-Parra J, Godoy R, Moreno N, Tejedor A, González-Aragoneses F, Bravo J-L, Alvarez FV, Camaño S, and Agustí A.** Abnormal mitochondrial function in locomotor and respiratory muscles of COPD patients. *European Respiratory Journal* 33: 1045-1052, 2009.
17. **Carew JS, and Huang P.** Mitochondrial defects in cancer. *Molecular cancer* 1: 1-12, 2002.
18. **VanderVeen BN, Fix DK, and Carson JA.** Disrupted skeletal muscle mitochondrial dynamics, mitophagy, and biogenesis during cancer cachexia: a role for inflammation. *Oxidative medicine and cellular longevity* 2017: 2017.
19. **Sung H, Ferlay J, Siegel RL, Laversanne M, Soerjomataram I, Jemal A, and Bray F.** Global cancer statistics 2020: GLOBOCAN estimates of incidence and mortality worldwide for 36 cancers in 185 countries. *CA: a cancer journal for clinicians* 71: 209-249, 2021.
20. **Onesti JK, and Guttridge DC.** Inflammation based regulation of cancer cachexia. *BioMed research international* 2014: 2014.
21. **Smith BD, Smith GL, Hurria A, Hortobagyi GN, and Buchholz TA.** Future of cancer incidence in the United States: burdens upon an aging, changing nation. *Journal of clinical oncology* 27: 2758-2765, 2009.

22. **Amano K, Maeda I, Morita T, Baba M, Miura T, Hama T, Mori I, Nakajima N, Nishi T, and Sakurai H.** C-reactive protein, symptoms and activity of daily living in patients with advanced cancer receiving palliative care. *Journal of cachexia, sarcopenia and muscle* 8: 457-465, 2017.
23. **Stojcev Z, Matysiak K, Duszewski M, and Banasiewicz T.** The role of dietary nutrition in stomach cancer. *Contemporary Oncology* 17: 343, 2013.
24. **Stene GB, Balstad TR, Leer ASM, Bye A, Kaasa S, Fallon M, Laird B, Maddocks M, and Solheim TS.** Deterioration in muscle mass and physical function differs according to weight loss history in cancer cachexia. *Cancers* 11: 1925, 2019.
25. **Dolly A, Dumas JF, and Servais S.** Cancer cachexia and skeletal muscle atrophy in clinical studies: what do we really know? *Journal of Cachexia, Sarcopenia and Muscle* 2020.
26. **Rosa-Caldwell ME, Fix DK, Washington TA, and Greene NP.** Muscle alterations in the development and progression of cancer-induced muscle atrophy: a review. *Journal of Applied Physiology* 128: 25-41, 2020.
27. **Barreto R, Mandili G, Witzmann FA, Novelli F, Zimmers TA, and Bonetto A.** Cancer and Chemotherapy Contribute to Muscle Loss by Activating Common Signaling Pathways. *Front Physiol* 7: 472, 2016.
28. **Bertram JS, and Janik P.** Establishment of a cloned line of Lewis Lung Carcinoma cells adapted to cell culture. *Cancer letters* 11: 63-73, 1980.
29. **Tanaka Y, Eda H, Tanaka T, Udagawa T, Ishikawa T, Horii I, Ishitsuka H, Kataoka T, and Taguchi T.** Experimental cancer cachexia induced by transplantable colon 26 adenocarcinoma in mice. *Cancer research* 50: 2290-2295, 1990.
30. **Beck SA, and Tisdale MJ.** Production of lipolytic and proteolytic factors by a murine tumor-producing cachexia in the host. *Cancer research* 47: 5919-5923, 1987.
31. **Bibby MC, Double JA, Ali SA, Fearon KCH, Brennan RA, and Tisdale MJ.** Characterization of a transplantable adenocarcinoma of the mouse colon producing cachexia in recipient animals. *Journal of the National Cancer Institute* 78: 539-546, 1987.
32. **Tessitore L, Bonelli G, and Baccino FM.** Early development of protein metabolic perturbations in the liver and skeletal muscle of tumour-bearing rats. A model system for cancer cachexia. *Biochemical Journal* 241: 153-159, 1987.

33. **Fukawa T, Yan-Jiang BC, Min-Wen JC, Jun-Hao ET, Huang D, Qian C-N, Ong P, Li Z, Chen S, and Mak SY.** Excessive fatty acid oxidation induces muscle atrophy in cancer cachexia. *Nature medicine* 22: 666-671, 2016.

34. **Batista ML, Neves RX, Peres SB, Yamashita AS, Shida CS, Farmer SR, and Seelaender M.** Heterogeneous time-dependent response of adipose tissue during the development of cancer cachexia. *Journal of Endocrinology* 215: 363-373, 2012.

35. **Baltgalvis KA, Berger FG, Peña MMO, Davis JM, White JP, and Carson JA.** Muscle wasting and interleukin-6-induced atrogen-1 expression in the cachectic Apc Min/+ mouse. *Pflügers Archiv-European Journal of Physiology* 457: 989-1001, 2009.

36. **White JP, Puppa MJ, Narsale A, and Carson JA.** Characterization of the male ApcMin/+ mouse as a hypogonadism model related to cancer cachexia. *Biol Open* 2: 1346-1353, 2013.

37. **Blum D, Omlin A, Baracos VE, Solheim TS, Tan BHL, Stone P, Kaasa S, Fearon K, Strasser F, and European Palliative Care Research C.** Cancer cachexia: a systematic literature review of items and domains associated with involuntary weight loss in cancer. *Critical reviews in oncology/hematology* 80: 114-144, 2011.

38. **Talbert EE, Cuitiño MC, Ladner KJ, Rajasekerea PV, Siebert M, Shakya R, Leone GW, Ostrowski MC, Paleo B, and Weisleder N.** Modeling human cancer-induced cachexia. *Cell reports* 28: 1612-1622, 2019.

39. **Frontera WR, and Ochala J.** Skeletal muscle: a brief review of structure and function. *Calcified tissue international* 96: 183-195, 2015.

40. **Evans WJ.** Skeletal muscle loss: cachexia, sarcopenia, and inactivity. *The American journal of clinical nutrition* 91: 1123S-1127S, 2010.

41. **Bye A, Sjøblom B, Wentzel-Larsen T, Grønberg BH, Baracos VE, Hjermsstad MJ, Aass N, Bremnes RM, Fløtten Ø, and Jordhøy M.** Muscle mass and association to quality of life in non-small cell lung cancer patients. *Journal of cachexia, sarcopenia and muscle* 8: 759-767, 2017.

42. **Welch N, Dasarathy J, Runkana A, Penumatsa R, Bellar A, Reen J, Rotroff D, McCullough AJ, and Dasarathy S.** Continued muscle loss increases mortality in cirrhosis: Impact of aetiology of liver disease. *Liver International* 40: 1178-1188, 2020.

43. **Attaway AH, Welch N, Hatipoğlu U, Zein JG, and Dasarathy S.** Muscle loss contributes to higher morbidity and mortality in COPD: An analysis of national trends. *Respirology* 26: 62-71, 2021.
44. **White JP, Puppa MJ, Sato S, Gao S, Price RL, Baynes JW, Kostek MC, Matesic LE, and Carson JA.** IL-6 regulation on skeletal muscle mitochondrial remodeling during cancer cachexia in the Apc Min/+ mouse. *Skeletal muscle* 2: 1-16, 2012.
45. **Rosa-Caldwell ME, and Greene NP.** Muscle metabolism and atrophy: let's talk about sex. *Biology of sex differences* 10: 1-14, 2019.
46. **Mauvais-Jarvis F.** Sex differences in metabolic homeostasis, diabetes, and obesity. *Biology of sex differences* 6: 1-9, 2015.
47. **Callahan DM, Bedrin NG, Subramanian M, Berking J, Ades PA, Toth MJ, and Miller MS.** Age-related structural alterations in human skeletal muscle fibers and mitochondria are sex specific: relationship to single-fiber function. *Journal of applied physiology* 116: 1582-1592, 2014.
48. **Haizlip KM, Harrison BC, and Leinwand LA.** Sex-based differences in skeletal muscle kinetics and fiber-type composition. *Physiology* 30: 30-39, 2015.
49. **Talbot J, and Maves L.** Skeletal muscle fiber type: using insights from muscle developmental biology to dissect targets for susceptibility and resistance to muscle disease. *Wiley Interdisciplinary Reviews: Developmental Biology* 5: 518-534, 2016.
50. **Picard M, Ritchie D, Thomas MM, Wright KJ, and Hepple RT.** Alterations in intrinsic mitochondrial function with aging are fiber type-specific and do not explain differential atrophy between muscles. *Aging cell* 10: 1047-1055, 2011.
51. **Gao Y, Arfat Y, Wang H, and Goswami N.** Muscle atrophy induced by mechanical unloading: mechanisms and potential countermeasures. *Frontiers in physiology* 9: 235, 2018.
52. **Brocca L, Cannavino J, Coletto L, Biolo G, Sandri M, Bottinelli R, and Pellegrino MA.** The time course of the adaptations of human muscle proteome to bed rest and the underlying mechanisms. *The Journal of physiology* 590: 5211-5230, 2012.
53. **De Jonghe B, Sharshar T, Lefaucheur J-P, Authier F-J, Durand-Zaleski I, Boussarsar M, Cerf C, Renaud E, Mesrati F, and Carlet J.** Paresis acquired in the intensive care unit: a prospective multicenter study. *Jama* 288: 2859-2867, 2002.

54. **Zhu Y, Shao X, Wang X, Liu L, and Liang H.** Sex disparities in cancer. *Cancer letters* 466: 35-38, 2019.
55. **Rebecca S, Siegel MPH, Kimberly D, Miller MPH, and Ahmedin Jemal DVM.** Cancer statistics. *Ca Cancer J Clin* 67: 7-30, 2017.
56. **Cook MB, Dawsey SM, Freedman ND, Inskip PD, Wichner SM, Quraishi SM, Devesa SS, and McGlynn KA.** Sex disparities in cancer incidence by period and age. *Cancer Epidemiology and Prevention Biomarkers* 18: 1174-1182, 2009.
57. **Cook MB, McGlynn KA, Devesa SS, Freedman ND, and Anderson WF.** Sex disparities in cancer mortality and survival. *Cancer Epidemiology and Prevention Biomarkers* 20: 1629-1637, 2011.
58. **Anderson LJ, Liu H, and Garcia JM.** Sex differences in muscle wasting. In: *Sex and Gender Factors Affecting Metabolic Homeostasis, Diabetes and Obesity* Springer, 2017, p. 153-197.
59. **Vagnildhaug OM, Blum D, Wilcock A, Fayers P, Strasser F, Baracos VE, Hjermsstad MJ, Kaasa S, Laird B, and Solheim TS.** The applicability of a weight loss grading system in cancer cachexia: a longitudinal analysis. *Journal of cachexia, sarcopenia and muscle* 8: 789-797, 2017.
60. **Baracos VE, Reiman T, Mourtzakis M, Gioulbasanis I, and Antoun S.** Body composition in patients with non-small cell lung cancer: A contemporary view of cancer cachexia with the use of computed tomography image analysis. *The American journal of clinical nutrition* 91: 1133S-1137S, 2010.
61. **Montalvo RN, Counts BR, and Carson JA.** Understanding sex differences in the regulation of cancer-induced muscle wasting. *Current opinion in supportive and palliative care* 12: 394, 2018.
62. **Oliván S, Calvo AC, Manzano R, Zaragoza P, and Osta R.** Sex differences in constitutive autophagy. *BioMed research international* 2014: 2014.
63. **Ogawa M, Kitano T, Kawata N, Sugihira T, Kitakaze T, Harada N, and Yamaji R.** Daidzein down-regulates ubiquitin-specific protease 19 expression through estrogen receptor β and increases skeletal muscle mass in young female mice. *The Journal of nutritional biochemistry* 49: 63-70, 2017.

64. **Hetzler KL, Hardee JP, Puppa MJ, Narsale AA, Sato S, Davis JM, and Carson JA.** Sex differences in the relationship of IL-6 signaling to cancer cachexia progression. *Biochimica et Biophysica Acta (BBA)-Molecular Basis of Disease* 1852: 816-825, 2015.
65. **Kilgour RD, Vigano A, Trutschnigg B, Lucar E, Borod M, and Morais JA.** Handgrip strength predicts survival and is associated with markers of clinical and functional outcomes in advanced cancer patients. *Supportive Care in Cancer* 21: 3261-3270, 2013.
66. **Isaac ST, Tan TC, and Polly P.** Endoplasmic Reticulum Stress, Calcium Dysregulation and Altered Protein Translation: Intersection of Processes That Contribute to Cancer Cachexia Induced Skeletal Muscle Wasting. *Curr Drug Targets* 17: 1140-1146, 2016.
67. **Close RI.** Dynamic properties of mammalian skeletal muscles. *Physiological reviews* 52: 129-197, 1972.
68. **Murphy KT, Chee A, Trieu J, Naim T, and Lynch GS.** Importance of functional and metabolic impairments in the characterization of the C-26 murine model of cancer cachexia. *Disease models & mechanisms* 5: 533-545, 2012.
69. **VanderVeen BN, Hardee JP, Fix DK, and Carson JA.** Skeletal muscle function during the progression of cancer cachexia in the male ApcMin/+ mouse. *Journal of Applied Physiology* 124: 684-695, 2018.
70. **Roberts BM, Frye GS, Ahn B, Ferreira LF, and Judge AR.** Cancer cachexia decreases specific force and accelerates fatigue in limb muscle. *Biochemical and biophysical research communications* 435: 488-492, 2013.
71. **Sodek KL, Ringuette MJ, and Brown TJ.** Compact spheroid formation by ovarian cancer cells is associated with contractile behavior and an invasive phenotype. *International journal of cancer* 124: 2060-2070, 2009.
72. **Al-Majid S, and McCarthy DO.** Resistance exercise training attenuates wasting of the extensor digitorum longus muscle in mice bearing the colon-26 adenocarcinoma. *Biological research for nursing* 2: 155-166, 2001.
73. **Patel TJ, and Lieber RL.** Force transmission in skeletal muscle: from actomyosin to external tendons. *Exercise and sport sciences reviews* 25: 321-363, 1997.
74. **Hardee JP, Mangum JE, Gao S, Sato S, Hetzler KL, Puppa MJ, Fix DK, and Carson JA.** Eccentric contraction-induced myofiber growth in tumor-bearing mice. *Journal of Applied Physiology* 120: 29-37, 2016.

75. **Egeblad M, and Werb Z.** New functions for the matrix metalloproteinases in cancer progression. *Nat Rev Cancer* 2: 161-174, 2002.
76. **Devine RD, Bicer S, Reiser PJ, Velten M, and Wold LE.** Metalloproteinase expression is altered in cardiac and skeletal muscle in cancer cachexia. *Am J Physiol Heart Circ Physiol* 309: H685-691, 2015.
77. **Fanzani A, Conraads VM, Penna F, and Martinet W.** Molecular and cellular mechanisms of skeletal muscle atrophy: an update. *Journal of cachexia, sarcopenia and muscle* 3: 163-179, 2012.
78. **Sandri M.** Protein breakdown in muscle wasting: role of autophagy-lysosome and ubiquitin-proteasome. *The international journal of biochemistry & cell biology* 45: 2121-2129, 2013.
79. **Smith KL, and Tisdale MJ.** Increased protein degradation and decreased protein synthesis in skeletal muscle during cancer cachexia. *Br J Cancer* 67: 680-685, 1993.
80. **White JP, Baynes JW, Welle SL, Kostek MC, Matesic LE, Sato S, and Carson JA.** The regulation of skeletal muscle protein turnover during the progression of cancer cachexia in the Apc Min/+ mouse. *PLoS one* 6: e24650, 2011.
81. **Brown JL, Lee DE, Rosa-Caldwell ME, Brown LA, Perry RA, Haynie WS, Huseman K, Sataranatarajan K, Van Remmen H, Washington TA, Wiggs MP, and Greene NP.** Protein imbalance in the development of skeletal muscle wasting in tumour-bearing mice. *J Cachexia Sarcopenia Muscle* 9: 987-1002, 2018.
82. **Brown JL, Lawrence MM, Ahn B, Kneis P, Piekarz KM, Qaisar R, Ranjit R, Bian J, Pharaoh G, Brown C, Peelor 3rd FF, Kinter MT, Miller BF, Richardson A, and Van Remmen H.** Cancer cachexia in a mouse model of oxidative stress. *Journal of Cachexia, Sarcopenia and Muscle* n/a: 2020.
83. **Waddell DS, Baehr LM, Van Den Brandt J, Johnsen SA, Reichardt HM, Furlow JD, and Bodine SC.** The glucocorticoid receptor and FOXO1 synergistically activate the skeletal muscle atrophy-associated MuRF1 gene. *American Journal of Physiology-Endocrinology and Metabolism* 295: E785-E797, 2008.
84. **Sandri M, Sandri C, Gilbert A, Skurk C, Calabria E, Picard A, Walsh K, Schiaffino S, Lecker SH, and Goldberg AL.** Foxo transcription factors induce the atrophy-related ubiquitin ligase atrogin-1 and cause skeletal muscle atrophy. *Cell* 117: 399-412, 2004.

85. **Xie Y, and Varshavsky A.** Physical association of ubiquitin ligases and the 26S proteasome. *Proceedings of the National Academy of Sciences* 97: 2497-2502, 2000.
86. **Bodine SC, Latres E, Baumhueter S, Lai VKM, Nunez L, Clarke BA, Poueymirou WT, Panaro FJ, Na E, and Dharmarajan K.** Identification of ubiquitin ligases required for skeletal muscle atrophy. *Science* 294: 1704-1708, 2001.
87. **Gomes MD, Lecker SH, Jagoe RT, Navon A, and Goldberg AL.** Atrogin-1, a muscle-specific F-box protein highly expressed during muscle atrophy. *Proceedings of the National Academy of Sciences* 98: 14440-14445, 2001.
88. **Petroski MD, and Deshaies RJ.** Mechanism of lysine 48-linked ubiquitin-chain synthesis by the cullin-RING ubiquitin-ligase complex SCF-Cdc34. *Cell* 123: 1107-1120, 2005.
89. **Yamao F.** Ubiquitin system: selectivity and timing of protein destruction. *The Journal of Biochemistry* 125: 223-229, 1999.
90. **Winston JT, Koepp DM, Zhu C, Elledge SJ, and Harper JW.** A family of mammalian F-box proteins. *Current Biology* 9: 1180-S1183, 1999.
91. **Seaborne RA, Hughes DC, Turner DC, Owens DJ, Baehr LM, Gorski P, Semenova EA, Borisov OV, Larin AK, and Popov DV.** UBR5 is a novel E3 ubiquitin ligase involved in skeletal muscle hypertrophy and recovery from atrophy. *The Journal of physiology* 597: 3727-3749, 2019.
92. **Ebert SM, Dyle MC, Kunkel SD, Bullard SA, Bongers KS, Fox DK, Dierdorff JM, Foster ED, and Adams CM.** Stress-induced skeletal muscle Gadd45a expression reprograms myonuclei and causes muscle atrophy. *Journal of Biological Chemistry* 287: 27290-27301, 2012.
93. **Bongers KS, Fox DK, Ebert SM, Kunkel SD, Dyle MC, Bullard SA, Dierdorff JM, and Adams CM.** Skeletal muscle denervation causes skeletal muscle atrophy through a pathway that involves both Gadd45a and HDAC4. *American Journal of Physiology-Endocrinology and Metabolism* 305: E907-E915, 2013.
94. **Cohen S, Brault JJ, Gygi SP, Glass DJ, Valenzuela DM, Gartner C, Latres E, and Goldberg AL.** During muscle atrophy, thick, but not thin, filament components are degraded by MuRF1-dependent ubiquitylation. *Journal of Cell Biology* 185: 1083-1095, 2009.
95. **Zhao J, Zhang Y, Zhao W, Wu Y, Pan J, Bauman WA, and Cardozo C.** Effects of nandrolone on denervation atrophy depend upon time after nerve transection. *Muscle & Nerve: Official Journal of the American Association of Electrodiagnostic Medicine* 37: 42-49, 2008.

96. **Silva KAS, Dong J, Dong Y, Dong Y, Schor N, Tweardy DJ, Zhang L, and Mitch WE.** Inhibition of Stat3 activation suppresses caspase-3 and the ubiquitin-proteasome system, leading to preservation of muscle mass in cancer cachexia. *Journal of Biological Chemistry* 290: 11177-11187, 2015.
97. **Mizushima N, and Komatsu M.** Autophagy: renovation of cells and tissues. *Cell* 147: 728-741, 2011.
98. **Mizushima N, Yoshimori T, and Ohsumi Y.** The role of Atg proteins in autophagosome formation. *Annual review of cell and developmental biology* 27: 107-132, 2011.
99. **Xie Z, and Klionsky DJ.** Autophagosome formation: core machinery and adaptations. *Nature cell biology* 9: 1102-1109, 2007.
100. **MacDonald AJ, Johns N, Stephens N, Greig C, Ross JA, Small AC, Husi H, Fearon KC, and Preston T.** Habitual Myofibrillar Protein Synthesis Is Normal in Patients with Upper GI Cancer Cachexia. *Clin Cancer Res* 21: 1734-1740, 2015.
101. **Bodine SC, Stitt TN, Gonzalez M, Kline WO, Stover GL, Bauerlein R, Zlotchenko E, Scrimgeour A, Lawrence JC, and Glass DJ.** Akt/mTOR pathway is a crucial regulator of skeletal muscle hypertrophy and can prevent muscle atrophy in vivo. *Nature cell biology* 3: 1014-1019, 2001.
102. **Bodine SC.** mTOR signaling and the molecular adaptation to resistance exercise. *Medicine and science in sports and exercise* 38: 1950-1957, 2006.
103. **Preiss T, and W. Hentze M.** Starting the protein synthesis machine: eukaryotic translation initiation. *Bioessays* 25: 1201-1211, 2003.
104. **Peterson TR, Laplante M, Thoreen CC, Sancak Y, Kang SA, Kuehl WM, Gray NS, and Sabatini DM.** DEPTOR is an mTOR inhibitor frequently overexpressed in multiple myeloma cells and required for their survival. *Cell* 137: 873-886, 2009.
105. **Gordon BS, Steiner JL, Lang CH, Jefferson LS, and Kimball SR.** Reduced REDD1 expression contributes to activation of mTORC1 following electrically induced muscle contraction. *American Journal of Physiology-Endocrinology and Metabolism* 307: E703-E711, 2014.
106. **Figueiredo VC, and McCarthy JJ.** Targeting cancer via ribosome biogenesis: the cachexia perspective. *Cellular and Molecular Life Sciences* 78: 5775-5787, 2021.

107. **Machida M, Takeda K, Yokono H, Ikemune S, Taniguchi Y, Kiyosawa H, and Takemasa T.** Reduction of ribosome biogenesis with activation of the mTOR pathway in denervated atrophic muscle. *Journal of cellular physiology* 227: 1569-1576, 2012.
108. **Connolly M, Paul R, Farre-Garros R, Natanek SA, Bloch S, Lee J, Lorenzo JP, Patel H, Cooper C, and Sayer AA.** miR-424-5p reduces ribosomal RNA and protein synthesis in muscle wasting. *Journal of cachexia, sarcopenia and muscle* 9: 400-416, 2018.
109. **Pearson G, Robinson F, Beers Gibson T, Xu B-e, Karandikar M, Berman K, and Cobb MH.** Mitogen-activated protein (MAP) kinase pathways: regulation and physiological functions. *Endocrine reviews* 22: 153-183, 2001.
110. **Johnson GL, and Lapadat R.** Mitogen-activated protein kinase pathways mediated by ERK, JNK, and p38 protein kinases. *Science* 298: 1911-1912, 2002.
111. **Wilde JM, Gumucio JP, Grekin JA, Sarver DC, Noah AC, Ruehlmann DG, Davis ME, Bedi A, and Mendias CL.** Inhibition of p38 mitogen-activated protein kinase signaling reduces fibrosis and lipid accumulation after rotator cuff repair. *Journal of shoulder and elbow surgery* 25: 1501-1508, 2016.
112. **Kramer HF, and Goodyear LJ.** Exercise, MAPK, and NF- κ B signaling in skeletal muscle. *Journal of applied physiology* 103: 388-395, 2007.
113. **McClung JM, Judge AR, Powers SK, and Yan Z.** p38 MAPK links oxidative stress to autophagy-related gene expression in cachectic muscle wasting. *American Journal of Physiology-Cell Physiology* 298: C542-C549, 2010.
114. **Sin TK, Zhang G, Zhang Z, Zhu JZ, Zuo Y, Frost JA, Li M, and Li Y-P.** Cancer-Induced Muscle Wasting Requires p38 β MAPK Activation of p300. *Cancer Research* 81: 885-897, 2021.
115. **Li Y-P, Chen Y, John J, Moylan J, Jin B, Mann DL, and Reid MB.** TNF- α acts via p38 MAPK to stimulate expression of the ubiquitin ligase atrogin1/MAFbx in skeletal muscle. *The FASEB Journal* 19: 362-370, 2005.
116. **Bossola M, Marzetti E, Rosa F, and Pacelli F.** Skeletal muscle regeneration in cancer cachexia. *Clinical and Experimental Pharmacology and Physiology* 43: 522-527, 2016.
117. **Talbert EE, and Guttridge DC.** Impaired regeneration: A role for the muscle microenvironment in cancer cachexia. *Semin Cell Dev Biol* 54: 82-91, 2016.

118. **He WA, Berardi E, Cardillo VM, Acharyya S, Aulino P, Thomas-Ahner J, Wang J, Bloomston M, Muscarella P, and Nau P.** NF- κ B-mediated Pax7 dysregulation in the muscle microenvironment promotes cancer cachexia. *The Journal of clinical investigation* 123: 4821-4835, 2013.
119. **Sakellariou GK, Pearson T, Lightfoot AP, Nye GA, Wells N, Giakoumaki II, Vasilaki A, Griffiths RD, Jackson MJ, and McArdle A.** Mitochondrial ROS regulate oxidative damage and mitophagy but not age-related muscle fiber atrophy. *Scientific reports* 6: 33944, 2016.
120. **Ježek J, Cooper KF, and Strich R.** Reactive oxygen species and mitochondrial dynamics: the yin and yang of mitochondrial dysfunction and cancer progression. *Antioxidants* 7: 13, 2018.
121. **Hurtley SM.** Mitochondrial quality control. *Science* 350: 1052-1053, 2015.
122. **Chan DC.** Mitochondrial fusion and fission in mammals. *Annu Rev Cell Dev Biol* 22: 79-99, 2006.
123. **Otera H, Wang C, Cleland MM, Setoguchi K, Yokota S, Youle RJ, and Mihara K.** Mff is an essential factor for mitochondrial recruitment of Drp1 during mitochondrial fission in mammalian cells. *Journal of Cell Biology* 191: 1141-1158, 2010.
124. **Huang P, Galloway CA, and Yoon Y.** Control of mitochondrial morphology through differential interactions of mitochondrial fusion and fission proteins. *PloS one* 6: e20655, 2011.
125. **Kobayashi S, Zhao F, Zhang Z, Kobayashi T, Huang Y, Shi B, Wu W, and Liang Q.** Mitochondrial Fission and Mitophagy Coordinately Restrict High Glucose Toxicity in Cardiomyocytes. *Frontiers in physiology* 11: 2020.
126. **Sanchis-Gomar F, Luis Garcia-Gimenez J, Carmen Gomez-Cabrera M, and V Pallardo F.** Mitochondrial biogenesis in health and disease. Molecular and therapeutic approaches. *Current pharmaceutical design* 20: 5619-5633, 2014.
127. **Boushel R, Lundby C, Qvortrup K, and Sahlin K.** Mitochondrial plasticity with exercise training and extreme environments. *Exercise and sport sciences reviews* 42: 169-174, 2014.
128. **Holloszy JO.** Regulation of mitochondrial biogenesis and GLUT4 expression by exercise. *Comprehensive Physiology* 1: 921-940, 2011.
129. **Johri A, Chandra A, and Beal MF.** PGC-1 α , mitochondrial dysfunction, and Huntington's disease. *Free Radical Biology and Medicine* 62: 37-46, 2013.

130. **Hayashi G, Jasoliya M, Sahdeo S, Saccà F, Pane C, Filla A, Marsili A, Puorro G, Lanzillo R, and Brescia Morra V.** Dimethyl fumarate mediates Nrf2-dependent mitochondrial biogenesis in mice and humans. *Human molecular genetics* 26: 2864-2873, 2017.
131. **Picca A, and Lezza AMS.** Regulation of mitochondrial biogenesis through TFAM-mitochondrial DNA interactions: useful insights from aging and calorie restriction studies. *Mitochondrion* 25: 67-75, 2015.
132. **Tzika AA, Fontes-Oliveira CC, Shestov AA, Constantinou C, Psychogios N, Righi V, Mintzopoulos D, Busquets S, Lopez-Soriano FJ, and Milot S.** Skeletal muscle mitochondrial uncoupling in a murine cancer cachexia model. *International journal of oncology* 43: 886-894, 2013.
133. **Guigni BA, Callahan DM, Tourville TW, Miller MS, Fiske B, Voigt T, Korwin-Mihavics B, Anathy V, Dittus K, and Toth MJ.** Skeletal muscle atrophy and dysfunction in breast cancer patients: role for chemotherapy-derived oxidant stress. *American Journal of Physiology-Cell Physiology* 315: C744-C756, 2018.
134. **de Castro GS, Simoes E, Lima JDCC, Ortiz-Silva M, Festuccia WT, Tokeshi F, Alcântara PS, Otoch JP, Coletti D, and Seelaender M.** Human cachexia induces changes in mitochondria, autophagy and apoptosis in the skeletal muscle. *Cancers* 11: 1264, 2019.
135. **Russell ST, Eley H, and Tisdale MJ.** Role of reactive oxygen species in protein degradation in murine myotubes induced by proteolysis-inducing factor and angiotensin II. *Cellular signalling* 19: 1797-1806, 2007.
136. **Ventura-Clapier R, Moulin M, Piquereau J, Lemaire C, Mericskay M, Veksler V, and Garnier A.** Mitochondria: a central target for sex differences in pathologies. *Clinical science* 131: 803-822, 2017.
137. **Santarelli R, Rossi R, Scimemi P, Cama E, Valentino ML, La Morgia C, Caporali L, Liguori R, Magnavita V, and Monteleone A.** OPA1-related auditory neuropathy: site of lesion and outcome of cochlear implantation. *Brain* 138: 563-576, 2015.
138. **Patten DA, Wong J, Khacho M, Soubannier V, Mailloux RJ, Pilon-Larose K, MacLaurin JG, Park DS, McBride HM, and Trinkle-Mulcahy L.** OPA1-dependent cristae modulation is essential for cellular adaptation to metabolic demand. *The EMBO journal* 33: 2676-2691, 2014.
139. **Anand R, Wai T, Baker MJ, Kladt N, Schauss AC, Rugarli E, and Langer T.** The i-AAA protease YME1L and OMA1 cleave OPA1 to balance mitochondrial fusion and fission. *Journal of Cell Biology* 204: 919-929, 2014.

140. **Fülöp L, Szanda G, Enyedi B, Várnai P, and Spät A.** The effect of OPA1 on mitochondrial Ca²⁺ signaling. *PLoS One* 6: e25199, 2011.
141. **Varanita T, Soriano ME, Romanello V, Zaglia T, Quintana-Cabrera R, Semenzato M, Menabò R, Costa V, Civileto G, and Pesce P.** The OPA1-dependent mitochondrial cristae remodeling pathway controls atrophic, apoptotic, and ischemic tissue damage. *Cell metabolism* 21: 834-844, 2015.
142. **Eiberg H, Kjer B, Kjer P, and Rosenberg T.** Dominant optic atrophy (OPA1) mapped to chromosome 3q region. I. Linkage analysis. *Human molecular genetics* 3: 977-980, 1994.
143. **Delettre C, Lenaers G, Griffoin J-M, Gigarel N, Lorenzo C, Belenguer P, Pelloquin L, Grosgeorge J, Turc-Carel C, and Perret E.** Nuclear gene OPA1, encoding a mitochondrial dynamin-related protein, is mutated in dominant optic atrophy. *Nature genetics* 26: 207-210, 2000.
144. **Carelli V, Musumeci O, Caporali L, Zanna C, La Morgia C, Del Dotto V, Porcelli AM, Rugolo M, Valentino ML, and Iommarini L.** Syndromic parkinsonism and dementia associated with OPA 1 missense mutations. *Annals of neurology* 78: 21-38, 2015.
145. **Giacomello M, Pyakurel A, Glytsou C, and Scorrano L.** The cell biology of mitochondrial membrane dynamics. *Nature reviews Molecular cell biology* 21: 204-224, 2020.
146. **Hanahan D, and Weinberg RA.** Hallmarks of cancer: the next generation. *cell* 144: 646-674, 2011.
147. **Herkenne S, and Scorrano L.** OPA1, a new mitochondrial target in cancer therapy. *Aging (Albany NY)* 12: 20931, 2020.
148. **Wee Y, Liu Y, Lu J, Li X, and Zhao M.** Identification of novel prognosis-related genes associated with cancer using integrative network analysis. *Scientific reports* 8: 1-11, 2018.
149. **Wang X, Li H, Zheng A, Yang L, Liu J, Chen C, Tang Y, Zou X, Li Y, and Long J.** Mitochondrial dysfunction-associated OPA1 cleavage contributes to muscle degeneration: preventative effect of hydroxytyrosol acetate. *Cell Death & Disease* 5: e1521-e1521, 2014.
150. **Baker N.** Muscle Stem Cell Fate is Directed by the Mitochondrial Fusion Protein OPA1. 2021.

151. **Szklarz LKS, and Scorrano L.** The antiapoptotic OPA1/Parl couple participates in mitochondrial adaptation to heat shock. *Biochimica et Biophysica Acta (BBA)-Bioenergetics* 1817: 1886-1893, 2012.
152. **Szabo A, Sumegi K, Fekete K, Hocsak E, Debreceni B, Setalo Jr G, Kovacs K, Deres L, Kengyel A, and Kovacs D.** Activation of mitochondrial fusion provides a new treatment for mitochondria-related diseases. *Biochemical pharmacology* 150: 86-96, 2018.
153. **Henstridge DC, Bruce CR, Drew BG, Tory K, Kolonics A, Estevez E, Chung J, Watson N, Gardner T, and Lee-Young RS.** Activating HSP72 in rodent skeletal muscle increases mitochondrial number and oxidative capacity and decreases insulin resistance. *Diabetes* 63: 1881-1894, 2014.

CHAPTER II: PROPOSAL

A. Specific Aims

SEX DIFFERENCES IN CANCER CACHEXIA AND A NOVEL THERAPEUTIC TARGET FOR CANCER-INDUCED MUSCLE WASTING

Cancer-cachexia (CC), a wasting syndrome, occurs in approximately 80% of cancer patients (2) and is responsible for 22-30% of cancer-related deaths (2, 3). However, current therapeutic approaches lack sufficient efficacy to prevent cachexia (3). Early biomarkers to manage tumor development and concurrent treatment using potential therapeutic targets to protect muscle mass are desperately needed to improve cancer outcomes. Recently, we identified for the first time that mitochondrial degeneration including **lower mitochondrial fusion protein, OPA1, preceded marked loss in skeletal muscle mass of tumor-bearing mice**, suggesting OPA1 might be a novel target for cancer-induced muscle loss. **However, the efficacy of OPA1 to prevent CC has not been assessed** (12, 81).

In addition, the majority of preexisting pre-clinical CC studies have been mainly focused on male animals (26, 45) although recent evidence demonstrates sex-related phenotypical differences in response to muscle atrophy (45, 58, 154, 155). Therefore, the **PURPOSE** of my dissertation project is to investigate skeletal muscle alterations during the development of CC in female tumor-bearing mice (Aim 1) and determine the efficacy of OPA1 as a therapeutic target for cancer-induced muscle atrophy (Aim 2). The **CENTRAL HYPOTHESES of this proposed work are: Aim 1)** Impaired muscle contractility, mitochondrial health, and altered protein turnover will present in the skeletal muscle of female tumor-bearing mice and **Aim 2)** Impaired muscular health in response to LLC implantation will be ameliorated via AAV-mediated OPA1 (mitochondrial fusion-associated) gene transfer.

AIM 1.**Define alterations in the development of cancer cachexia in female tumor-bearing mice.**

Our laboratory has previously completed animal experiments for Aim 1. Female mice were injected with Lewis Lung Carcinoma (LLC) and harvested at 1, 2, 3, and 4 wks to determine skeletal muscle alterations during the development of CC. We utilized a similar experimental design that we used with male mice (12), where we found mitochondrial degenerations in a pre-cachectic state. Therefore, to define alterations of mitochondrial health in female mice, we measured mitochondrial respiratory control ratio (RCR) and reactive oxygen species (ROS) emission, oxidative phenotype, mitochondrial quality control markers. In addition, the cancer-induced muscle wasting mechanism has been well characterized in male animals and is associated with a poor cancer outcome and reduced survival rate¹³ although that of females remains elusive. To determine the muscle wasting process from pre- to cachectic state, we further assessed 24h protein fractional synthetic rate (FSR), protein degradation signaling via ubiquitin proteasomal system (UPS) and autophagic-lysosomal pathway (ALP), pro-inflammatory markers, and myogenic markers via immunoblotting and RT-qPCR. As muscle mass is directly associated with strength, we finally assessed skeletal muscle contractility (force production and fatigability) via *in vivo* electrical stimulation in lower limb muscles. The outcome of this project may provide **novel insight into potential mechanisms** that may explain biological sex as a crucial variable in cancer cachexia.

AIM 2.

Define if genetic overexpression of OPA1 (OPA1/AAV) serves as a novel therapeutic target for cancer-induced muscle wasting.

The research idea for aim 2 was developed from our prior studies of CC development to define a mechanistic target of onset in CC. I will systemically determine the efficacy of promoting mitochondrial quality by OPA1 gene manipulation in LLC-induced tumor-bearing mice to mitigate cancer-induced muscle wasting. I will apply adeno-associated virus (AAV)-mediated gene transfer of OPA1 gene into the muscle to prevent CC. Intra-muscular AAV has been applied in muscle-related disease (156). Previously, we observed reduced OPA1 protein content during the early development of CC which remained lower through development of the cachectic phenotype. Therefore, the initial treatment and duration of the AAV intervention will begin at 1 wk following LLC injection, and the gene transfer will continue throughout the animal experiment. To determine if OPA1 AAV gene transfer attenuates CC, I will assess a diverse analysis to examine skeletal muscle health. Specific skeletal muscle measurements will be followed as Aim 1. Briefly, muscle contractile functions, fiber typing, protein turnover, mitochondrial oxidative phenotype, and mitochondrial quality control will be assessed. The outcome of Aim 2 will provide **mechanistic** evidence utilizing pre-CC signature for efficacious target in CC prevention.

***Note – our contingency plan for AAV was to utilize OPA1 transgenic mice to the same purpose. As we did not have AAV prepared for this experiment in Aim 2 I present data collected to date utilizing the OPA1 transgenic mice.**

PUBLIC HEALTH IMPACT: Proposed project may significantly advance the current CC study via providing a fundamental understanding of CC development in both males and females and a mechanistic target to effectively prevent CC, contributing to improved overall cancer outcomes.

C. RESEARCH STRATEGY

i. SIGNIFICANCE

Cancer-cachexia (CC), a wasting syndrome, characterized by marked weight loss that occurs in approximately 80% of cancer patients (2) and is responsible for 20-30% of cancer-related deaths (2, 20). However, current therapeutic approaches lack sufficient efficacy to prevent or reverse (3) and it is often poorly diagnosed (3). Understanding underlying mechanisms for the development of CC are crucial for the development of therapies to treat CC and improve cancer outcomes. **Therefore, there remains a critical need to identify key underlying mechanisms in the development of cancer cachexia in females to enhance therapeutic potential.** The OVERARCHING GOAL of this proposal is to understand alterations in skeletal muscle during the development of CC in female tumor-bearing mice and determine if genetic intervention to promote mitochondrial fusion protects muscle from wasting and attenuates CC. Therefore, the **CENTRAL HYPOTHESES of this proposed work are: Aim 1)** Impaired muscle contractility, mitochondrial health, and altered protein turnover will present in the skeletal muscle of female tumor-bearing mice and **Aim 2)** Impaired muscular health in response to LLC implantation will be ameliorated via AAV-mediated OPA1 (mitochondrial fusion-associated) gene transfer. Therefore, this proposal will **SIGNIFICANTLY** address these critical needs and advance the study of cancer cachexia via:

1. Providing **FUNDAMENTAL** evidence for alterations or degenerating processes in the development of CC in female tumor-bearing mice as well as potential therapeutic strategies to prevent CC via utilizing genetic manipulations (overexpression) of OPA1 based on our previous findings (12). Furthermore, I will combine recent outcome measures incorporating more complete assessments of mitochondrial health including mitochondrial function, oxidative phenotype, quality control markers, and protein turnover including protein synthesis

by 24h protein FSR as well as muscle contractile function to provide the most comprehensive assessment of muscular health in CC development.

2. Providing **MECHANISTIC** evidence for targeting pre-muscle wasting alterations utilizing genetic approaches. The AAV/OPA1 intervention will be employed with timing of onset based upon the timing of concurrent alterations to endogenous target during the early development of CC, which will provide the importance of specific timing-derived treatments and systemic effects of the intervention to prevent CC.

ii. RIGOR OF PRIOR RESEARCH

Our prior evidence using a pre-clinical mouse model of CC in a time-course manner showed progressive deteriorations(12, 81), representing for the first time to define the pre-

cachectic signatures of skeletal muscle in the development of CC in male tumor-bearing mice (Table 1). These preliminary data indicate that CC is responsible for muscle atrophy and mitochondrial dysfunction in male tumor-bearing

Variable	1 week	2 weeks	3 weeks	4 weeks
Mitochondrial ROS	↑	↑	↑	↑
Satellite Cell/Myogenesis	↓	↓	↓	↓
Opa1	↓	↓	↓	↓
MitoTimer		↑	↑	↑
RCR			↓	↓
BNIP3			↑	↑
Atrogin/MuRF1			↑	↑
Ubiquitination				↑
Autophagy Machinery				↑
MAPK				↑
Fis1				↑
SDH/COXIV/VDAC				↑
Deptor			↑	
Muscle mass				↓

Table 1. Summary of alterations in development of LLC-induced muscle atrophy

mice, and it is speculated that certain biological markers may initiate these degenerating processes during the initial stages of CC. Therefore, it is imperative to understand underlying molecular mechanisms in both males and females during the development and progression of CC to guide sex-based therapeutic strategies to prevent CC. This proposed project extends our

prior studies in male mice (12, 81), and the outcomes of this proposal will help to advance efficacious therapies for CC. Taken together, our preliminary studies show CC induces muscle atrophy and mitochondrial dysfunction in the muscle of male tumor-bearing mice and supporting the experimental rationale for the central hypothesis of this project.

D. APPROACH

Overall Approach. In **Aim 1**, I will provide **novel evidence** of pre-cachectic alterations in the skeletal muscle during the early stages of CC via utilizing a time-course cancer development design in female tumor-bearing mice. This time-course approach will allow us to identify and compare degenerating mechanisms involved in muscle contractility, protein turnover, and mitochondrial quality in the skeletal muscle during the development of CC, thus providing foundational evidence in cachectic phenotypes in females. In **Aim 2**, I will provide **mechanistic evidence** for targeting cancer-induced muscle wasting via utilizing a genetic intervention to determine if rescuing OPA1 expression prevents CC-induced muscle wasting and cachectic phenotypes. This **approach** will provide critical mechanistic insight into the development of CC in females as well as a potential therapeutic target for cancer-induced muscle wasting in both sexes. This combined strategy will allow us to shift from identifying pre-cachectic phenotypes in females (Aim 1) towards advancing a mechanistic strategy to target CC (Aim 2).

i. BIOLOGICAL SEX AS AN IMPORTANT VARIABLE.

Although it has been reported that muscle phenotype of both males and females respond distinctively during different forms of muscle atrophy including disuse- (10) and inflammation-induced muscle atrophy (45), existing pre-clinical CC studies have been conducted predominantly with male animals and **it has not been tested if biological sex differentially regulates**

muscular health in the development of CC. Therefore, our animal experiments were performed in female mice for **Aim 1** to compare with previous male CC studies (12, 15, 35, 80, 81) and will be performed in both sexes for **Aim 2** to determine if there are distinct molecular alterations in the skeletal muscle in response to genetic intervention between tumor-bearing males and females within a study. Our unique research design may elucidate ambiguous roles in biological sex in CC research.

ii. RIGOR AND REPRODUCIBILITY.

Researchers involved in analyzing data will be blinded to experimental conditions although binding to the tumor-bearing state during animal experiments are not feasible due to subcutaneous allograft. Coding and analyzing data for immunoblotting, real-time PCR, mitochondrial function and FSR will be blinded to laboratory members. Since our pre-clinical animal model of CC is limited for translating into that of the human model, we have opted for a relatively robust effect size ($\beta > 0.8$) for power calculation. This robust effect size in highly controlled pre-clinical models is more likely to translate into clinically meaningful results in human models.

E. AIM 1:

DEFINE ALTERATIONS IN THE DEVELOPMENT OF CANCER CACHEXIA IN FEMALE TUMOR-BEARING MICE.

i. EXPERIMENTAL RATIONALE.

With **Aim 1**, I will provide foundational insights into the development of CC and molecular mechanisms involved during the early stages of CC. Prior investigations examining CC progression have extensively focused on cachectic or refractory cachectic (late) states and alterations during pre-cachectic (pre-weight loss) states remain elusive (80, 157), suggesting a critical need in the study of CC. However, recent investigations from our group revealed that disruptions of mitochondrial network (12) and satellite cell and myogenesis-associated genes (81) precedes the development of cachectic phenotype in skeletal muscle in a mouse model of CC and these markers are closely associated with mitochondrial respiratory function and muscle loss that are often seen in cachectic states. Nevertheless, it remains unknown if these degenerating processes are present in females during the development of CC. Prior observations demonstrated that skeletal muscle undergoes marked atrophy and mitochondrial dysfunction in both tumor-bearing male (12, 15) and female (82, 158) animals. However, females are known to be less sensitive to inflammation-induced muscle atrophy compared to their male counterparts (45). Therefore, I **hypothesize** altered muscle contractility, protein turnover, and impaired mitochondrial quality/function in the skeletal muscle will be present during CC in female tumor-bearing mice, but to a lesser extent compared to previous male CC studies (12, 81). However, the pre-cachectic signature of female mice is not yet elucidated. Accordingly, determining and comparing degenerative mechanisms between male and female skeletal muscle during the development of CC will be critical to improve therapeutic strategies for the cancer treatment. Since decreased muscle quality limits overall survival for cancer patients (159), identifying degenerative mechanisms in the female during early stages of CC and specifically targeting these mechanisms

will be a key step to reverse/prevent the cachectic state and improve cancer outcomes. Therefore, we will determine if molecular degenerations occur in females during the development of CC.

ii. *EXPERIMENTAL DESIGN AND APPROACH.*

Animal model and experimental design. Animal experiments and tissue analysis for Aim 1 were already completed, therefore, Aim 1 will be described in the past tense. With Aim 1, I utilized the LLC-induced mouse model of CC in a time-course manner to determine muscle degenerating mechanism during the development of CC. LLC is a well-accepted allograft animal model of CC and it has been widely used in various pre-clinical cancer researches (12, 81, 160) due to enhanced experimental control including precise dosing making them an excellent research model. Our novel time-course experimental design divides mice into 5 groups (1, 2, 3, 4 wks, and PBS control) and 1-4 wks mice were given LLC cells (1×10^6) suspended in PBS were implanted to the hind flank at 8 wks of age. The tumors were allowed to develop for 1, 2, 3, and 4 wks and PBS-injected control mice were age-matched to the 4 wks of LLC-implanted mice and

tissues were harvested at 4 different designated time points as described in **Figure 1** (12). However, after 3 or 4 wks of tumor growth, we observed a clear dichotomy in

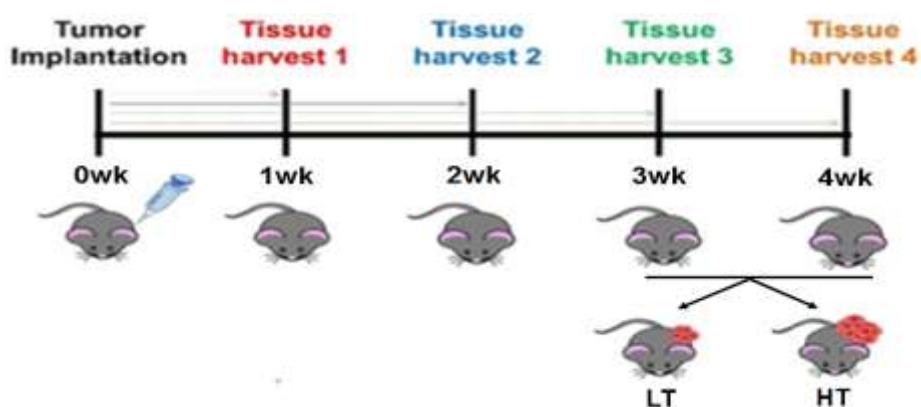


Figure 1. Animal experimental design for Aim 1. ~60 mice (12 mice per each group) will be injected either PBS (control) or LLC (1×10^6) at a designated time points (1, 2, 3, or 4-week). However, due to dichotomy in tumor size between 3 and 4-week animals, I regroup them by Low Tumor (LT; $\leq 1.2g$) and High Tumor (HT; $\geq 2g$) weight. Tissues were harvested at designated time points.

tumor size among 3 and 4 wks animals. Therefore, 3 and 4 wks mice were regrouped by Low

Tumor (LT; $\leq 1.2\text{g}$) and High Tumor (HT; $\geq 2\text{g}$) weight after collecting the tissues, which allowed us to determine and compare molecular changes occurred during CC between pre-cachectic and cachectic states. A total of ~60 mice were utilized for Aim 1.

iii. DEPENDENT VARIABLES.

To determine alterations in the skeletal muscle of female tumor-bearing mice in response to LLC implantation, I set to assess dependent variables, which are as follows: **1) Muscle contractility** (peak isometric torque, $\frac{1}{2}$ muscle relaxation time, time to maximal contraction, and fatigability) of the dorsiflexor muscles of the lower limb was examined via utilizing *in vivo* electrical stimulation as previously described (161, 162). This *in vivo* configuration system will allow me to assess ankle torsion of the animal's hind limb, as opposed to direct force. In addition, this experiment is physiologically relevant and does not require surgical isolation nor neurovascular alteration. The measurement of torque is normalized to estimates of cross-sectional area of the plantaris muscle. Muscle contractility was measured 48 hours prior to the tissue harvest to ensure any muscle damages occurred during the electrical stimulation are fully recovered prior to the tissue harvest. **2) Protein turnover:** Protein synthesis was assessed via 24h protein FSR via Deuterium oxide (D_2O) labeled amino acid (alanine) incorporation using gas chromatography-mass spectrometry (GC-MS) as previously described (81). 24 hours of FSR of incorporated amino acid will allow an assessment to occur over a full light/dark cycle and in the fed state, providing a more direct reflection of protein synthesis in normal conditions. In addition, signaling for both protein synthesis (via IGF/mTOR and its downstream pathways) and two major protein degradation pathways via ubiquitin-proteasome system (UPS) and autophagic-lysosomal pathway (ALP) were measured as previously reported by us using immunoblot and real-time PCR(81). **3) Mitochondrial quality** was assessed as we previously reported (12). Measures were

mitochondrial RCR and ROS emission in permeabilized muscle fibers (12), mitochondrial network using the fluorescent reporter gene; MitoTimer (12, 163), and mitochondrial quality control (MQC) markers (mitochondrial biogenesis, dynamics, and mitophagy) via immunoblot and real-time qPCR (12, 163). Mitochondrial RCR, ROS emission, and MitoTimer measurements were performed at the time of tissue harvest and data analysis was already completed.

iv. EXPECTED/OBSERVED OUTCOMES.

Based on what we (12, 81) and others (69, 80) observed from previous male CC studies, we originally expected impaired muscle contractile function, mitochondrial quality, and abnormal protein turnover in the skeletal muscle in tumor-bearing female mice compared to PBS-injected control mice. We also expected a protective effect in tissue wasting and CC signatures in female tumor-bearing mice in that females are less sensitive to inflammation-induced muscle atrophy than males. Overall, female tumor-bearing mice developed cancer-induced muscle degenerations including tissue weight loss, muscle contractility, abnormal protein turnover, and compromised mitochondrial quality, but to a lesser extent compared to previous male tumor-bearing mice reported previously (12, 81). More specifically, female tumor-bearing mice appear to have a protective mechanism to prevent cancer-induced cachectic phenotypes including tumor development, mitochondrial degeneration, and muscle wasting compared to previous male studies.

v. POTENTIAL PITFALLS AND CONTINGENCY PLAN.

Proposed animal experiments for Aim 1 were already completed, therefore we do not anticipate any problems with study completion. However, the animal model I am utilizing in this

project is Lewis Lung Carcinoma-induced, which may not necessarily represent other cancer types. This potential problem is likely to be solved via part of studies from our recently funded NIH research grant/project (R01 AR075794-01A1/AR/NIAMS), which will test overall skeletal muscle health assessments including skeletal muscle contractility, mitochondrial quality, and protein turnover in different animal models of CC including C26 (colon cancer), and Azoxymethane (colon cancer)-induced mouse models in both sexes, which will provide a more generalized view of CC mechanisms in preclinical animal models.

vi. *STATISTICS AND SAMPLE SIZE DETERMINATION.*

Data from each experiment will be assessed in two biological sexes independently. We utilized a One-way analysis of variance (ANOVA) with independent factors of five different animal groups. Where significant F-ratios were found, statistical differences among means were determined by Tukey's post hoc test. With an anticipated Cohen's f effect size of 0.35, $\alpha=0.05$, and $\beta=0.80$ and I required 10-12 animals per condition.

F. AIM 2.

DETERMINE IF MITOCHONDRIA-TARGETED INTERVENTION PREVENTS CC.*i. EXPERIMENTAL RATIONALE.*

Our laboratory has shown that mitochondrial inner membrane fusion protein (OPA1) is downregulated during the early development of cancer and remains suppressed until cachectic phenotypes occur in male tumor-bearing mice (**Figure 2.**) (12). Therefore, I will apply a novel therapeutic strategy (a timing-dependent OPA1 gene manipulation) to attenuate LLC-induced muscle atrophy via the mitochondria-targeted genetic methodology. Although whether the downregulation of OPA1 observed in male tumor-bearing mice would

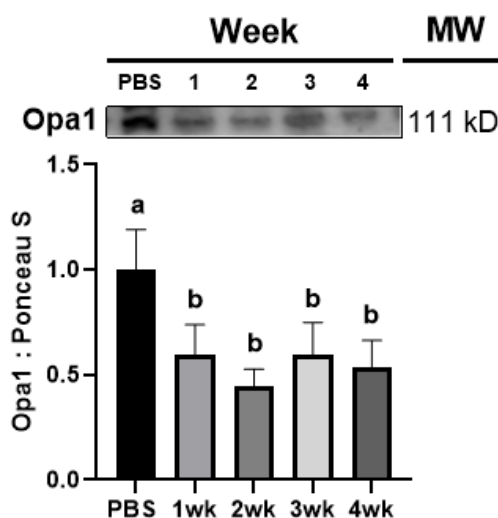


Figure 2. Changes in Opa1 protein content during development of LLC-induced CC³. ~50% down-regulation in mitochondrial fusion factor Opa1 at 1-wk following tumor implantation. Data adapted from Brown et al, JCSM, 2017.

appear in females was unknown, prior evidence from our laboratory demonstrated lower *OPA1* mRNA level in both male and female mice of disuse-induced muscle atrophy. This experiment will allow a guided approach to preventative treatment in cancer-induced muscle wasting while providing crucial mechanistic insight into the development of CC. Optic atrophy 1 (OPA1) is the mitochondrial inner membrane remodeling protein and acts as a fusion factor via combining two mitochondrial pieces (fusion). OPA1 has a dual role in maintaining morphology and energetics via mediating inner membrane fusion and regulating cristae structure (164). OPA1 also plays a crucial role in mitochondrial oxidative phosphorylation and calcium homeostasis (165). In addition, prior evidence demonstrated conditional OPA1 deletion resulted in lower muscle mass as well as elevation of catabolic signaling and suppression of protein synthesis (166). Meanwhile, overexpression of OPA1 improved motor function, respiratory chain activity, and increased

lifespan in a pre-clinical mouse model of mitochondrial disease (167). Despite the therapeutic potential of rescuing OPA1 on muscle mass, the efficacy of OPA1 has not been assessed in certain forms of muscle atrophy including cancer-induced muscle atrophy. Previously, we observed impaired mitochondrial quality control markers including OPA1 (**Figure 2**) during the early development of CC **prior to a marked muscle loss (12)**. Here I suggest rescuing OPA1 may be critical to have protective

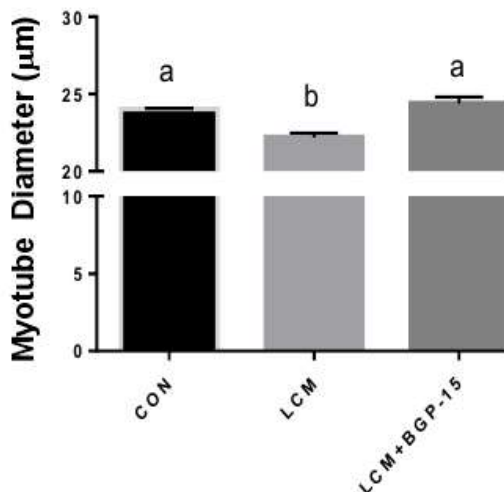


Figure 3. Opa1 target (BGP-15) prevents CC *in vitro*. BGP-15 –known to induce Opa1. BGP-15 prevent an ~10% loss in myotube diameter by LLC conditioned media (LCM) in C2C12 myotubes.

effects on mitochondrial degeneration and protein catabolism in CC. Smuder et al revealed that **HSP72** overexpression via **BGP-15** (a nicotinic amidoxime derivative, which **induces OPA1 and HSP72 expression**) administration had protective effects against mechanical ventilation-induced oxidative stress and transcriptional activities of protein degradation (168). Accordingly, we assessed the efficacy of OPA1 via using **BGP-15** in LLC-conditioned media (LCM)-mediated myotube atrophy *in vitro* and we found myotube atrophy induced via LCM was rescued with BGP-15 overexpression (**Figure 3**). These preliminary data led us to pursue *in vivo* animal studies using a mouse model of OPA1 (AAV-mediated gene transfer) to determine the role of OPA1 in tumor-mediated muscle atrophy *in vivo*. By using this experimental design, I **hypothesize** that reduced muscle tissue weights via tumor implantation will be attenuated in mice treated with AAV-mediated gene transfer. Moreover, prior evidence demonstrated that OPA1 plays an imperative role in both mitochondrial oxidative phosphorylation and protein turnover (165, 166). Therefore, our experimental intervention utilizing genetic overexpression of OPA1 in mice is likely to rescue mitochondrial and muscular degenerations induced via tumor growth.

***Note – our contingency plan for AAV was to utilize OPA1 transgenic mice to the same purpose. As we did not have AAV prepared for this experiment in Aim 2 I present data collected to date utilizing the OPA1 transgenic mice.**

ii. *EXPERIMENTAL DESIGN AND APPROACH.*

First, a **mouse model of cancer cachexia** will be applied using LLC implantation in C57BL6/J male and female mice and allow to grow the tumor for 4 wks to become a cachectic state. I will use AAV-mediated gene transfer to the tibialis anterior (TA) of tumor-bearing mice at a designated time point (from 1 wk after the tumor-implantation). AAV will allow high efficiency (90%) and stability of gene transfer, which has been successfully used for long-term gene expression *in vivo* in various tissues including skeletal muscle (156, 169). AAV plasmid will be driven by the U6 polIII promoter and express a green fluorescent protein (GFP) to allow identification of transfection positive fibers and efficiency. AAV/OPA1 (overexpression vector) will be transferred via intramuscular injection into both TA muscles while control mice will be given

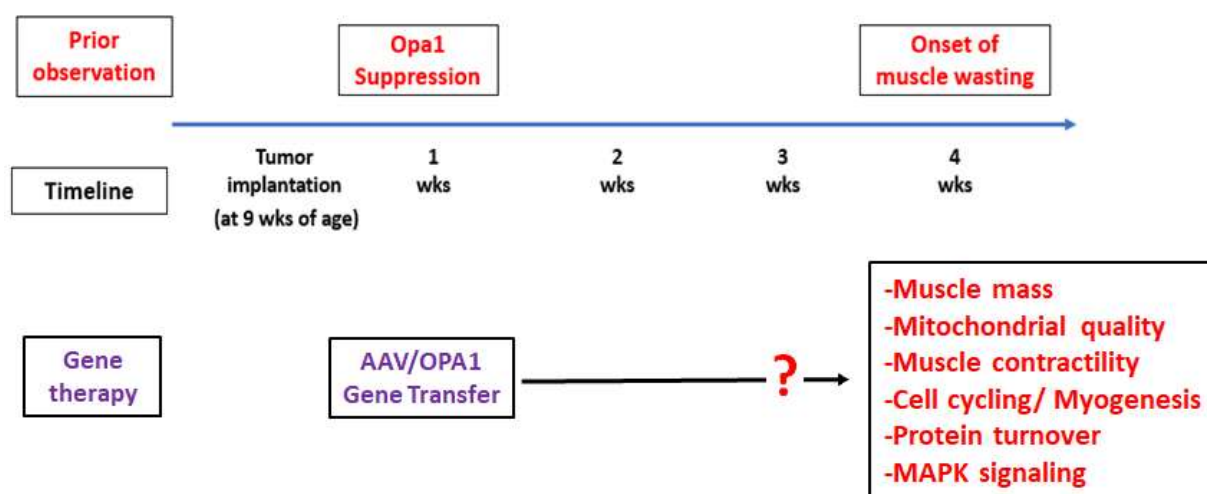


Figure 4. Experimental design for Aim 2. Uppermost portion demonstrate time of onset for changes to targets in LLC tumor bearing mice based on our previous work³. The Opa1 genetic approach will be employed with timing of onset based on timing of concurrent alteration to endogenous target during development of CC³.

the appropriate control vector AAV. Further efficiency of AAV plasmid transfer will be provided

with immunohistochemistry and RT-qPCR data. This will provide an excellent method of temporal OPA1 gene transfer, allowing me to investigate skeletal muscle health including muscle contractility, protein turnover, and mitochondrial quality in response to LLC-induced muscle atrophy (**Figure 4**). The total number of animals for Aim 2 will be ~88 mice. Specifically, there will be 4 animal groups (12 animals per group) within each sex for each approach (PBS-Control/AAV vs PBS-OPA1/AAV vs LLC-Control/AAV vs LLC-OPA1/AAV). By utilizing these gene manipulation method, I will not only provide fundamental information regarding the efficacy of OPA1 genetic intervention in cancer-induced muscle atrophy but also proof of concept for the efficacy of timed interventions to stage of tumor development.

iii. DEPENDENT VARIABLES.

Dependent variables will be the same for both Approach 1 and 2. To determine overall muscular health in response to genetic intervention (AAV OPA1 gene transfer and OPA1 TG), I set to assess dependent variables including **1) Muscle contractility**, **2) Protein turnover**, and **3) Mitochondrial quality** will be assessed as in Aim 1.

iv. EXPECTED OUTCOMES.

1) 4 wks of LLC implantation will induce significant tissue wasting including skeletal muscle and fat as we have seen previously (12, 81) **2)** 4-wk of LLC implantation will also induce muscle degenerating effects including impaired muscle contractility, abnormal protein turnover, and degenerated mitochondrial health. **3)** Genetic overexpression of OPA1 will attenuate LLC-induced muscle degenerations including muscle atrophy, abnormal protein turnover, impaired muscle contractility, and mitochondrial health. **4)** Based on previous evidence (12, 45, 61, 81,

170), I also expect to observe sex differences in **1), 2)** and **3)**. Specifically, I expect relatively less severe tissue wasting, muscle fatigability, and mitochondrial oxidative capacity in female mice than previous male studies (12, 81).

v. *POTENTIAL PITFALLS AND CONTINGENCY PLAN.*

Approach 1 in Aim 2 is required specific techniques including AAV subcloning, production, and utilization. These procedures will be led by Dr. Christopher Nelson who is experienced in the required skills; therefore, I do not anticipate any technical problems. However, in case of difficulties in AAV mediated gene expression, I will concomitantly perform experiments with OPA1 TG mice. These mice were developed and validated by the laboratory of Dr. Luca Scorrano (167). Skeletal muscle specific OPA1 TG mice will be given LLC-implantation and the tumors will develop for 4 wks and the same assessments for Aim 2 will be applied to determine if OPA1 TG mice exhibit any protection effects against cancer-induced muscle degenerations.

***Due to unavailability of OPA1 AAV plasmid, OPA1 TG animals were used to test my central hypothesis for Aim 2. In addition to OPA1 TG animals, BGP-15 (pharmacological target of OPA1) was utilized in both *in vitro* and *in vivo* to further test the efficacy of OPA1.**

vi. *STATISTICS AND SAMPLE SIZE DETERMINATION.*

Data from each experiment will be assessed in both biological sexes. Data will be assessed by two-way analysis of variance (ANOVA) with independent factors of sex (males/females) by tumor-bearing (tumor vs control) by plasmid (AAV/OPA1 vs AAV/empty vector control). When significant F ratios are found, pairwise comparisons will be Tukey Post-hoc

adjusted. With an anticipated Cohen's f interaction effect size of 0.35, $\alpha=0.05$, and $\beta=0.80$ we anticipate requiring 12 animals/condition.

G. PROPOSED TIMELINE OF ENTIRE PROJECT.

All proposed experiments are planned based on logical relationships and expected time to complete the entire project within 12 months as described in the timeline table. Aims are designed independently of each other, and the proposed arrangement will allow me to facilitate this project in a timely progress manner. There are no anticipated budget problems to complete both aims as well (**Table 2**).

Proposed Timeline for work (month)	1, 2	3, 4	5, 6	7, 8
AIM 1				
Mitochondrial measurements	Complete			
Protein balance measurements	Complete			
Data analysis	Complete			
Dissemination of findings	Complete			
AIM 2				
Animal experiments				
Tissue prep & assays				
Data analysis				
Dissemination of findings				

Table 2. Proposed timeline for the dissertation project.

H. REFERENCES

1. **Fearon KCH, Glass DJ, and Guttridge DC.** Cancer cachexia: mediators, signaling, and metabolic pathways. *Cell metabolism* 16: 153-166, 2012.
2. **Fearon K, Strasser F, Anker SD, Bosaeus I, Bruera E, Fainsinger RL, Jatoi A, Loprinzi C, MacDonald N, and Mantovani G.** Definition and classification of cancer cachexia: an international consensus. *The lancet oncology* 12: 489-495, 2011.
3. **Brown JL, Rosa-Caldwell ME, Lee DE, Blackwell TA, Brown LA, Perry RA, Haynie WS, Hardee JP, Carson JA, and Wiggs MP.** Mitochondrial degeneration precedes the development of muscle atrophy in progression of cancer cachexia in tumour-bearing mice. *Journal of cachexia, sarcopenia and muscle* 8: 926-938, 2017.
4. **Brown JL, Lee DE, Rosa-Caldwell ME, Brown LA, Perry RA, Haynie WS, Huseman K, Sataranatarajan K, Van Remmen H, Washington TA, Wiggs MP, and Greene NP.** Protein imbalance in the development of skeletal muscle wasting in tumour-bearing mice. *J Cachexia Sarcopenia Muscle* 9: 987-1002, 2018.
5. **Rosa-Caldwell ME, Fix DK, Washington TA, and Greene NP.** Muscle alterations in the development and progression of cancer-induced muscle atrophy: a review. *Journal of Applied Physiology* 128: 25-41, 2020.
6. **Rosa-Caldwell ME, and Greene NP.** Muscle metabolism and atrophy: let's talk about sex. *Biology of sex differences* 10: 1-14, 2019.
7. **Anderson LJ, Liu H, and Garcia JM.** Sex differences in muscle wasting. In: *Sex and Gender Factors Affecting Metabolic Homeostasis, Diabetes and Obesity* Springer, 2017, p. 153-197.
8. **Canon ME, and Crimmins EM.** Sex differences in the association between muscle quality, inflammatory markers, and cognitive decline. *The journal of nutrition, health & aging* 15: 695-698, 2011.
9. **Colom B, Oliver J, and Garcia-Palmer FJ.** Sexual dimorphism in the alterations of cardiac muscle mitochondrial bioenergetics associated to the ageing process. *Journals of Gerontology Series A: Biomedical Sciences and Medical Sciences* 70: 1360-1369, 2015.
10. **Nelson CE, Hakim CH, Ousterout DG, Thakore PI, Moreb EA, Rivera RMC, Madhavan S, Pan X, Ran FA, and Yan WX.** In vivo genome editing improves muscle function in a mouse model of Duchenne muscular dystrophy. *Science* 351: 403-407, 2016.

11. **Onesti JK, and Guttridge DC.** Inflammation based regulation of cancer cachexia. *BioMed research international* 2014: 2014.
12. **Rosa-Caldwell ME, Lim S, Haynie WA, Brown JL, Deaver JW, Morena Da Silva F, Jansen LT, Lee DE, Wiggs MP, and Washington TA.** Female mice may have exacerbated catabolic signalling response compared to male mice during development and progression of disuse atrophy. *Journal of Cachexia, Sarcopenia and Muscle* 2021.
13. **Baltgalvis KA, Berger FG, Peña MMO, Davis JM, White JP, and Carson JA.** Muscle wasting and interleukin-6-induced atrogen-1 expression in the cachectic Apc Min/+ mouse. *Pflügers Archiv-European Journal of Physiology* 457: 989-1001, 2009.
14. **White JP, Baltgalvis KA, Puppa MJ, Sato S, Baynes JW, and Carson JA.** Muscle oxidative capacity during IL-6-dependent cancer cachexia. *American Journal of Physiology-Regulatory, Integrative and Comparative Physiology* 300: R201-R211, 2011.
15. **White JP, Baynes JW, Welle SL, Kostek MC, Matesic LE, Sato S, and Carson JA.** The regulation of skeletal muscle protein turnover during the progression of cancer cachexia in the Apc Min/+ mouse. *PLoS one* 6: e24650, 2011.
16. **Bonetto A, Aydogdu T, Kunzevitzky N, Guttridge DC, Khuri S, Koniaris LG, and Zimmers TA.** STAT3 activation in skeletal muscle links muscle wasting and the acute phase response in cancer cachexia. *PLoS one* 6: e22538, 2011.
17. **Hetzler KL, Hardee JP, LaVoie HA, Murphy EA, and Carson JA.** Ovarian function's role during cancer cachexia progression in the female mouse. *American Journal of Physiology-Endocrinology and Metabolism* 312: E447-E459, 2017.
18. **Brown JL, Lawrence MM, Ahn B, Kneis P, Piekarcz KM, Qaisar R, Ranjit R, Bian J, Pharaoh G, Brown C, Peelor 3rd FF, Kinter MT, Miller BF, Richardson A, and Van Remmen H.** Cancer cachexia in a mouse model of oxidative stress. *Journal of Cachexia, Sarcopenia and Muscle* n/a: 2020.
19. **Hamo CE, and Bloom MW.** Cancer and heart failure: understanding the intersection. *Cardiac Failure Review* 3: 66, 2017.
20. **O'Reilly MS, Holmgren L, Shing Y, Chen C, Rosenthal RA, Moses M, Lane WS, Cao Y, Sage EH, and Folkman J.** Angiostatin: a novel angiogenesis inhibitor that mediates the suppression of metastases by a Lewis lung carcinoma. *cell* 79: 315-328, 1994.
21. **Call JA, McKeehen JN, Novotny SA, and Lowe DA.** Progressive resistance voluntary wheel running in the mdx mouse. *Muscle & nerve* 42: 871-880, 2010.

22. **Nichenko AS, Sorensen JR, Southern WM, Qualls AE, Schifino AG, McFaline-Figueroa J, Blum JE, Tehrani KF, Yin H, and Mortensen LJ.** Lifelong Ulk1-mediated autophagy deficiency in muscle induces mitochondrial dysfunction and contractile weakness. *International journal of molecular sciences* 22: 1937, 2021.

23. **Laker RC, Xu P, Ryall KA, Sujkowski A, Kenwood BM, Chain KH, Zhang M, Royal MA, Hoehn KL, Driscoll M, Adler PN, Wessells RJ, Saucerman JJ, and Yan Z.** A novel MitoTimer reporter gene for mitochondrial content, structure, stress, and damage in vivo. *J Biol Chem* 289: 12005-12015, 2014.

24. **VanderVeen BN, Hardee JP, Fix DK, and Carson JA.** Skeletal muscle function during the progression of cancer cachexia in the male ApcMin/+ mouse. *Journal of Applied Physiology* 124: 684-695, 2018.

25. **Lee H, and Yoon Y.** Mitochondrial membrane dynamics—functional positioning of OPA1. *Antioxidants* 7: 186, 2018.

26. **Fülöp L, Rajki A, Maka E, Molnár MJ, and Spät A.** Mitochondrial Ca²⁺ uptake correlates with the severity of the symptoms in autosomal dominant optic atrophy. *Cell Calcium* 57: 49-55, 2015.

27. **Tezze C, Romanello V, Desbats MA, Fadini GP, Albiero M, Favaro G, Ciciliot S, Soriano ME, Morbidoni V, and Cerqua C.** Age-associated loss of OPA1 in muscle impacts muscle mass, metabolic homeostasis, systemic inflammation, and epithelial senescence. *Cell metabolism* 25: 1374-1389, 2017.

28. **Civiletto G, Varanita T, Cerutti R, Gorletta T, Barbaro S, Marchet S, Lamperti C, Viscomi C, Scorrano L, and Zeviani M.** Opa1 overexpression ameliorates the phenotype of two mitochondrial disease mouse models. *Cell metabolism* 21: 845-854, 2015.

29. **Smuder AJ, Morton AB, Hall SE, Wiggs MP, Ahn B, Wawrzyniak NR, Sollanek KJ, Min K, Kwon OS, and Nelson WB.** Effects of exercise preconditioning and HSP72 on diaphragm muscle function during mechanical ventilation. *Journal of cachexia, sarcopenia and muscle* 10: 767-781, 2019.

30. **Wang B, Li J, and Xiao X.** Adeno-associated virus vector carrying human minidystrophin genes effectively ameliorates muscular dystrophy in mdx mouse model. *Proceedings of the National Academy of Sciences* 97: 13714-13719, 2000.

31. **Montalvo RN, Counts BR, and Carson JA.** Understanding sex differences in the regulation of cancer-induced muscle wasting. *Current opinion in supportive and palliative care* 12: 394, 2018.

32. **Zhong X, and Zimmers TA.** Sex Differences in Cancer Cachexia. *Current Osteoporosis Reports* 1-9, 2020.

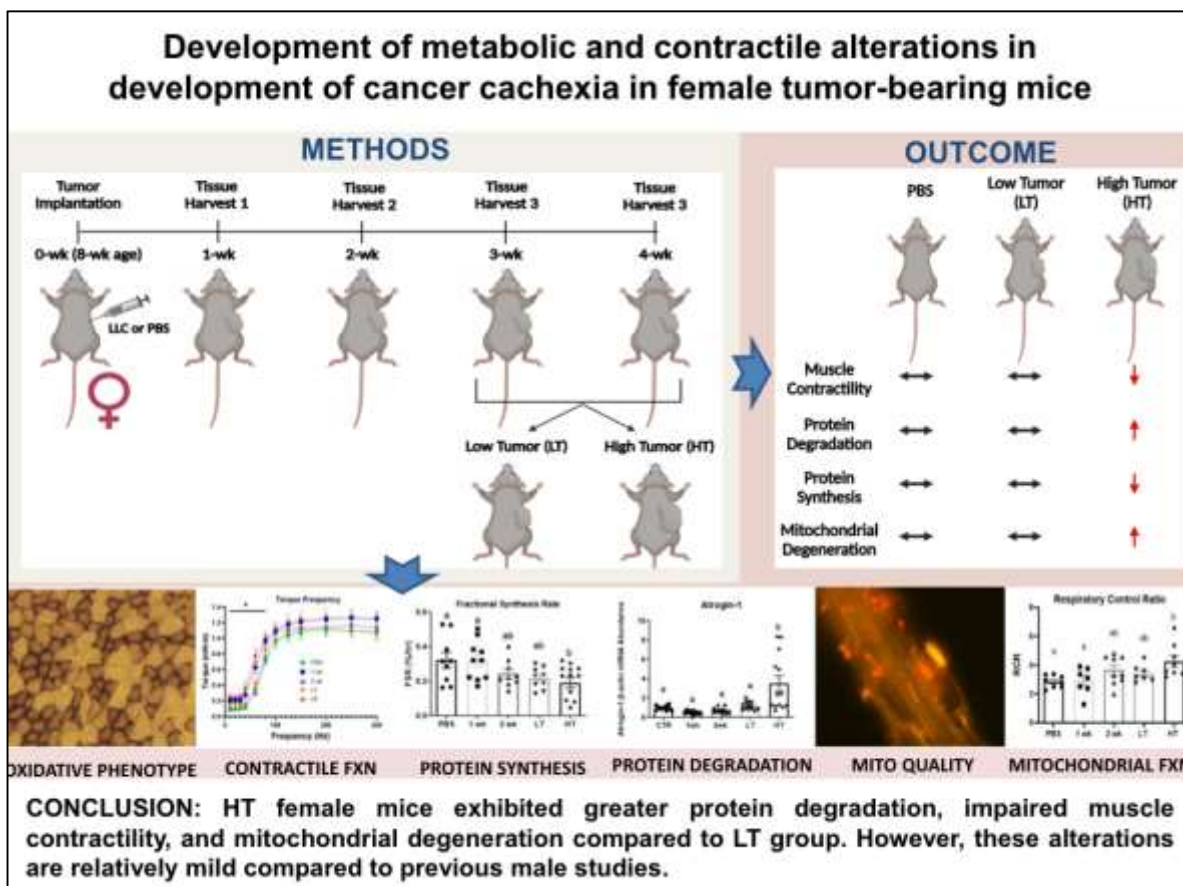
CHAPTER III: Manuscript from Specific Aim I

Development of metabolic and contractile alterations in development of cancer cachexia in female tumor-bearing mice.

Seongkyun Lim & Nicholas P. Greene

Published in Journal of Applied Physiology on 05 JAN 2022

A. Graphical Abstract



B. ABSTRACT

Cancer cachexia (CC) results in impaired muscle function and quality of life and is the primary cause of death for ~20-30% of cancer patients. We demonstrated mitochondrial degeneration as a precursor to CC in male mice, however, if such alterations occur in females is currently unknown. The purpose of this study was to elucidate muscle alterations in CC development in female tumor-bearing mice. 60 female C57BL/6J mice were injected with PBS or Lewis Lung Carcinoma at 8 wks age, and tumors developed for 1, 2, 3, or 4 wks to assess the time course of cachectic development. *In vivo* muscle contractile function, protein fractional synthetic rate (FSR), protein turnover, and mitochondrial health were assessed. 3- and 4-wk tumor-bearing mice displayed a dichotomy in tumor growth and were reassigned to High Tumor (HT) and Low Tumor (LT) groups. HT mice exhibited lower soleus, TA, and fat weights compared to PBS. HT mice showed lower peak isometric torque and slower one-half relaxation time compared to PBS. HT mice had lower FSR compared to PBS while E3 ubiquitin ligases were greater in HT compared to other groups. *Bnip3* (mitophagy) and pMitoTimer red puncta (mitochondrial degeneration) were greater in HT while *Pgc1α1* and *TFAM* (mitochondrial biogenesis) were lower in HT compared to PBS. We demonstrate alterations in female tumor-bearing mice where HT exhibited greater protein degradation, impaired muscle contractility, and mitochondrial degeneration compared to other groups. Our data provide novel evidence for a distinct cachectic development in tumor-bearing female mice compared to previous male studies.

KEYWORDS: Mitochondrial function, muscle atrophy, mitochondrial quality control, Lewis Lung Carcinoma, and skeletal muscle contractility.

NEW & NOTEWORTHY Our study demonstrates divergent tumor development and tissue wasting within 3- and 4-wk mice, where approximately half the mice developed large tumors and subsequent cachexia. Unlike previous male studies, where metabolic perturbations precede the onset of cachexia, females appear to exhibit protections from the metabolic perturbations and cachexia development. Our data provide novel evidence for divergent cachectic development in tumor-bearing female mice compared to previous male CC studies, suggesting different mechanisms of CC between sexes.

C. INTRODUCTION

Cancer is the second leading cause of death worldwide and about 600,000 people die from cancer each year in the United States (171). 50-80% of cancer patients experience the wasting syndrome known as cancer cachexia (CC) which is inversely associated with health-related quality of life (3, 172). CC is a multifactorial wasting syndrome characterized by significant skeletal muscle mass loss with or without loss of fat mass that may not be reversed by nutritional intervention alone and is responsible for 20-30% of cancer-related deaths (3). Moreover, cachexia is often clinically defined by greater than 5% unintentional weight loss over the past 6 months, which often is associated with progressive dysfunctions or degenerations in multiple tissues and organs (3). Unfortunately, there are limited treatments that mitigate the effects of CC. Therefore, appropriate early diagnosis and treatment of cancer-induced cachexia continues to be the most effective strategy to alleviate this condition. Furthermore, understanding the pre-cachectic processes and the development of preventive approaches become crucial. However, while we have provided recent evidence for such pre-cachectic processes in male tumor-bearing mice (12, 81, 173), to date there is limited understanding of pre-cachectic processes in females.

Previous evidence has suggested impaired skeletal muscle oxidative capacity may reduce muscle mass in the cachectic state (15), although the initial mechanisms remain elusive. Accordingly, we have focused on aspects of mitochondrial health including mitochondrial respiratory control ratio (RCR) and reactive oxygen species (ROS) emission during the development of CC in male mice revealing that mitochondrial degeneration precedes the cachectic phenotypes in skeletal muscle of tumor-bearing male mice (12). Prior evidence denoted that elevated oxidative stress has been linked to altered protein turnover and skeletal muscle integrity (174). Oxidative stress to proteins yields increases in the hydrophobicity of both intracellular and cytoplasmic proteins, which are often toxic and can threaten cell viability, inducing protein aggregation, thereby undergoing selective proteolysis (175). Specifically, we

found smaller cross-sectional area (CSA) of muscle fibers and lower protein fractional synthesis rates (FSR), as well as altered cellular signaling associated with protein turnover in LLC (Lewis Lung Carcinoma)-induced cachectic male mice (81), in line with the previous works (15, 176).

There is a growing body of evidence suggesting distinct biological sex differences in different models of animal muscle atrophy (10), with phenotypical disparities between males and females having been found in different forms of human cancers including lung cancer (177). In fact, males appear more susceptible to inflammation-mediated muscle atrophies with greater ubiquitin-proteasome system (UPS) (12, 45) while females seem more susceptible to disuse-induced muscle atrophies with lower UPS compared to males (45, 62). Moreover, recent evidence from our laboratory suggests sex-based differences in the development of muscle disuse atrophy (10). Notably in cancer cachexia male $Apc^{Min/+}$ mice demonstrate a high IL-6 dependency for cachexia development while female mice exhibit an IL-6 independence (9, 15, 64). While the initial development of cancer cachexia in male mice is a relatively understudied topic, investigations of the same pathology in female mice are very few despite suggestions of differing atrophic mechanisms between biological sexes. Therefore, the purpose of this study was to assess the pre-cachectic signature of skeletal muscle in the development of CC in female tumor-bearing mice. Specifically, herein, we have focused assessment on aspects of muscle contractile function, protein turnover, and mitochondrial health.

Footnote: All figures can be found at the end of chapter III.

D. METHODS

i. Animal Interventions

All animal methods were approved by the Institutional Animal Care and Use Committee of the University of Arkansas. 60 female C57BL/6J mice (n=10-14/cohort) were purchased from Jackson Laboratories (000664, Bar Harbor, ME, USA) and kept on a 12:12-h light-dark cycle, housed at 72 degrees Fahrenheit, and given *ad libitum* access to normal rodent chow and water for the duration of the study. At 8 wks of age, mice were subcutaneously given an injection of either Lewis Lung Carcinoma (LLC) cells (1×10^6) suspended in 100 μ L sterile phosphate-buffered saline (PBS) or an equal volume of sterile PBS as a control to the left hind flank. Per our prior works (12, 173), tumors were allowed to develop for 1, 2, 3, or 4 wks. PBS control mice were age-matched with 4 wks tumor-bearing mice at time of tissue collection. After 3 or 4 wks of tumor growth, we noted a clear dichotomy in tumor size, with some females having greater tumor development than others within 3 and 4 wks animals. Therefore, 3 and 4 wks mice were combined and regrouped by Low Tumor (LT; ≤ 1.2 g) and High Tumor (HT; ≥ 2 g) bearing groups (**Supplemental Figure 1A-B**). Tissue collection was performed at 12 wks of age for 4 wks as well as PBS mice and the rest of the mice were euthanized at the designated time points and tissue wet weight was measured. Plasma was separated from the blood by centrifugation to determine female sex hormones. Tissue and plasma samples were then snap-frozen in liquid nitrogen and stored at -80 °C for further analysis. All tissue weights were normalized to their tibia length to account for different body sizes (81). Final groups for analysis included PBS, 1wk, 2wk, LT, and HT.

ii. Lewis Lung Carcinoma Cell Culture

LLC cells (CRL-1642, ATCC, Manassas, VA, USA) were plated in 250 mL culture flasks in DMEM (11965092, Life Technologies, Carlsbad, CA, USA) containing 10% fetal bovine serum (26140079, Life Technologies) supplemented with 1% penicillin/streptomycin (15140122, Life Technologies) and media was changed every 48 hours. Upon ~80% confluence, cells were trypsinized, suspended via centrifugation, and diluted in PBS prior to tumor implantation as previously described (12).

iii. Plasmid DNA Amplification and Electroporation

DH5- α Escherichia coli containing pMitoTimer plasmid were amplified and plasmid DNA isolated using PureLink HiPure Plasmid Filter Maxiprep kit (K211017, Life Technologies). At 6 wks of age, pMitoTimer plasmid transfection into the right flexor digitorum brevis (FDB) muscle was performed as described previously (12, 163). Briefly, while mice were anesthetized (isoflurane), 10 μ L of 0.36 mg/mL of hyaluronidase in saline was injected using an insulin syringe with a 30-gauge needle subcutaneously under footpad. The needle penetrates the skin at a point close to the heel of the foot and advances the needle subcutaneously towards the base of the toe for $\frac{1}{4}$ which is above the FDB muscle. After 60-min, mice were anesthetized again and a total of 20 μ g of the plasmid DNA for MitoTimer was injected subcutaneously in the footpad with the same procedure described for the hyaluronidase injection. Anesthesia was disconnected after the plasmid DNA injection for 10-min and reconnected for electroporation. Two gold-plated acupuncture needles were connected to an electrical stimulator placed under the skin near the heel and a second one near the base of the toes. Electrodes were perpendicular to the long axis of the foot and parallel to each other. 10 electrical pulses with 20 ms in duration/each, at 1 Hz and 75 V were applied using an S88 electrical stimulator (Grass Telefactor, West Warwick, RI, USA).

iv. In vivo Muscle Contractility Test

Approximately 48 hours prior to tissue harvest, *in vivo* peak isometric torque, isometric torque frequencies, frequency at half maximum torque, 1/2 relaxation time, time to maximal contraction, and fatigability (susceptibility to fatigue) of the anterior crural (shin) muscles were performed as described (161). Briefly, while mice were anesthetized, the left hindlimb was shaved and an ethanol pad applied to clean the skin. The foot was placed in a footplate attached to a servomotor (Model 300B-LR, Aurora Scientific, Aurora, Ontario, Canada) using surgical tape while their body temperature was maintained at 37 °C using a heating pad. Two platinum electrodes (Model E2-12, Grass Technologies) were then inserted percutaneously on either side of the peroneal nerve. Consistent instant stimulation was monitored to ensure the electrodes were neither too deep nor too proximal as to yield recruitment of the posterior crural muscles. Muscle contractions were induced via electrical stimulator and stimulus isolation unit (Model S48 and SIU5, respectively; Grass Technologies). After resting the hindlimb for 1-min, torque and M-wave as a function of stimulation frequency were measured during 12 isometric contractions with the duration of 150 ms at various stimulation frequencies (10, 20, 30, 40, 60, 80, 100, 125, 150, 200, 250, and 300 Hz) to determine hindlimb motor unit recruitment based on two different physiological conditions: [1] hindlimb motor unit recruitments during normal movement, which occurs between 60 and 100 Hz (178). [2] During supra-maximal stimulation frequencies (i.e., >200 Hz) can reveal different contractile phenotypes such as low-frequency fatigue (179) followed by resting the hindlimb for 4-min. After measurement of submaximal and maximal isometric torques at 150 Hz, the anterior crural muscles underwent a fatigability test via applying 120 isometric contractions with duration of 150 ms per each stimulation at 40 Hz for a total protocol time of 2-min. During the recovery following the fatigability test, the normal movement of experimental mice was closely monitored to determine any injuries during the *in vivo* muscle force production and fatigability test.

v. Deuterium (D₂O) Injection & 24 hours Muscle Fractional Synthesis Rate (FSR)

FSR was quantified using gas chromatography-mass spectrometry (GC-MS) (7890A and 5977A, Agilent, Santa Clara, CA, USA) as described (10, 81). Briefly, mice were given an intraperitoneal (IP) injection of 99.9% D₂O (151882-1L, Millipore Sigma, Burlington, MA, USA) at 20 µL/g body weight 24 hours prior to tissue harvest. Drinking water was thereafter supplemented with 4% D₂O to maintain the plasma pool of D₂O until tissue harvest (180). Mice were not fasted at tissue collection. 15 mg of gastrocnemius and TA muscles were powdered and homogenized in a 10% TCA solution for FSR. Mixed protein fractions were then washed three times with 10% TCA solution by centrifugation to eliminate cytosolic amino acids. Proteins were then placed in a tube with 200 µL of 6 M HCL and heated at 100 °C to hydrolyze proteins into amino acids for 24 hours. An aliquot of the hydrolysate was dried down and derivatized with a 3:2:1 v/v solution of methyl-8, methanol, and acetonitrile to determine 2H labeling of alanine on its methyl-8 derivative. The solution was then placed in a GC-MS capillary column (7890A GC HP-5 ms capillary column, Agilent) and positioned in the GC-MS; 1 µL of the solution was run on the GC-MS at a 20:1 split. GC-MS settings have previously been described (79). A ratio of deuterated alanine over alanine was employed to assess protein synthesis. The precursor pool of 2 H₂O in the plasma was reacted with 10 M NaOH and a 5% solution of acetone in acetonitrile for 24 hours to conjugate the free 2 H₂O to acetone. The solution was extracted by adding Na₂SO₄ and chloroform and placed in capillary columns to be analyzed on the GC-MS to detect acetone at a 20:1 split. FSR of mixed proteins were calculated using the equation $EA \times [EBW \times 3.7 \times t (h)] - 1 \times 100$, where EA represents the amount of protein-bound [2H] alanine (mole% excess), EBW is the quantity of 2H₂O in body water (mole % excess), 3.7 represents the exchange of 2H between body water and alanine (3.7 of 4 carbon-bound hydrogens of alanine exchange with water) and t (h) represents the time the label was present in hours.

vi. Fluorescence Microscopy for pMitoTimer

pMitoTimer was analyzed as previously described (12). Briefly, at the time of tissue harvesting, freshly collected FDB muscles were fixed with 4% paraformaldehyde (PFA) for 20-min followed by 5-min incubation with PBS at room temperature. Muscles were then spread out on a gelatin-coated glass slide using 2 forceps and mounted with a drop of 50% glycerol in PBS as mounting media. A coverslip was added on the top of the mounted sample and 4 drops of nail polish were applied at the corners to anchor the coverslip. pMitoTimer images were acquired at x100 magnification using the FITC (green; excitation/emission, 488/518 nm) and TRITC (red; excitation/emission, 543/572 nm) fluorescent channels on a Nikon Eclipse Ti-S inverted epifluorescent microscope (Nikon, Melville, NY, USA) with LED-based light source. Standardized acquisition parameters were established and followed for all imaging to match across samples. All assessments were performed in congruence with Laker et al (163). A specially generated MATLAB program, a generous gift from Dr. Zhen Yan (U. Virginia), was used to analyze pMitoTimer red to green ratio (a mitochondrial oxidative stress marker) and pure red puncta number (a marker for completely degenerated mitochondria) (163).

vii. Cryosection & Succinate Dehydrogenase (SDH) Histological Staining

Cryosections and all histological staining methods were performed as described (12). Plantaris muscle was embedded with optimal cutting temperature (OCT) and frozen in liquid nitrogen-cooled isopentane. Each section was cut at 10 μ m using a Leica CM1860 cryostat (Leica Biosystems, Wetzlar, Germany). Sections were stained for SDH. Sections were in incubation media (50 mM sodium succinate, 50 mM phosphate buffer, 0.12 M KH_2PO_4 , and 0.88 M Na_2PHO_4 , 0.5 mg/mL nitroblue tetrazolium) for 40-min in a 37 $^\circ\text{C}$ water bath. Slides were washed for 3-min with dH_2O and imaged. Images were collected with Nikon Sight DS-Vi1 camera mounted on an Olympus CKX41 inverted microscope. ~25 individual fibers of SDH+ (purple or oxidative) and

SDH- fibers (non-purple or glycolytic) per each muscle were counted and both fibers were manually circled for cross-sectional area (CSA) using Nikon Basic Research Imaging Software (Melville, NY, USA). All fiber measurements were performed by a blinded investigator. Plantaris muscle was initially chosen to compare current SDH data with our previous male CC study (12).

viii. Preparation of Separated and Permeabilized Muscle Fibers

During tissue harvesting, ~15 mg of fresh plantaris muscle was collected and placed in 100 mm rounded petri dish containing ice-cold buffer X (60 mM K-MES, 35 mM KCl, 7.23 mM K₂EGTA, 2.77 mM CaK₂EGTA, 20 mM imidazole, 0.5 mM DTT, 20 mM taurine, 5.7 mM ATP, 15 mM phosphocreatine, and 6.56 mM MgCl₂ at pH 7.1). Connective tissues and blood clots were eliminated, and the fiber bundles were gently separated into a near-single fiber bundle to maximize their surface area under an upright stereoscopic microscope (Fisher Scientific, Waltham, MA, USA) using a pair of extra-sharp forceps (Fisher Scientific). The finely separated fiber bundles were then permeabilized in a tube with saponin (50 µg/mL) in ice-cold buffer X on a rotator for 30-min at 4 °C. The permeabilized fiber bundles were washed in ice-cold buffer Z (110 mM K-MES, 35 mM KCl, 1 mM EGTA, 5 mM K₂HPO₄, 3 mM MgCl₂, 0.005 mM glutamate, 0.02 mM malate, and 0.5 mg/ml BSA at pH 7.1) for 5-min x 3 times as previously described (12, 181). The permeabilized fiber bundles were then used for both mitochondrial RCR and ROS emission (12).

ix. Mitochondrial Respiratory Control Ratio (RCR)

Mitochondrial oxygen consumption was measured by polarography in a respiration chamber maintained at 37 °C (Oxygraph+, Hansatech Instruments, King's Lynn, UK) as described (12) and this method was adapted from Min et al (181). Briefly, permeabilized plantaris muscles

were transferred to a respiratory chamber filled with 1 mL of respiration buffer Z containing creatine (20 mM) to saturate creatine kinase and allowed to equilibrate with the tissue for 5- to 10-min before adding any substrate. State 2 respiration was assessed by the addition of malate and pyruvate (5mM) using 10 μ L 701RN Syringes (Hamilton, Reno, NV, USA) followed by maximal ADP-stimulated respiration (State 3) by adding ADP (0.25 Mm) and then basal mitochondrial respiration (State 4) by the addition of oligomycin (10 μ g/mL) to inhibit ATP synthesis. State 3 and 4 respiration rates were normalized to dry tissue weight. The respiratory control ratio (RCR) was calculated by dividing State 3 by State 4 respiration.

x. ROS Emission

ROS emission was determined using Amplex UltraRed Reagent (Molecular Probes, Eugene, OR, USA) in permeabilized muscle fibers as previously described (12). This assay is based on the concept that amplex red reacts with H_2O_2 in a 1:1 stoichiometric ratio in the presence of horseradish peroxidase to produce the red fluorescent oxidation product; resorufin. Following the addition of the permeabilized plantaris muscle, baseline H_2O_2 production was measured followed by induction of H_2O_2 production by the addition of supraphysiological concentrations of succinate. The rate of H_2O_2 was normalized to dry weight of the tissue and calculated based on the rate of change from baseline to succinate and then concentrations we calculated using a standard curve. Plantaris muscle was used for both mitochondrial respiration and ROS emission analysis.

xi. Immunoblotting

Frozen gastrocnemius muscle samples were powdered, and 20 mg tissue samples were suspended in 250 μ L 2x protein sample buffer (50 mM Tris-HCl, 1% sodium dodecyl sulfate

(SDS), 10% glycerol, dithiothreitol (20 Mm), 2-mercaptoethanol (127 mM), and 0.01% bromophenol blue combined with protease inhibitors, and phosphatase inhibitors at pH 6.8) and homogenized. Protein concentration was determined using the RC/DC assay (5000122, Bio-Rad, Hercules, CA, USA). 40 µg total protein in protein sample buffer was loaded into 10% gel and resolved by SDS-PAGE at 100 V for 2 hours, transferred to a PVDF membrane at 20 V for 1.5 hours. Ponceau S stain was applied to membranes. The membranes were then incubated with 5% of milk in TBS at room temperature for 1 hour, then the membranes were incubated with primary antibodies with 1:500-1000 dilution rate in LI-COR blocking buffer with 0.2% tween 20. The membranes were incubated overnight for primary antibodies specific to COX-IV (4844S, Cell Signaling), VDAC (4866S , Cell Signaling), Deptor (ABS222, Millipore Sigma), Ubiquitin (3933, Cell signaling), Beclin-1 (3737, Cell Signaling), LC3 (4108, Cell signaling), p62 (p0067, Sigma), p-p38 MAPK (9211, Cell signaling; T180/182), p38 MAPK (9212, Cell signaling), p-ERK 1/2 MAPK (4370, Cell signaling; T202/Y204), ERK 1/2 MAPK (4695, Cell signaling), PGC-1 α (sc-13067, Santa Cruz), PPAR α (sc-9000, Santa Cruz), PPAR δ (sc-7197, Santa Cruz), TFAM (7495, Cell Signaling), MFN1 (sc-50330, Santa Cruz), MFN2 (sc-50331, Santa Cruz), OPA1 (sc-367890, Santa Cruz), DRP1 (14647, Cell Signaling), and FIS1 (NB100-56646, Novus). BNIP3 (3769, Cell Signaling), SOD1 (GTX100554, Genetex), SOD2 (131945, Cell Signaling), SOD3 (AF4817, R & D Systems), and Catalase (140975, Cell Signaling). Following overnight incubation with primary antibodies, membranes were washed with TBS with 0.1% tween 20 (TBST) for 5-min x 3 times and conjugated with HRP secondary antibodies (LI-COR Biosciences, Lincoln, NE, USA) with 1:10,000 dilution rate were used according to the manufacturer's protocol for an hour at room temperature. Membranes were then washed with TBST for 5-min x 3 times followed by an image scan on LiCor Odyssey FC via IR detection. All bands were normalized to the 45 kDa actin band of Ponceau S stain as a loading control as previously described (12, 182, 183).

xii. RNA isolation, cDNA synthesis, and quantitative real-time PCR

Frozen gastrocnemius muscle samples were powdered, and 20 mg tissue samples were suspended in 1 mL of TRIzol reagent and homogenized using Polytron for ~5-sec x 5 times before being transferred into a 1.5 mL microtube placed on ice. After 15-min at room temperature, 200 μ L of chloroform was added and samples were centrifuged for 25-min. The clear portion of the solution from the top was transferred into a new tube. An equal amount of 70% of Diethyl Pyrocarbonate (DEPC) treated ethanol was added, and the samples were loaded into a RNeasy column. RNA isolation was then processed using an RNA isolation kit (K145002; Invitrogen, Carlsbad, CA, USA). 30 μ L of DNase treated RNA was collected and RNA concentration and purity were determined by fluorometry using 260/280 nm ratios read on a Bio-Tek Power Wave XC microplate reader (BioTek Instruments Inc., Winooski, VT, USA) with Take3 microvolume plate using Gen5 software. Subsequently, 1 μ g of RNA was reverse transcribed into cDNA using VILO Superscript reagent (11755050, Invitrogen) and cDNA was diluted to 1:100 (10 ng/ μ L). Quantitative real-time PCR was performed using TaqMan probe reagent and QuantStudio3 PCR instrument (ThermoFisher Scientific, Waltham, MA, USA), and Ct values were analyzed according to the manufacturer's instructions. PCR was as follows: 4-min of incubations, 45 cycles of denaturation, annealing, and extension at 95 °C, 60 °C, and 72 °C, respectively. Target TaqMan probes for *β -actin* (Mm00607939_g1), *Cox4i1* (Mm01250094_m1), *Igf1* (Mm00439560_m1), *Redd1* (Mm00512504_g1), *Deptor* (Mm01195339_m1), *Ubc* (Mm02525934_g1), *Gadd45a* (Mm00432802_m1), *Atrogin1* (Mm00499523_m1), *Murf1* (Mm01185221_m1), *IL-6* (Mm00446190_m1), *Tnf* (Mm00443258_m1), *NF- κ B* (Mm00476361_m1), *Lc3* (Mm00458724_m1), *p62* (Mm01700766_M1), *Cyclin-D1* (Mm00432359_m1), *Pax7* (Mm01354484_m1), *MyoD* (Mm01203489_g1), *Myogenin* (Mm00446194_m1), *Mki67* (Mm01278617_m1), *Pgc1 α 1* (Mm01208835_m1), *Ppar γ* (Mm01184322_m1), *Nrf2* (Mm_00477784m1), *Drp1* (Mm_00432881_m1), and *Mtif2* (Mm00505356_m1) were purchased from Applied Biosystems (Life Technologies). Additional custom primer pairs specific for *Vdac*,

Pgc1α4, *Beclin-1*, *Bnip3*, *Ppara*, *Tfam*, *OPA1*, *Mfn1*, *Mfn2*, *Mff*, *Fis1*, *TuFM*, *Taco1*, and *Mtif3* were used in which primer information has been reported previously (12, 81, 184). Final quantification of mRNA level was calculated using the $\Delta\Delta\text{CT}$ method as described previously (182, 184). All targets were normalized to the β -actin Ct value, which did not differ between experimental groups.

xiii. Statistics

A one-way ANOVA with a factor of group was utilized as the global analysis for each dependent variable. Where significant F-ratios were found, statistical differences among means were determined by Tukey's post hoc test. The comparison-wise error rate, α , was set at 0.05 for all statistical tests. Only differences that reached significance by the global F test and significant differences by Tukey-adjusted pairwise comparison are presented. All data were analyzed using GraphPad Prism (La Jolla, CA, USA) and figures were compiled using GraphPad Prism as well. Data expressed as mean \pm Standard error of the mean (SEM).

E. RESULTS

i. Lower muscle and fat tissue weights with HT animals.

Tissue weights from all animals are presented in **Table 1**. In soleus muscle, HT had ~14% and ~12% lower compared to PBS ($p=0.003$) and LT ($p=0.024$). In TA muscle, HT had ~12% and ~9% lower weights compared to PBS ($p<0.001$) and LT ($p=0.017$), respectively. In EDL and plantaris muscles, no significant differences were observed. In addition, spleen weight, a surrogate marker for the inflammatory state, was ~63% and ~296% greater in LT ($p=0.010$) and HT ($p<0.001$) compared to PBS. Similarly, Liver weight was ~16% and ~32% greater in LT ($p=0.006$) and HT ($p<0.001$) compared to PBS. Lung weight was ~19% greater in HT compared

to PBS ($p < 0.001$). Gonadal fat mass was ~34% and ~38% lower in 1 LT ($p = 0.030$) and HT ($p = 0.008$) compared to PBS. Tumor weight was ~290% higher in HT compared to LT ($p < 0.001$; **Table 1**). These data suggest the HT group displayed mild cachexia compared to our prior male CC study (12).

ii. Reduced female sex hormones with LLC injection.

Female sex hormone levels in plasma were assessed to determine hormonal changes during CC. Both estrogen and progesterone levels in plasma had ~67% and 42% lower in 1 wk following LLC injection, which remained suppressed in all tumor-bearing groups ($p = 0.05-0.038$, **Table 1**).

iii. Unchanged oxidative phenotype in tumor-bearing female mice

The mean percentage of SDH+ fibers in the plantaris muscle was not different among experimental groups ($p = 0.350$; **Figure 1A-B**). Moreover, fiber CSA distribution and mean fiber CSA of both SDH+ and SDH- tended to be greater in the HT group compared to other groups although statistically non-significant ($p = 0.089$; **Figure 1C-F**). mRNA abundance of *Vdac* was ~40-54% lower in HT compared to PBS ($p < 0.001$), 1 wk ($p = 0.071$), 2 wks ($p = 0.003$), and LT ($p = 0.041$; **Figure 1G**) while protein contents of mitochondrial content (COX IV and VDAC) were not different across the groups (**supplemental figure 2A**).

iv. Impaired skeletal muscle contractility with HT animals

In vivo isometric torque frequency data (unnormalized) demonstrated HT had ~77-121% higher isometric torque during lower frequencies (10-60 Hz) than PBS ($p = 0.002-0.040$; **Figure 2A**). Peak isometric torque (unnormalized) was not different between experimental groups

(**Figure 2B**). Stimulation frequency at 50% peak torque was ~18% lower in HT compared to other groups ($p=0.001-0.013$; **Figure 2C**). One-half relaxation time was ~71% slower in HT compared to PBS ($p=0.054$; **Figure 2D**). Time to maximal contraction was ~127% slower in HT compared to other experimental groups ($p<0.001$; **Figure 2E**). The fatigability test revealed no statistical difference between PBS and LT or HT although 2 wks animals had ~12-42% greater fatigability compared to 1 wk, LT, and HT at various time-points (10-30s and 60-70s; $p=0.005-0.046$; **Figure 2F**).

v. Inhibition of muscle protein anabolism

To determine protein synthetic function, we assessed 24 hours FSR determined by D₂O labeling and cell signaling markers associated with protein synthesis. Mixed gastrocnemius muscle FSR was ~40% lower in HT compared to PBS ($p=0.043$; **Figure 3A**) although there were no statistical differences in TA (**Supplemental Figure 3A**). mRNA content of *Pgc1 α 4* was ~62% lower in 1 wk compared to LT ($p=0.015$) and insulin growth factor-1 (*Igf1*) was greater in 2 wks compared to LT (~66%, $p=0.009$) and HT (~57%, $p=0.016$), respectively (**Figure 3B**). *Redd1* mRNA content was ~17-fold greater in 1 wk compared to PBS ($p=0.001$), and ~3-6-fold greater compared to 2 wks, LT, and HT ($p=0.004-0.014$, **Figure 3C**). Protein content of Deptor was greater in LT compared to PBS (~3-fold; $p=0.067$) and 2 wks (~1.8-fold, $p=0.012$; **Figure 3D**) while mRNA content of *Deptor* was ~45.1% greater in 2 wks compared to HT ($p=0.046$; **Figure 3E**).

vi. Atrophy-associated genes are upregulated with tumor development

We assessed mRNA content of genes from gastrocnemius within the UPS, autophagy-lysosomal pathway, and markers of inflammation to assess protein degradation systems during the development of CC (**Figure 4**). First, mRNA content of *Ubc* (Ubiquitin C), *Atrogin1*, and *Murf1*

were ~2.8-fold ($p=0.019$), ~3.5-fold ($p<0.001$), and ~4.5-fold ($p=0.004$) greater in HT compared to other groups, respectively while *Gadd45a* demonstrated no difference from PBS (**Figure 4A**). Regarding autophagy, the protein content of Beclin1 (a central marker for autophagy, initiating autophagosome formation) was ~54% higher in 1 wk compared to PBS ($p=0.021$) and LC3 II/I ratio (indication of autophagic activity) was ~190% higher in HT compared to 2 wks ($p=0.038$) although there were no significant differences in total LC3 and p62 (a cargo protein that targets other proteins that bind to it for selective autophagy) protein content (**Figure 4B-C**). On the other hand, the mRNA content of *Beclin1* was ~44% lower in HT compared to PBS ($p=0.035$) and *Lc3* was ~39% higher in 2 wks compared to PBS and HT ($p=0.019-0.040$). No significant differences in *p62* content were observed (**Figure 4D**). Regarding inflammatory markers, *IL-6* mRNA content was ~90% greater in HT compared to other groups ($p<0.001$) and *Tnfa* was ~185% greater in 2 wks and LT compared to 1 wk ($p=0.021-0.027$; **Figure 4E**). There was no statistical difference was found in *NF- κ B* mRNA content (**Figure 4E**).

vii. Extrinsic regulators of skeletal muscle mass are altered during CC development

To examine extrinsic regulators of skeletal muscle mass, we assessed mRNA contents from gastrocnemius for cell cycling and myogenesis. *Cyclin-D1* (essential regulator of the G1-S transition) was ~2.5-fold greater in 2 wks compared to other experimental groups ($p<0.001$). *Mki67* (cell proliferation marker) was ~2.5-fold greater in HT compared to PBS (~149%, $p<0.001$), 2 wks (~109%, $p=0.002$), and LT (~99%, $p=0.003$). *Acta2* (a marker of myofibroblast) was ~57% higher in 1 wk and 2 wks compared to PBS and HT ($p=0.001$; **Figure 5A**). Both *Pax7* (the essential regulator for muscle precursor cell proliferation) and *MyoD* (regulating both skeletal muscle proliferation) were ~31-41% lower in HT compared to 1 and 2 wks ($p=0.001-0.045$). No changes were observed in *Myogenin* (muscle differentiation marker) mRNA content (**Figure 5B**).

viii. Mitochondrial degeneration in HT

Histological assessment of MitoTimer (redox-sensitive reporter gene) data demonstrated lower red to green ratio (oxidative stress) in 1 wk compared to LT (~27%, $p=0.042$) and HT (~30%, $p=0.009$; **Figure 6A and B**). Greater pure red puncta numbers (completely degenerated mitochondria) were observed in HT compared to PBS and 1 wk (~50%, $p=0.005-0.022$, **Figure 6A and C**). In addition, Mitochondrial respiratory function measured by the mitochondrial RCR was ~49% higher in HT compared to PBS and 1 wk ($p=0.021-0.036$, **Figure 6D**) while mtROS emission was not statistically different across experimental groups (**Figure 6E**).

ix. LLC impairs mitochondrial quality control and mitophagy in HT, but not in LT

Mitochondrial quality control was determined via assessing markers of mitochondrial biogenesis, dynamics, translation initiation factors, and mitophagy from gastrocnemius. In mitochondrial biogenesis, *Pgc1 α 1* mRNA levels were ~44% lower in HT compared to PBS, 1 wk, and 2wks ($p=0.009-0.019$; **Figure 7A**). *Tfam* mRNA levels were ~28% lower in HT and ~25% lower in 1wk compared to PBS ($p<0.001$; **Figure 7A**). *Nrf2* mRNA content was ~38% greater in HT compared to PBS ($p=0.026$) and 1 wk ($p=0.029$) while there were no statistical differences in *Ppara* or *Ppar δ* (**Figure 7A**). In mitochondrial dynamics, *Drp1* and *Mff* were higher in 2 wks and lower in HT compared to PBS (~32%; $p=0.024$ and ~43%; $p=0.002$, respectively) while HT was not different from PBS (**Figure 7B**). *Mfn1* mRNA content was ~34% lower in HT compared to PBS ($p=0.014$) while there were no statistical differences in *Fis1* and *OPA1* (**Figure 7B**). In mitochondrial translation, *TuFM*, *Taco1*, and *Mtif2* showed similar patterns that were gradually elevated in 2 wks and reduced in HT ($p=0.001-0.013$) while no changes were observed in *Mtif3* (**Figure 7C**). In mitophagy, both protein and mRNA content of BNIP3 was ~63% ($p=0.010$) and

~147% ($p < 0.001$) greater in HT compared to other groups, respectively (**Figure 7D-E**). There were no statistical differences in protein contents for mitochondrial biogenesis and dynamics (**Supplemental Figure 2A, B, and D**).

x. Antioxidant enzymes are unchanged during CC

The protein content of SODs -1, -2, and -3 and Catalase from gastrocnemius were not statistically different among experimental groups (**Supplemental figure 2C**).

xi. Altered MAPK signaling in LT group

MAPK signaling from gastrocnemius was determined via assessing the phosphorylation status of p38 and ERK. Although there were no statistical differences in protein content of p-p38^{T180/Y182}/p38, p-ERK1/2^{T202/Y204}/ERK was ~7.3-fold higher in LT compared to PBS ($p = 0.034$; **Supplemental figure 4A**).

F. DISCUSSION

In this study, we aimed to assess alterations in the development of CC in LLC tumor-bearing female mice. To do so, we assessed aspects of skeletal muscle contractile function and metabolism including protein turnover and mitochondrial health. In addition, we observed a distinct dichotomous effect in tissue wasting and cachectic phenotype within the 3 and 4 wk animals where approximately half of the mice exhibited a relatively low tumor mass (<1.2 grams), and the other half exhibited a substantially greater tumor mass (>2 grams). This was a particularly interesting finding, as previous studies in male mice have shown gradual tumor development over time following tumor implantation (12, 185). Furthermore, animals with HT exhibited higher protein

degradation, impaired skeletal muscle contractility, and accelerated mitochondrial degeneration while LT mice did not exhibit such cachectic phenotypes, despite up to 4 wks of tumor growth. Our prior works have demonstrated impaired metabolic health in male mice prior to the onset of cachexia itself (12, 81), compared to those works the current data suggest a relative protection of muscle contractile and metabolic functions in female tumor-bearing mice in these earlier stages of tumor development.

First, we observed a clear dichotomy in tumor burden among 3- and 4-wk tumor-bearing female mice, wherein mice with higher tumor burdens developed a cachectic phenotype. This dichotomy suggests a significant reliance upon tumor burden for the development of cancer cachexia in female mice whereby timeframe of tumor development may not directly reflect increases to tumor burden and corresponding cachectic phenotype. Considering, these effects we regrouped 3- and 4- wk mice to low and high tumor bearing conditions to better reflect the developmental process of cachexia in female mice. Our findings suggest LT mice may have a protective mechanism to prevent cancer-induced cachectic phenotypes including tumor development and muscle wasting although additional investigations are required to elucidate this mechanism. Despite marked muscle loss in HT mice, this atrophy was less overt compared to previous studies utilizing tumor-bearing male mice (12, 18). Specifically, females revealed ~3-14% overall muscle loss with significant muscle wasting in two muscles (TA and soleus) while males underwent ~11-16% overall muscle loss with significant muscle wasting in four muscles (gastrocnemius, TA, plantaris, and soleus muscle) out of five (12). Furthermore, CSA distribution for oxidative and glycolytic muscle fibers as well as oxidative phenotype via SDH staining did not differ between experimental groups although these markers were significantly lower in our previous study using tumor-bearing male mice (12). These findings imply that while female HT mice exhibit mild cachexia, female mice may have a protective effect on cancer-induced muscle

wasting compared to male counterparts consistent with suggestions that females may be less sensitive to inflammation-mediated muscle atrophies compared to males (45).

In addition to muscle wasting, impaired muscle contractile function is a strong indicator of lower survival rate and impaired functional outcomes in advanced cancer patients (65). CC is often associated with impaired muscle contractility including force production and fatigability (69). Here, we observed impaired muscle contractility in HT mice, in agreement with findings from a previous study (69). Indeed, we observed lower torque frequency at half maximum torque, slower muscle contraction and relaxation times in HT mice, which was in line with prior works (186). While speculative these data suggest preferential protection of slower twitch fibers in early phases of cachexia itself, which aligns with preservation of oxidative fibers previously observed by our group (12). Prior evidence also demonstrated decreased isometric muscle force production and elevated muscle fatigue in male *Apc*^{Min/+} mice (colorectal cancer model) (69). However, another study demonstrated unaltered fatigability in tumor-bearing female mice (187) as observed here which may be associated with the relatively mild cachectic phenotype in our study. Collectively, although fatigability may not be altered with early-stage CC, likely due to preferential survival of slow-twitch fibers, muscle contractile function does still appear to be impaired with high tumor development in female mice.

One of the major features of CC is the net loss of skeletal muscle protein as protein degradation exceeds protein synthesis. Therefore, we assessed muscle protein anabolism and catabolism across tumor development. In line with previous works (79, 81), we observed lower muscle protein FSR in gastrocnemius of female mice with greater tumor burdens. We postulate this is due to altered function of the protein anabolic system during the development of CC, specifically the induction of anabolic/mTORC1 repressors, *Deptor* and *Redd1*, which were observed greater prior to the onset of the cachectic phenotype (**Figure 3C-D**). We previously observed a similar pattern in male tumor-bearing mice, whereby *Deptor* content was higher in

pre-cachectic male mice (81), suggesting inductions of anabolic repressors precede cachexia and may account for diminished protein synthetic rates as early-stage cachexia develops. It is noteworthy to mention that although gastrocnemius FSR was lower in HT mice, this muscle mass was intact. We speculate that unlike males, female gastrocnemius muscle mass appears to be protected during the development of CC and may begin the wasting process at later stages of cancer, which may not be enough to detect the significant muscle loss at the time of tissue collection in the current study.

Protein degradation in skeletal muscle is largely mediated by two major processes, the UPS and the autophagy-lysosomal pathway. Of note, we observe induction of E3 ligases, *Atrogin1* & *Murf1*, as well as *UBC (10)* in the HT mice (**Figure 4A**), in accordance with previous male CC studies (35, 81). Moreover, we observed greater LC3II/I ratio in HT while p62 level did not change, indicating an increase in autophagy initiation but not necessarily resolution in HT mice. In addition, cancer-induced protein degradation is often associated with elevated inflammation (15, 188) and inflammatory cytokines are well-known mediators of muscle wasting during CC (35, 188, 189). The elevated *IL-6* mRNA content observed in the HT group have also been demonstrated previously in both clinical (189) and pre-clinical models of CC (15, 188). Furthermore, these effects are of local induction of inflammatory cytokines at the level of the muscle suggesting tumor-induced local inflammation in cachectic mice. Taken together, these upregulated E3 ligases and proinflammatory cytokines appear to coincide and associate with muscle wasting as well as tumor development in tumor-bearing female mice.

Adult skeletal muscle has a capacity to regenerate in response to proper stimuli (190) and is often altered in various myopathologies including CC (81). Of note, previous evidence suggests alteration to satellite cell function including the markers *Pax7*, *Myogenin*, *MyoD*, and *Cyclin-D1* in tumor-bearing male mice (81, 118). However, here we observed lower *Pax7* and *MyoD* in only the HT group (**Figure 5B**), suggesting a relative protection of myogenic regulators in females

compared to previous male CC study (81). Further in-depth research on the cell cycle and myogenic function is warranted to elucidate the regulation of muscle regeneration during CC, especially within female mice.

Prior evidence demonstrates cancer-induced muscle mitochondrial degeneration including diminished mitochondrial RCR, ATP production, and elevated mtROS emission (12, 18). In addition, we have demonstrated these mitochondrial degenerations occur prior to muscle loss in tumor-bearing male mice (12). Interestingly, here we report female mice exhibited unchanged mtROS emission and greater mitochondrial RCR in HT, in direct contrast to lowered RCR in cachectic male mice (12) and suggesting specific protection of mitochondrial health during cancer cachexia in female mice. These data closely align with recent findings suggesting early mitochondrial degeneration in male, but not female mice during disuse atrophy (11). Combined data suggest a mechanism of mitochondrial degeneration to induce muscle atrophy is preserved across pathologies specifically in male mice; yet in females these mitochondrial mechanisms may be more nuanced in relation to muscle atrophy. Impaired mitochondrial function is often associated with dysregulated mitochondrial autophagy (mitophagy) (12, 191), which contributes to exacerbated mitochondrial degeneration. We observed induction of BNIP3 and an increase in pMitoTimer pure red puncta in HT mice, reflecting the induction of mitophagy and accumulation of damaged mitochondria in female mice upon onset of the cachectic phenotype (**Figure 6-7**). While similar data are observed in male mice by our group (12) as well as others (192), in our prior work these effects were observed well prior to onset of the cachectic phenotype in males in contrast to later development in females. Further studies applying either pharmacological or transgenic animal models of BNIP3 is warranted to determine its precise role in CC. Considering data from the current study as well as other recent works (5, 183), we hypothesize that female mice specifically protect mitochondrial health during myopathologies. This specific mitochondrial protection may lead to attenuation of inflammatory forms of atrophy (i.e., CC) while prioritizing

mitochondrial health at the expense of muscle mass in non-inflammatory forms of atrophy (i.e., disuse).

Together with aforementioned mitophagy, mitochondrial quality control (MQC) is the accumulation of systems required for maintaining mitochondrial integrity and function and is an important defense mechanism for the cell's survival from mitochondrial damage (121), often altered in cancer (12). Herein, we observed altered mitochondrial biogenesis markers in HT mice. Specifically, we found lower *Pgc1 α 1* and *Tfam*, and greater *Nrf2* contents in HT although these effects were absent in previous male CC studies (12). In addition, some mitochondrial fission markers (*Drp1* and *Mff*) and translational factors (*Taco1* and *Mtif2*) within females revealed a similar pattern of elevation at 2 wks of tumor-bearing state, which may reflect mechanisms to protect muscle mitochondrial health during early stages of tumor development. By contrast, several of these mitochondrial biogenesis and dynamics markers were suppressed during the development of CC in our previous male study (12) further exemplifying dichotomous effects between biological sexes relative to maintenance of mitochondrial health during atrophic pathologies.

Recent studies have addressed phenotypical differences between sexes in response to different types of muscle atrophy such as those induced by disuse and cancer (45, 61, 170, 193), with females possibly having exacerbated wasting compared to males in some myopathies such as disuse, with the opposite being true in males and cancer. However, prior pre-clinical CC studies have primarily focused on male animals, making it difficult to isolate the fundamental role of biological sex during CC. Previously, Hetzler et al (64) demonstrated sex differences in IL-6 content in CC, whereby *Apc*^{Min/+} male mice had higher plasma IL-6 content than female counterparts. However, to our knowledge, the current study is one of the first studies to demonstrate various alterations in skeletal muscle during the initial development of CC in female tumor-bearing mice. While some responses appear preserved between sexes, we observed distinct differences in response to tumor development in females compared to prior male CC

studies (12, 81). Specifically, both sexes exhibit impaired protein anabolism, upregulated E3 ligase-mediated protein degradation, and mitophagy in mice with greater tumor burden. However, there were clear differences in oxidative phenotype, myogenic markers, MAPK signaling, mitochondrial RCR, mtROS emission, and mitochondrial dynamics between sexes, wherein many of these cellular alterations appear relatively protected in females while that of males was significantly impaired prior to the onset of cachexia itself (12, 81). Among protected effects in females compared to previous male studies, mitochondrial protection during the development of CC appears to serve as a major contributor to preserve muscle mass although further investigations regarding mitochondrial regulation in CC are warranted. Our findings suggest distinct biological sex differences in development of CC and these differentially regulated targets/pathways may be crucial in the protective mechanism in tissue wasting during CC in females. Therefore, a critical need remains to directly investigate comparative alterations in the skeletal muscle during the development of CC between males and females within a single study using various cancer types to better delineate the role of biological sex in CC.

It is worth mentioning a limitation of this study is the use of younger mice (8 to 12 wks old) to compare outcomes with prior works in male mice (12, 81, 194-196). However, with a majority of human cancers are most prevalent in older adults (197). Therefore, future studies should utilize aged animals to better recapitulate these clinical scenarios.

In conclusion, we set to investigate the initial development of CC in tumor-bearing female mice revealing various metabolic and contractile impairments with tumor development. Specifically, while many metabolic perturbations precede the onset of cachexia in males, female tumor-bearing mice exhibit multiple protections in both metabolic and contractile functions in these earlier stages of tumor development. These data suggest female mice may have a defense system protecting them from tumor-induced muscle degeneration via maintaining muscle regenerative processes, mitochondrial respiratory capacity, mitochondrial dynamics, and oxidative capacity during the development of CC. Our data strongly imply females exhibit an

enhanced capacity to mitigate aberrations associated with the onset of CC in the early stage of tumor development. However, further works are necessary to delineate these specific protections in female mice and their potential clinical utility.

G. TABLES

	PBS (N = 10)	1 week (N = 11)	2 weeks (N = 12)	LT (N = 13)	HT (N = 14)
Body Weight (g/mm)	1.154 ± 0.014 ab	1.075 ± 0.013 c	1.125 ± 0.011 bc	1.197 ± 0.017 ad	1.287 ± 0.026 e
Tumor Weight (mg/mm)	N/A	2.376 ± 0.29 a	14.86 ± 2.24 a	43.85 ± 6.37 b	171.2 ± 9.23 c
Body Weight –Tumor (g/mm)	1.154 ± 0.014 a	1.073 ± 0.013 b	1.110 ± 0.011 ab	1.153 ± 0.016 a	1.115 ± 0.025 ab
Gastrocnemius (mg/mm)	5.542 ± 0.068 a	5.211 ± 0.045 b	5.346 ± 0.06 ab	5.602 ± 0.073 a	5.369 ± 0.062 ab
Soleus (mg/mm)	0.449 ± 0.01 a	0.403 ± 0.01 ab	0.418 ± 0.016 ab	0.437 ± 0.009 a	0.385 ± 0.014 b
Plantaris (mg/mm)	0.789 ± 0.016	0.762 ± 0.019	0.753 ± 0.015	0.797 ± 0.02	0.736 ± 0.015
EDL (mg/mm)	0.510 ± 0.017	0.488 ± 0.007	0.479 ± 0.013	0.488 ± 0.013	0.475 ± 0.016
TA (mg/mm)	2.282 ± 0.057 a	2.174 ± 0.043 ab	2.151 ± 0.039 ab	2.213 ± 0.04 a	2.017 ± 0.042 b
Fat (mg/mm)	19.23 ± 1.856 a	17.6 ± 1.516 ab	16.77 ± 1.17 ab	18.14 ± 1.526 a	12 ± 1.359 b
Heart (mg/mm)	6.336 ± 0.18	6.275 ± 0.072	6.22 ± 0.163	6.346 ± 0.154	6.268 ± 0.165
Liver (mg/mm)	47.11 ± 1.948 a	46.74 ± 1.994 a	48.85 ± 1.218 ab	54.78 ± 1.863 bc	62.3 ± 2.36 d
Lungs (mg/mm)	7.695 ± 0.146 a	7.529 ± 0.211 a	7.607 ± 0.228 a	8.146 ± 0.238 a	9.131 ± 0.263 b
Spleen (mg/mm)	4.967 ± 0.217 a	4.274 ± 0.186 a	5.471 ± 0.371 a	8.104 ± 0.531 b	19.46 ± 1.123 c
Tibia Length (mm)	16.57 ± 0.053 a	16.15 ± 0.043 b	16.30 ± 0.079 bc	16.62 ± 0.057 ad	16.64 ± 0.049 ad
Estrogen (pg/mL)	67.61 ± 14.85 a	22.43 ± 4.40 b	28.27 ± 4.78 b	32.09 ± 4.19 b	21.77 ± 4.36 b
Progesterone (pg/mL)	9.58 ± 1.28 a	5.55 ± 1.55 ab	3.66 ± 0.63 b	5.55 ± 0.86 ab	3.59 ± 1.21 b

Table 1. Characteristics

Tissue weights are recorded as wet weights. All tissue weights were normalized to their tibia length to account for different body sizes. All values are represented as means ± SEM. Different letters represent statistical differences at Tukey-adjusted with alpha value set at $p \leq 0.05$. An N of 10-14 per group was used.

H. FIGURES

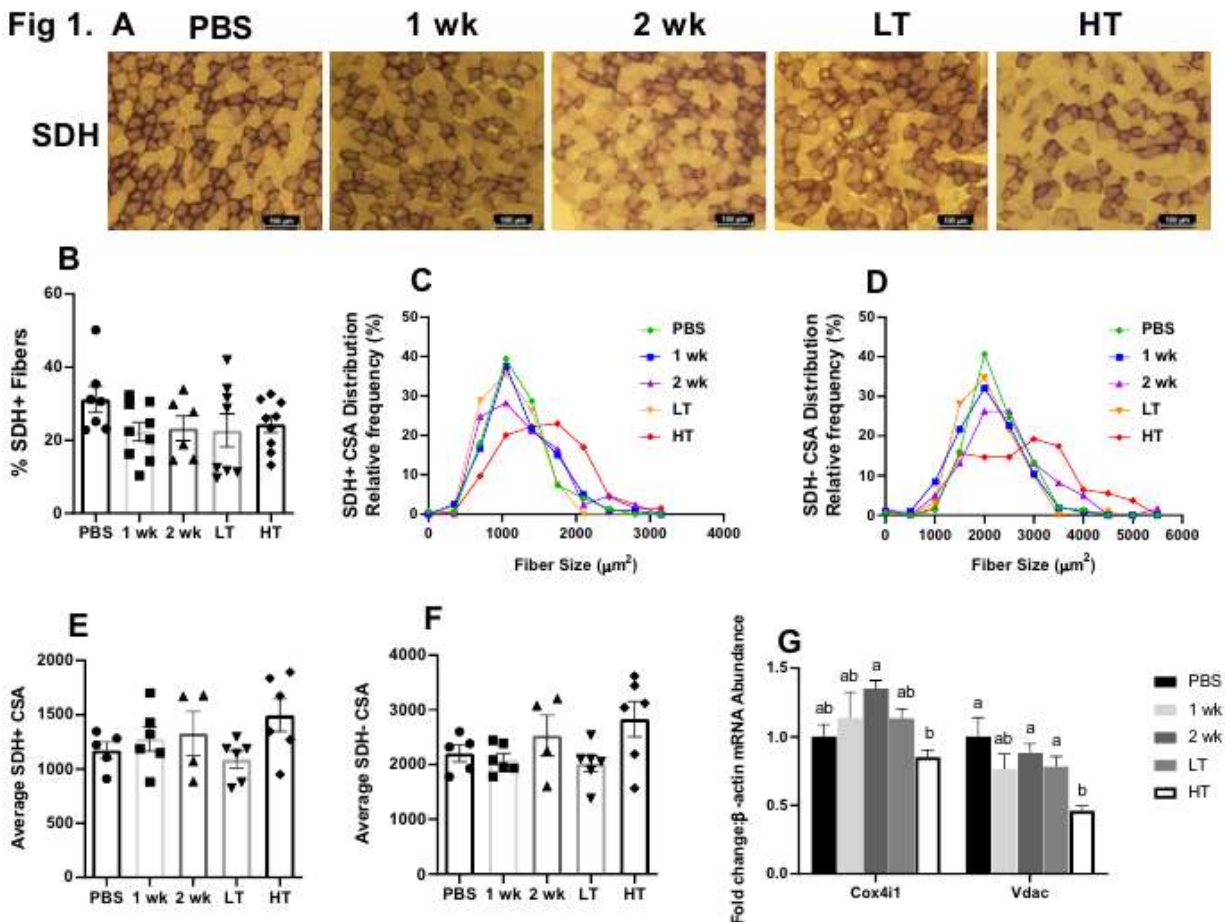


Figure 1. Oxidative Phenotype

Plantaris muscle used for SDH staining. (A) SDH staining images are representative of the five experimental groups. (B) Representative of the development of cancer cachexia through % of SDH+ fibers. (C) Distribution through relative frequency (%) of cross-sectional area for SDH+ fibers and (D) SDH- fibers. (E) and Average cross-sectional area for SDH+ and (F) SDH- fibers. (G) mRNA abundance for mitochondrial specific markers *Cox4i1* and *Vdac* by utilizing the Gastrocnemius muscle. Different letters represent statistical differences at Tukey-adjusted with alpha value set at $p \leq 0.05$. An N of 4-9 per group was used.

Fig 2.

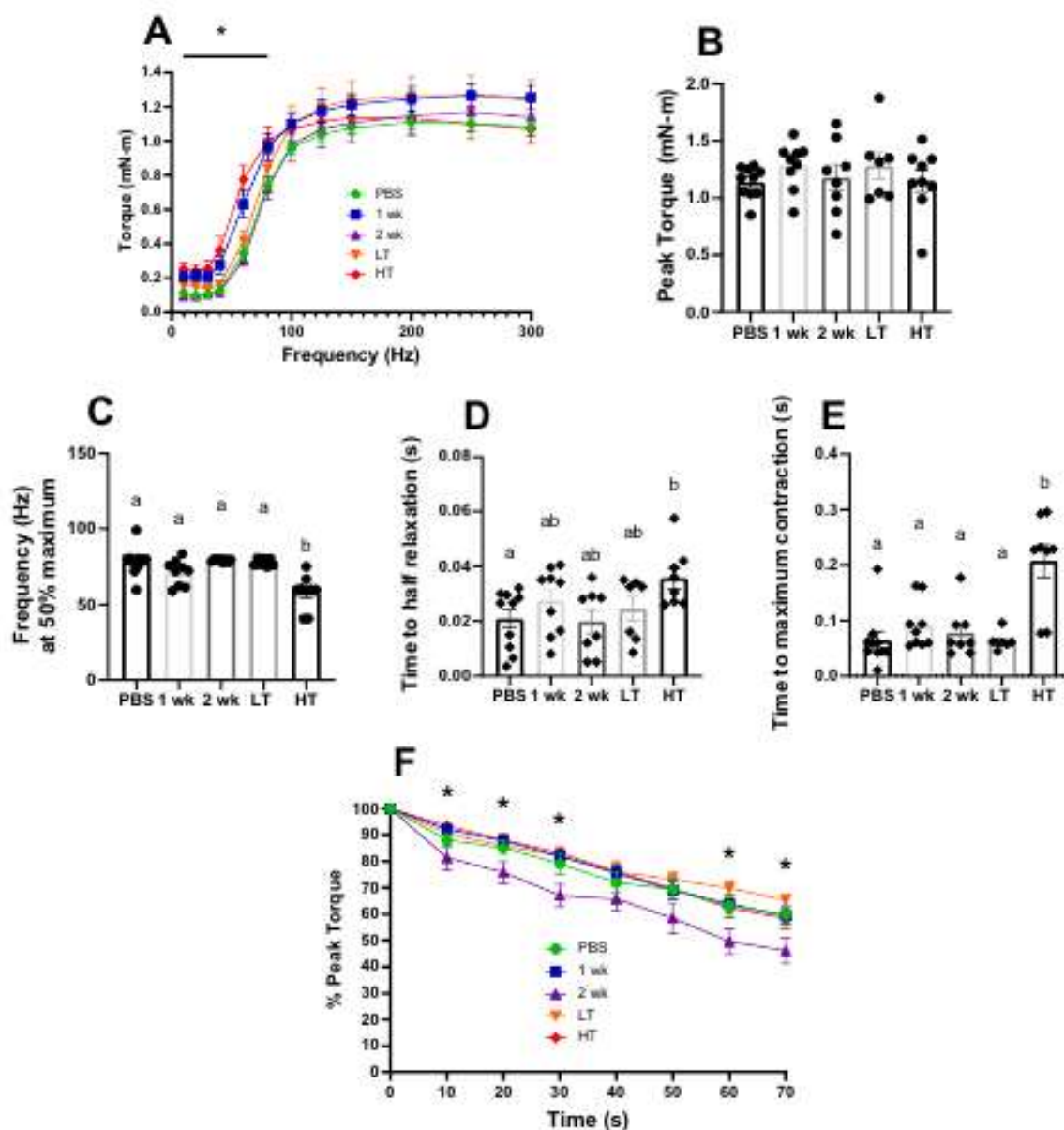


Figure 2. Skeletal Muscle Contractility

(A) Unnormalized isometric torque-frequency curve measured in mN·m for experimental animal groups. (B) Unnormalized average peak torque (mN·m) across experimental groups. (C) Frequency (Hz) delivered at 50% maximum torque across experimental groups. (D) Time (s) for muscle to achieve half relaxation across experimental groups. (E) Time to maximal contraction (s). (F) % peak torque measured over time (s) across experimental groups during fatiguing protocol induced via continuous peroneal nerve stimulation. Different letters represent statistical differences at Tukey-adjusted with alpha value set at $p \leq 0.05$. An N of 7-10 per group was used.

Fig 3.

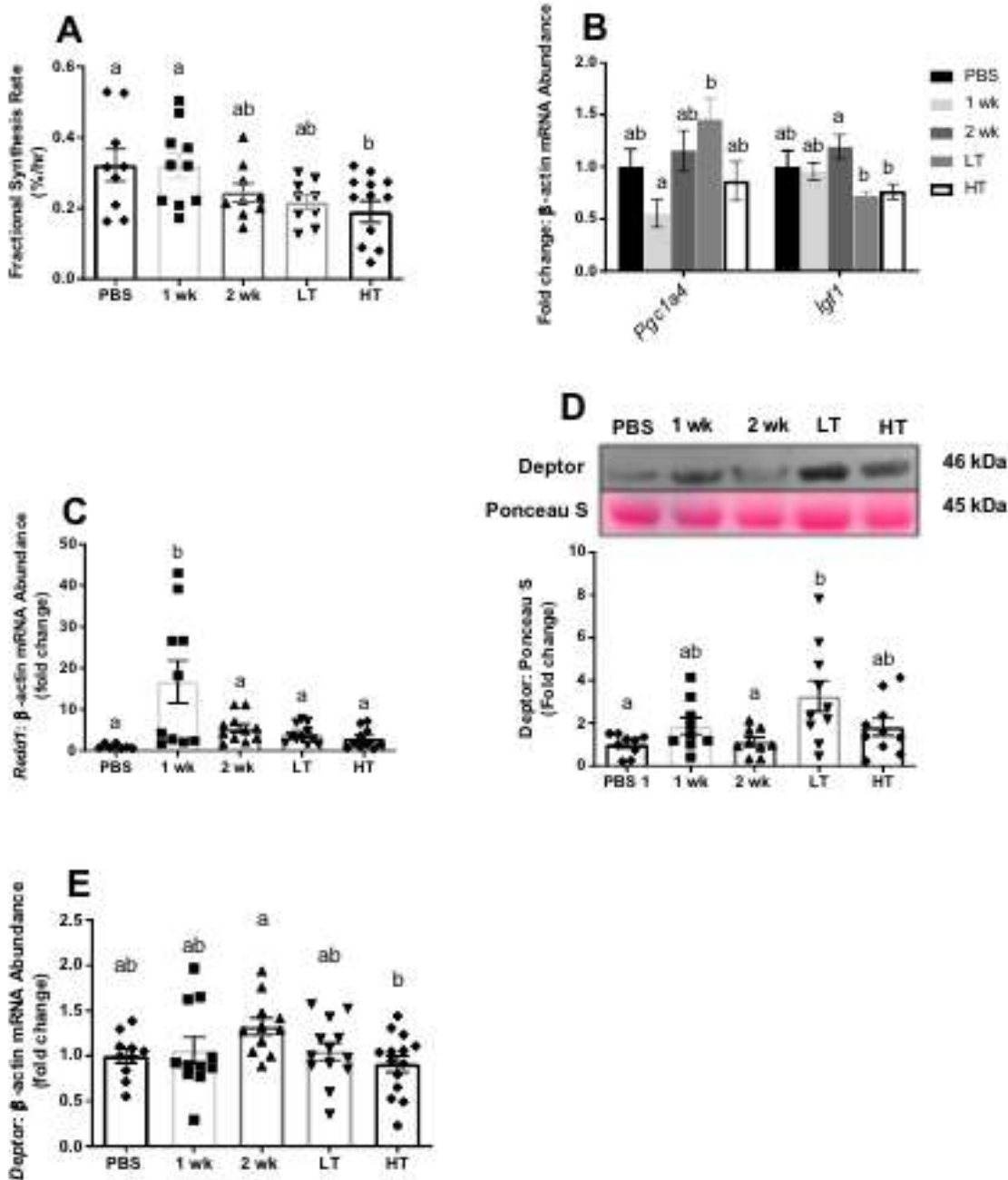


Figure 3. Protein Synthesis

(A) 24 hours mixed muscle fractional synthesis rates (%/hr) across experimental groups. (B) *Pgc1a4* and *Igf1* mRNA abundance measured among experimental groups. (C) *Redd1* mRNA abundance measured among experimental groups. (D) Protein content of Deptor relative to Ponceau S among experimental groups. Both mRNA and protein contents were analyzed from gastrocnemius muscle. Different letters represent statistical differences at Tukey-adjusted with alpha value set at $p \leq 0.05$. An N of 9-14 per group was used.

Fig 4.

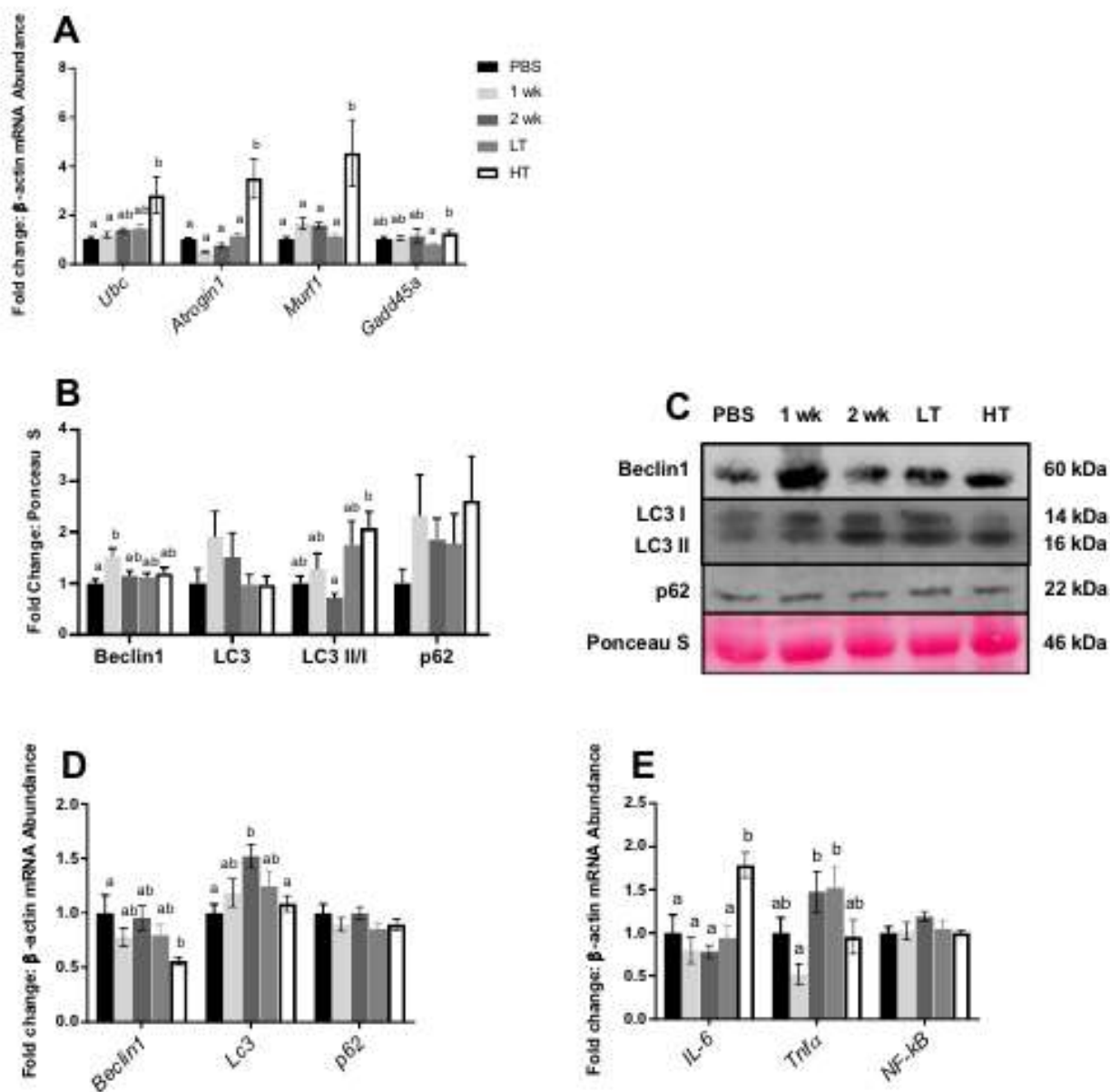


Figure 4. Protein Degradation & Inflammation

(A) Protein degradation measured by mRNA abundance for *Ubc*, *Atrogin-1*, *Murf1* and *Gadd45a*. (B) Protein content of autophagy-related markers; Beclin-1, LC3, LC3 II/I and p62 normalized to Ponceau S. (C) Representative immunoblot image for autophagy related markers from the same membrane. (D) mRNA abundance of autophagy-related markers for *Beclin-1*, *Lc3* and *p62*. (E) mRNA abundance of inflammation markers; *IL-6*, *Tnfa* and *NF-kB*. Both mRNA and protein contents were analyzed from gastrocnemius muscle. Different letters represent statistical differences at Tukey-adjusted with alpha value set at $p \leq 0.05$. An N of 10-14 per group was used.

Fig 5.

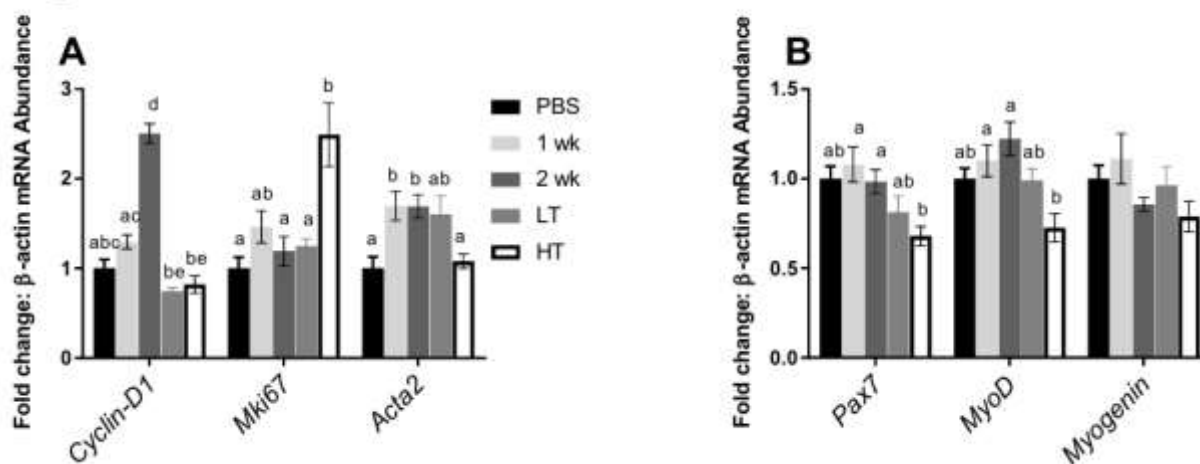


Figure 5. Myogenic & Cell Proliferation Factors

(A) Cell proliferation and (B) myogenic factors measured for mRNA abundance. (A) mRNA abundance measured for *Cyclin-D1*, *Mki67* and *Acta2*. (B) mRNA abundance measured for *Pax7*, *MyoD* and *Myogenin*. mRNA contents were analyzed from gastrocnemius muscle. Different letters represent statistical differences at Tukey-adjusted with alpha value set at $p \leq 0.05$. An N of 9-14 per group was used.

Fig 6.

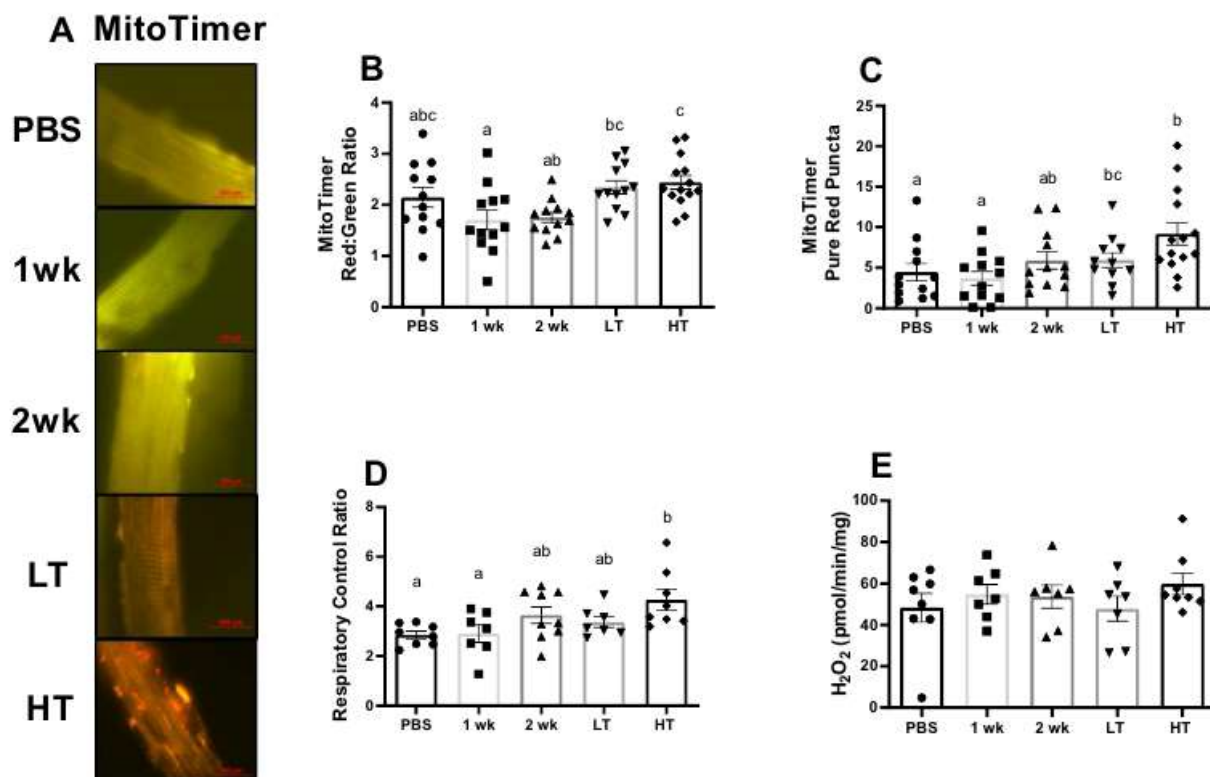


Figure 6. Mitochondrial Function & Network

(A) Representative images of MitoTimer in the FDB muscle taken at 100x magnification. Scale bar set at 100 μ m. (B-C) Quantifications of MitoTimer in FDB muscle. (B) Quantification of red to green ratio and (C) pure red puncta numbers quantified for MitoTimer. Pure red puncta are representative of mitochondria that are marked for autophagy. (D-E) Mitochondrial function and mtROS emission measurements of the plantaris muscle. (D) Respiratory Control Ratio (state 3: state 4 respiration) and (E) H_2O_2 emission of mitochondria measured with permeabilized plantaris. Different letters represent statistical differences at Tukey-adjusted with alpha value set at $p \leq 0.05$. An N of 7-9 per group was used.

Fig 7.

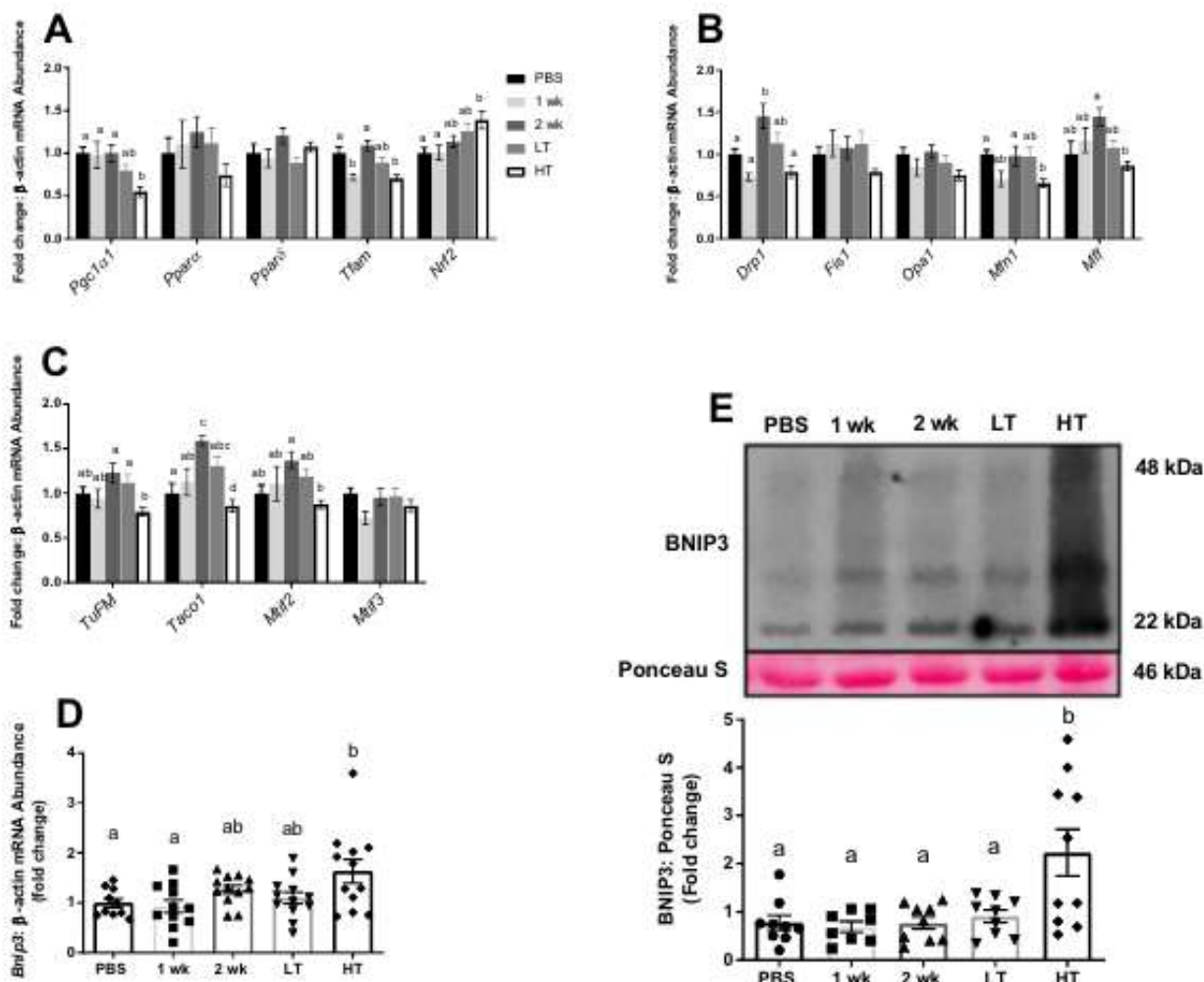
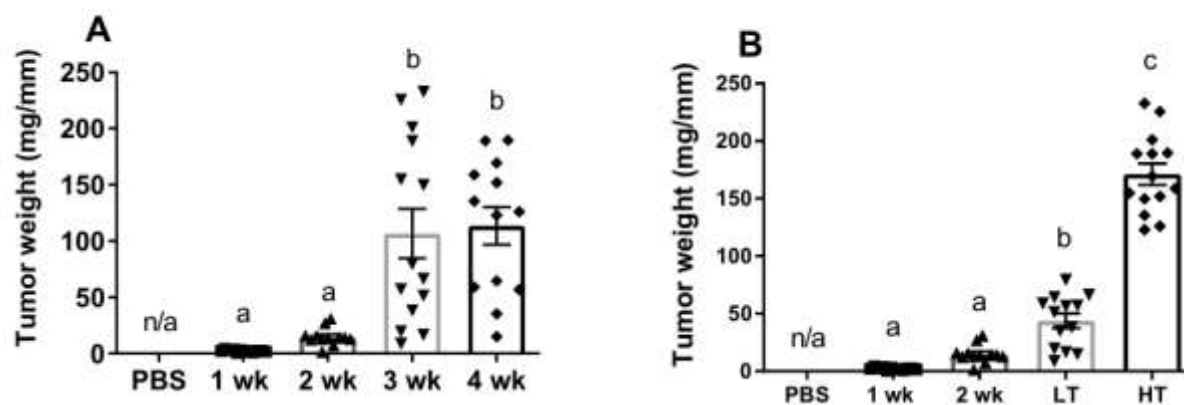


Figure 7. Mitochondrial Quality Control

(A) mRNA abundance of mitochondrial biogenesis controllers for *Pgc1α*, *Pparaα*, *Pparaδ*, *Tfam* and *Nrf2* among experimental groups. (B) mRNA abundance of mitochondrial dynamic controllers for *Drp1*, *Fis1*, *OPA1*, *Mfn1*, and *Mff* among experimental groups. (C) mRNA abundance of mitochondrial translation factors for *TuFM*, *Taco1*, *Mtif2* and *Mtif3* among experimental groups. (D-E) Mitophagy regulator, BNIP3, measured for (D) mRNA abundance and (E) protein content relative to Ponceau S with a representative image of immunoblot for Bnip3 and Ponceau S among experimental groups. Both mRNA and protein contents were analyzed from gastrocnemius muscle. Different letters represent statistical differences at Tukey-adjusted with alpha value set at $p < 0.05$. An N of 10-14 per group was used.

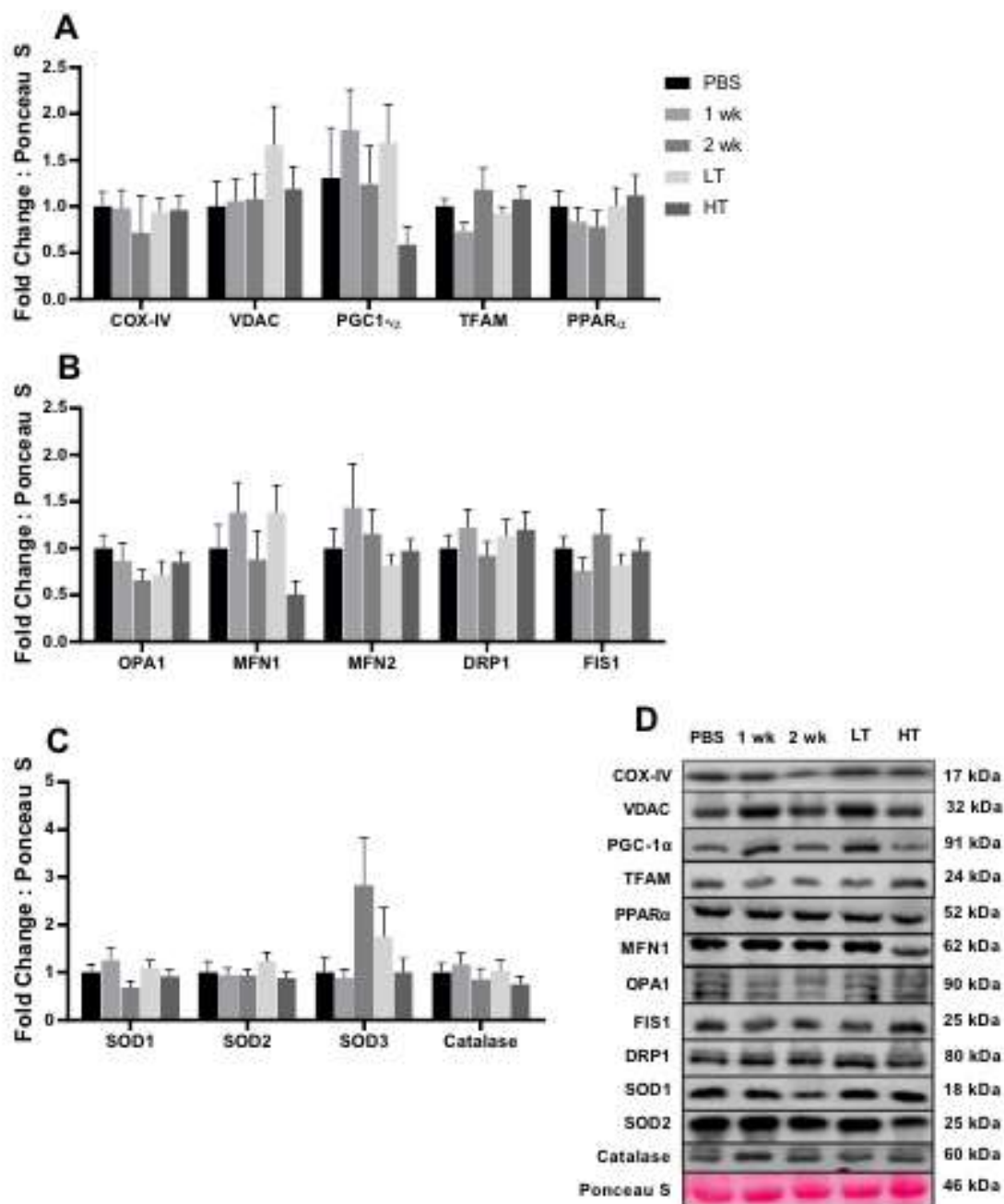
I. SUPPLEMENTAL FIGURES

Fig S1.

**Supplemental Figure 1. Original and Regrouped Tumor Weights**

(A) Original tumor weight distribution from 1 through 4 wks. (B) Regrouped animal experimental groups within 3- and 4-wk animals based on their tumor weight. LT; low tumor and HT; high tumor. An N of 10-14 per group was used.

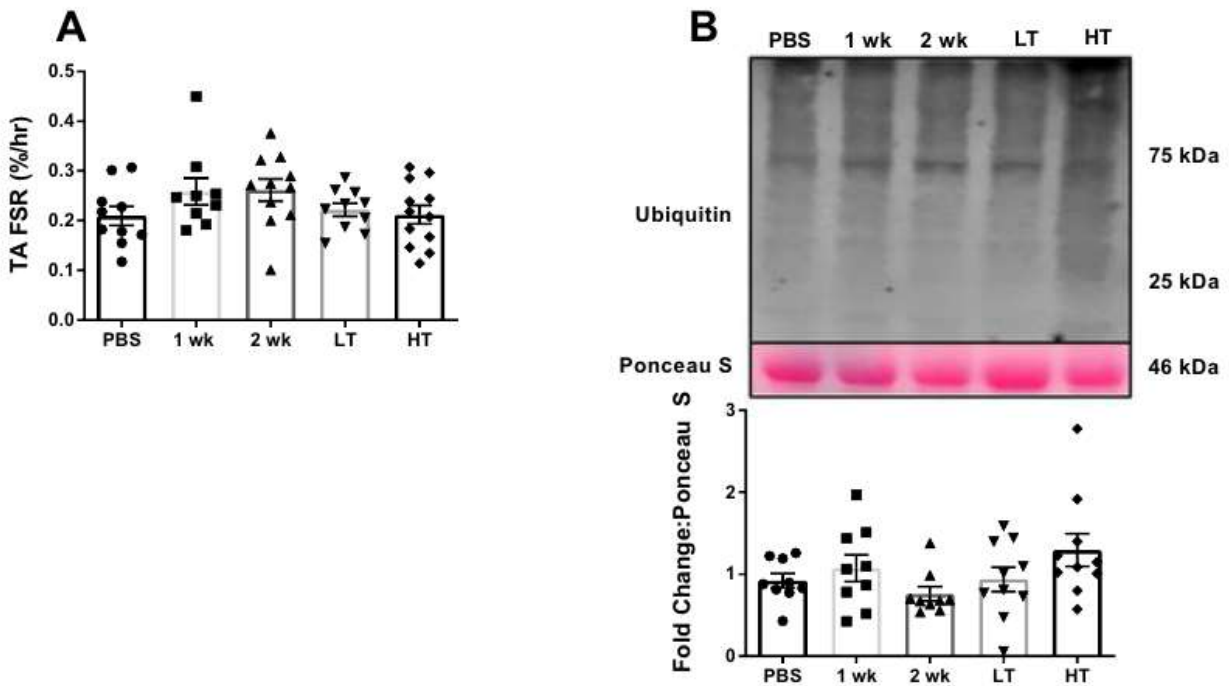
Fig S2.



Supplemental Figure 2. Mitochondrial markers

(A-C) Quantification of immunoblots for mitochondrial quality controllers among experimental groups. (A) Protein content for mitochondrial content and biogenesis controllers. (B) Protein content for mitochondrial dynamics controllers. (C) Protein content for antioxidant enzymes. (D) Representative image of immunoblot for mitochondrial quality controllers among experimental groups. Both mRNA and protein contents were analyzed from gastrocnemius muscle. An N of 10-14 per group was used.

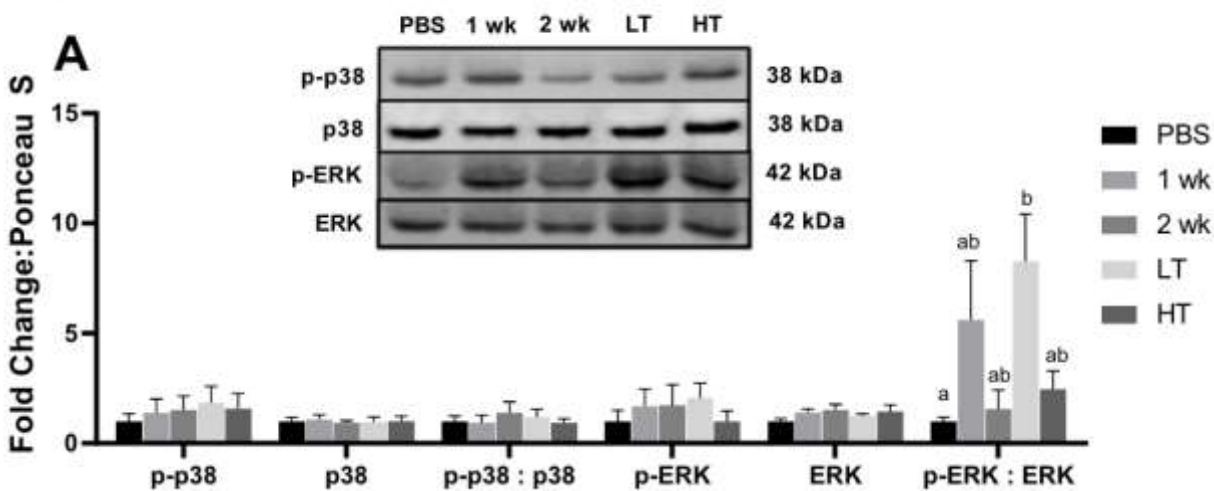
Fig S3.



Supplemental Figure 3. Protein Turnover

(A) TA muscle protein fractional synthesis rates (FSR) across experimental groups. (B) Representative image and protein content of immunoblot for Ubiquitin relative to Ponceau S. Protein content data was analyzed from gastrocnemius muscle. Different letters represent statistical differences at Tukey-adjusted with alpha value set at $p \leq 0.05$. An N of 9-14 per group was used.

Fig S4.



Supplemental Figure 4. MAPK Signaling

(A) Representative image and protein content of immunoblot for MAPK signaling specific markers (p-p38, p38, p-ERK, and ERK). Phosphorylation site of both p38 and ERK was normalized to their total protein content. Protein content data was analyzed from gastrocnemius muscle. Different letters represent statistical differences at Tukey-adjusted with alpha value set at $p \leq 0.05$. An N of 9-14 per group was used.

I. REFERENCES

1. **Ryerson AB, and Massetti GM.** Peer reviewed: CDC's public health surveillance of cancer. *Preventing chronic disease* 14: 2017.
2. **Fearon K, Strasser F, Anker SD, Bosaeus I, Bruera E, Fainsinger RL, Jatoi A, Loprinzi C, MacDonald N, and Mantovani G.** Definition and classification of cancer cachexia: an international consensus. *The lancet oncology* 12: 489-495, 2011.
3. **Kasvis P, Vigano M, and Vigano A.** Health-related quality of life across cancer cachexia stages. *Annals of palliative medicine* 8: 33-42, 2019.
4. **Brown JL, Rosa-Caldwell ME, Lee DE, Blackwell TA, Brown LA, Perry RA, Haynie WS, Hardee JP, Carson JA, and Wiggs MP.** Mitochondrial degeneration precedes the development of muscle atrophy in progression of cancer cachexia in tumour-bearing mice. *Journal of cachexia, sarcopenia and muscle* 8: 926-938, 2017.
5. **Brown JL, Lee DE, Rosa-Caldwell ME, Brown LA, Perry RA, Haynie WS, Huseman K, Sataranatarajan K, Van Remmen H, Washington TA, Wiggs MP, and Greene NP.** Protein imbalance in the development of skeletal muscle wasting in tumour-bearing mice. *J Cachexia Sarcopenia Muscle* 9: 987-1002, 2018.
6. **Blackwell TA, Cervenka I, Khatri B, Brown JL, Rosa-Caldwell ME, Lee DE, Perry RA, Jr., Brown LA, Haynie WS, Wiggs MP, Bottje WG, Washington TA, Kong BC, Ruas JL, and Greene NP.** Transcriptomic analysis of the development of skeletal muscle atrophy in cancer-cachexia in tumor-bearing mice. *Physiol Genomics* 50: 1071-1082, 2018.
7. **White JP, Baltgalvis KA, Puppa MJ, Sato S, Baynes JW, and Carson JA.** Muscle oxidative capacity during IL-6-dependent cancer cachexia. *American Journal of Physiology-Regulatory, Integrative and Comparative Physiology* 300: R201-R211, 2011.
8. **Dasuri K, Zhang L, and Keller JN.** Oxidative stress, neurodegeneration, and the balance of protein degradation and protein synthesis. *Free Radical Biology and Medicine* 62: 170-185, 2013.
9. **Shringarpure R, Grune T, and Davies KJA.** Protein oxidation and 20S proteasome-dependent proteolysis in mammalian cells. *Cellular and Molecular Life Sciences CMLS* 58: 1442-1450, 2001.
10. **Norton JA, Shamberger R, Stein TP, Milne GWA, and Brennan MF.** The influence of tumor-bearing on protein metabolism in the rat. *Journal of Surgical Research* 30: 456-462, 1981.

11. **Rosa-Caldwell ME, Lim S, Haynie WA, Brown JL, Deaver JW, Morena Da Silva F, Jansen LT, Lee DE, Wiggs MP, and Washington TA.** Female mice may have exacerbated catabolic signalling response compared to male mice during development and progression of disuse atrophy. *Journal of Cachexia, Sarcopenia and Muscle* 2021.
12. **Ryberg D, Hewer A, Phillips DH, and Haugen A.** Different susceptibility to smoking-induced DNA damage among male and female lung cancer patients. *Cancer research* 54: 5801-5803, 1994.
13. **Rosa-Caldwell ME, and Greene NP.** Muscle metabolism and atrophy: let's talk about sex. *Biology of sex differences* 10: 1-14, 2019.
14. **Oliván S, Calvo AC, Manzano R, Zaragoza P, and Osta R.** Sex differences in constitutive autophagy. *BioMed research international* 2014: 2014.
15. **White JP, Puppa MJ, Gao S, Sato S, Welle SL, and Carson JA.** Muscle mTORC1 suppression by IL-6 during cancer cachexia: a role for AMPK. *American Journal of Physiology-Endocrinology and Metabolism* 304: E1042-E1052, 2013.
16. **Hetzler KL, Hardee JP, Puppa MJ, Narsale AA, Sato S, Davis JM, and Carson JA.** Sex differences in the relationship of IL-6 signaling to cancer cachexia progression. *Biochimica et Biophysica Acta (BBA)-Molecular Basis of Disease* 1852: 816-825, 2015.
17. **Laker RC, Xu P, Ryall KA, Sujkowski A, Kenwood BM, Chain KH, Zhang M, Royal MA, Hoehn KL, Driscoll M, Adler PN, Wessells RJ, Saucerman JJ, and Yan Z.** A novel MitoTimer reporter gene for mitochondrial content, structure, stress, and damage in vivo. *J Biol Chem* 289: 12005-12015, 2014.
18. **Call JA, McKeehen JN, Novotny SA, and Lowe DA.** Progressive resistance voluntary wheel running in the mdx mouse. *Muscle & nerve* 42: 871-880, 2010.
19. **Gorassini M, Eken T, Bennett DJ, Kiehn O, and Hultborn H.** Activity of hindlimb motor units during locomotion in the conscious rat. *Journal of neurophysiology* 83: 2002-2011, 2000.
20. **Jones LA, and Hunter IW.** Force sensation in isometric contractions: a relative force effect. *Brain research* 244: 186-189, 1982.
21. **Gasier HG, Riechman SE, Wiggs MP, Previs SF, and Fluckey JD.** A comparison of 2H₂O and phenylalanine flooding dose to investigate muscle protein synthesis with acute exercise in rats. *American Journal of Physiology-Endocrinology and Metabolism* 297: E252-E259, 2009.

22. **Smith KL, and Tisdale MJ.** Increased protein degradation and decreased protein synthesis in skeletal muscle during cancer cachexia. *Br J Cancer* 67: 680-685, 1993.
23. **Min K, Smuder AJ, Kwon O-s, Kavazis AN, Szeto HH, and Powers SK.** Mitochondrial-targeted antioxidants protect skeletal muscle against immobilization-induced muscle atrophy. *Journal of applied physiology* 111: 1459-1466, 2011.
24. **Rosa-Caldwell ME, Jansen LT, Lim S, Dunlap KR, Haynie WS, Washington TA, and Greene NP.** Neither autophagy nor exercise training mode affect exercise-induced beneficial adaptations in high fat-fed mice. *Sports Medicine and Health Science* 2020.
25. **Rosa-Caldwell ME, Lim S, Haynie WS, Jansen LT, Westervelt LC, Amos MG, Washington TA, and Greene NP.** Altering aspects of mitochondrial quality to improve musculoskeletal outcomes in disuse atrophy. *Journal of Applied Physiology* 2020.
26. **Greene NP, Lee DE, Brown JL, Rosa ME, Brown LA, Perry RA, Henry JN, and Washington TA.** Mitochondrial quality control, promoted by PGC-1 α , is dysregulated by Western diet-induced obesity and partially restored by moderate physical activity in mice. *Physiological reports* 3: e12470, 2015.
27. **Cosper PF, and Leinwand LA.** Cancer causes cardiac atrophy and autophagy in a sexually dimorphic manner. *Cancer Res* 71: 1710-1720, 2011.
28. **VanderVeen BN, Fix DK, and Carson JA.** Disrupted skeletal muscle mitochondrial dynamics, mitophagy, and biogenesis during cancer cachexia: a role for inflammation. *Oxidative medicine and cellular longevity* 2017: 2017.
29. **Kilgour RD, Vigano A, Trutschnigg B, Lucar E, Borod M, and Morais JA.** Handgrip strength predicts survival and is associated with markers of clinical and functional outcomes in advanced cancer patients. *Supportive Care in Cancer* 21: 3261-3270, 2013.
30. **VanderVeen BN, Hardee JP, Fix DK, and Carson JA.** Skeletal muscle function during the progression of cancer cachexia in the male ApcMin/+ mouse. *Journal of Applied Physiology* 124: 684-695, 2018.
31. **Inaba S, Hinohara A, Tachibana M, Tsujikawa K, and Fukada S-i.** Muscle regeneration is disrupted by cancer cachexia without loss of muscle stem cell potential. *PLoS one* 13: e0205467, 2018.
32. **Greenman AC, Albrecht DM, Halberg RB, and Diffie GM.** Sex differences in skeletal muscle alterations in a model of colorectal cancer. *Physiological reports* 8: e14391, 2020.

33. **Baltgalvis KA, Berger FG, Peña MMO, Davis JM, White JP, and Carson JA.** Muscle wasting and interleukin-6-induced atrogen-I expression in the cachectic Apc Min/+ mouse. *Pflügers Archiv-European Journal of Physiology* 457: 989-1001, 2009.

34. **Carson JA, and Baltgalvis KA.** Interleukin 6 as a key regulator of muscle mass during cachexia. *Exerc Sport Sci Rev* 38: 168-176, 2010.

35. **Knüpfer H, and Preiss R.** Serum interleukin-6 levels in colorectal cancer patients—a summary of published results. *International journal of colorectal disease* 25: 135-140, 2010.

36. **Forcina L, Cosentino M, and Musarò A.** Mechanisms regulating muscle regeneration: Insights into the interrelated and time-dependent phases of tissue healing. *Cells* 9: 1297, 2020.

37. **He WA, Berardi E, Cardillo VM, Acharyya S, Aulino P, Thomas-Ahner J, Wang J, Bloomston M, Muscarella P, and Nau P.** NF- κ B-mediated Pax7 dysregulation in the muscle microenvironment promotes cancer cachexia. *The Journal of clinical investigation* 123: 4821-4835, 2013.

38. **Rosa-Caldwell ME, Lim S, Haynie WS, Brown JL, Lee DE, Dunlap KR, Jansen LT, Washington TA, Wiggs MP, and Greene NP.** Mitochondrial aberrations during the progression of disuse atrophy differentially affect male and female mice. *Journal of Cachexia, Sarcopenia and Muscle* 2021.

39. **Williams JA, Ni H-M, Ding Y, and Ding W-X.** Parkin regulates mitophagy and mitochondrial function to protect against alcohol-induced liver injury and steatosis in mice. *American journal of physiology-gastrointestinal and liver physiology* 309: G324-G340, 2015.

40. **Sowter HM, Ratcliffe PJ, Watson P, Greenberg AH, and Harris AL.** HIF-1-dependent regulation of hypoxic induction of the cell death factors BNIP3 and NIX in human tumors. *Cancer research* 61: 6669-6673, 2001.

41. **Ballarò R, Lopalco P, Audrito V, Beltrà M, Pin F, Angelini R, Costelli P, Corcelli A, Bonetto A, and Szeto HH.** Targeting mitochondria by SS-31 ameliorates the whole body energy status in cancer-and chemotherapy-induced cachexia. *Cancers* 13: 850, 2021.

42. **Hurtley SM.** Mitochondrial quality control. *Science* 350: 1052-1053, 2015.

43. **Zhong X, and Zimmers TA.** Sex Differences in Cancer Cachexia. *Current Osteoporosis Reports* 1-9, 2020.

44. **Montalvo RN, Counts BR, and Carson JA.** Understanding sex differences in the regulation of cancer-induced muscle wasting. *Current opinion in supportive and palliative care* 12: 394, 2018.
45. **Lim S, Brown JL, Washington TA, and Greene NP.** Development and Progression of Cancer Cachexia: Perspectives from Bench to Bedside. *Sports Medicine and Health Science* 2020.
46. **Puppa MJ, Gao S, Narsale AA, and Carson JA.** Skeletal muscle glycoprotein 130's role in Lewis lung carcinoma–induced cachexia. *The FASEB Journal* 28: 998-1009, 2014.
47. **Au ED, Desai AP, Koniaris LG, and Zimmers TA.** The MEK-inhibitor selumetinib attenuates tumor growth and reduces IL-6 expression but does not protect against muscle wasting in Lewis lung cancer cachexia. *Frontiers in physiology* 7: 682, 2017.
48. **Chiappalupi S, Sorci G, Vukasinovic A, Salvadori L, Sagheddu R, Coletti D, Renga G, Romani L, Donato R, and Riuzzi F.** Targeting RAGE prevents muscle wasting and prolongs survival in cancer cachexia. *Journal of cachexia, sarcopenia and muscle* 11: 929-946, 2020.
49. **Cinar D, and Tas D.** Cancer in the elderly. *Northern clinics of Istanbul* 2: 73, 2015.

CHAPTER IV: Manuscript from Specific Aim II

Targeting OPA1 for prevention of cancer-induced muscle loss.

Seongkyun Lim & Nicholas P. Greene

Formatted for Submission to *Journal of Applied Physiology*

A. ABSTRACT

Cancer Cachexia (CC) occurs in approximately 80% of cancer patients and is responsible for 20-40% of cancer-related death although current therapeutic approaches lack sufficient efficacy to prevent it. We previously demonstrated suppressed mitochondrial fusion protein, Optic atrophy 1 (OPA1), during the early development of CC in male tumor-bearing mice. Moreover, prior investigations revealed that loss of OPA1 is associated with lower muscle mass and impaired muscle function. Conversely, overexpression of OPA1 ameliorated the phenotypes of mitochondrial-associated diseases. However, the function of OPA1 as a therapeutic target in CC has not been assessed. The purpose of current study was to elucidate the function of OPA1 in CC using both pharmacological using BGP-15 (*in vitro* and *in vivo*) and genetic overexpression of OPA1 (OPA1 TG) *in vivo*. For pharmacological *in vitro* experiments, C2C12 myotubes were treated with Lewis Lung Carcinoma (LLC)-conditioned media (LCM) with or without BGP-15 (OPA1 drug target). BGP-15 was also administered in LLC-induced tumor-bearing male mice to determine regulation of muscle mass and function. For genetic overexpression experiments, we utilized wildtype (WT) and OPA1 TG mice to further assess the efficacy of OPA1 in tumor-bearing mice. Both BGP-15 *in vitro* and OPA1 TG *in vivo* experiments demonstrated attenuation of muscle loss in response to LLC and LCM-induced CC. BGP-15 *in vitro* mRNA data further suggests the protective effect on muscle wasting with BGP-15 treatment, which appears to be associated with

suppressed inflammatory cytokine and autophagic-lysosomal pathway (ALP) activities mediated via targeting OPA1. Our data suggests OPA1 as a potential therapeutic target for cancer-induced muscle wasting.

KEYWORDS: Mitochondrial fusion, cancer cachexia, skeletal muscle, chemotherapy, and atrophy.

NEW & NOTEWORTHY Our study demonstrates targeting of OPA1 utilizing both BGP-15 administration (*in vivo* & *in vitro*) and genetic overexpression (*in vivo*) were sufficient to attenuate cancer-induced muscle wasting. Our data provide novel evidence that OPA1 may serve as a potential therapeutic target for cancer-induced muscle wasting.

B. INTRODUCTION

Cancer is the 1st or 2nd leading cause of death in more than 110 countries (19). There are approximately 19.3 million new cases of cancer incidence and 9.9 million deaths annually (19). More importantly, the number of new cases is anticipated to grow up to 28 million by 2040 (19). Up to 80% of cancer patients undergo cancer cachexia, a wasting syndrome, which is clinically defined as weight loss (mainly skeletal muscle and adipose tissue) more than 5% in the past 6 months (3). Skeletal muscle mass and function are considered important indicators for quality of life and survival rate among cancer patients. A recent study demonstrated that recurring gastric cancer patients with lower skeletal muscle mass were closely associated with lower survival rates compared to gastric cancer patients with higher relative skeletal muscle mass (198). Along with lower skeletal muscle mass and muscle function, impaired mitochondrial quality has been implicated in both clinical and pre-clinical models of CC (12, 18, 69, 81, 199).

Mitochondrial quality is maintained by four major processes: mitochondrial biogenesis, dynamics (mitochondrial fusion and fission), autophagy, and the mitochondrial permeability transition pore (184, 200). Mitochondrial quality is the basis for maintaining the stability and integrity of mitochondria and is an important defense mechanism against mitochondrial damage (121). However, these mechanisms are often impaired during inflammation-induced diseases including cancer (12, 18). White and coworkers (44) reported dysregulated mitochondrial dynamics in a mouse model of CC. Mitochondrial dynamics are composed of two distinct mechanisms, mitochondrial fusion and fission, the balance between these two determines mitochondrial network health (121). Mitochondrial fusion occurs when two or more mitochondria fuse/converse into one, forming constantly changing tubular organelles, leading to mitochondrial elongation (121). Conversely, mitochondrial fission involves a mechanism by which a mitochondrion pinches off the membrane to form daughter mitochondria (121). Cellular health relies on a delicate balance between mitochondrial fusion and fission (145). Previous evidence

revealed higher fission proteins and lower fusion proteins in a mouse model of CC (44). Interestingly, we found comparable results that tumor-bearing male mice revealed higher mitochondrial fission and lower fusion protein content. Specifically, Optic atrophy 1 (OPA1), a mitochondrial fusion marker, protein content was ~50% lower during the early development of CC and this suppression was maintained into the development of marked atrophy (12).

OPA1 is enriched in the mitochondrial membrane and regulates the fusion of the inner mitochondrial membrane and contributes to ATP synthesis and apoptosis (137-139). Loss of OPA1 is associated with impaired skeletal muscle health including lower muscle mass and function, leading to lower survival rates (166). In addition, OPA1 overexpression ameliorated the phenotype of mitochondrial-associated disease mouse models (167). This prior evidence suggests OPA1 plays a significant role in maintenance of skeletal muscle health and might serve as a potential therapeutic target for skeletal muscle-associated diseases. However, the efficacy of OPA1 as a therapeutic target in cancer-induced muscle atrophy has not been explored. Therefore, the purpose of this study was to determine if pharmacological or genetic targeting of OPA1 may attenuate cancer-induced skeletal muscle atrophy and degeneration including impaired protein turnover, muscle contractile function, and mitochondrial quality utilizing both *in vivo* and *in vitro* models of CC. To determine viability of utilizing currently available compounds to attenuate CC via OPA1, BGP-15 was utilized. BGP-15 known as HSP-72 co-inducer (201), has recently been reported to promote OPA1 protein content (152), and has been demonstrated to attenuate other forms of atrophy (202, 203). To more specifically test the function of OPA1 in CC we utilized previously developed OPA1 transgenic mice which have been demonstrated to attenuate a cachectic phenotype of mitochondrial-associated disease (167). Herein, we demonstrate *in vitro* BGP-15 treatment can attenuate cancer-induced atrophy, and while this effect was absent *in vivo* BGP-15 administration experiment. However, transgenic overexpression of OPA1 ameliorated LLC-induced muscle wasting.

C. METHODS

I. Cell Culture Experiments

C2C12 murine myoblasts (CRL-1772, ATCC, Manassas, VA, USA) were plated in six-well plates (5×10^4 cells/well) in 2 mL Dulbecco's Modified Eagle Medium (DMEM; 11965092, Life Technology, Carlsbad, CA, USA) combined with 10% Fetal Bovine Serum (FBS) and 1% Penicillin/Streptomycin (P/S). Cells were incubated at 37°C with 5% CO₂ and media was changed every 48 hours. Upon ~80% confluence, growth media was replaced with DMEM supplemented with 2% horse serum, 1% P/S, 5% 4-(2-hydroxyethyl)-1-piperazineethanesulfonic acid (HEPES; 15-630-106, ThermoFisher Scientific, Waltham, MA, USA), 0.75% transferrin, and 0.75% insulin for cell differentiation. C2C12 cells were differentiated for 5 days to become mature myotubes. Cell proliferation and differentiation were performed as previously described (81, 204).

i. Lewis Lung Carcinoma Conditioned Media (LCM) and BGP-15 Drug Treatment

To collect LCM, Lewis Lung Carcinoma were grown up to 100% confluence as previously described (81). LLC cells were then incubated in fresh DMEM supplemented with 10% FBS and 1% P/S for 24 hours. The media were then collected and centrifuged. The supernatant was collected and diluted to 25% total volume of LLC media in serum free media (DMEM with 1% P/S). For the control group 25% total volume of CCM (C2C12-conditioned media, prepared as per LCM) was diluted in serum free media. Mature C2C12 myotubes were then treated with either CCM or LCM for 72 hours. The media was changed every 24 hours as described (205). To assess the efficacy of OPA1 in myotubes we treated myotubes either CCM or LCM with or without 10 μ M of BGP-15 (OPA1 target). BGP-15 is primarily described as HSP-72 co-inducer and has been described to promote OPA1 (152). Control cells were treated with same amount of dimethyl

sulfoxide (DMSO). Six replicates (wells) per condition was used and each condition was assessed in two independent experiments (three replicates per each experiment).

ii. C2C12 Myotube Diameter

After myotubes were treated with either LCM or CCM with or without BGP-15 for 72 h, myotubes were imaged with 10x and 40x objective with 5 images per well and 4-5 myotubes examined per well.

iii. FSR in Cell Culture

FSR was assessed using gas chromatography-mass spectrometry (GC-MS) (7890 A and 5977 A, Agilent, Santa Clara, CA, USA) as described (81, 206). Briefly, 4% deuterium (D_2O ; 151882-1 L, Millipore Sigma, Burlington, MA) enrichment was diluted in 1.5 mL of culture media in each 6-well plate 24 hours prior to cell harvest. Upon cell harvest, 6-well plate was washed with PBS twice and added with 300 μ L of 10% trichloroacetic acid (TCA) solution per well and cell lysates were collected using cell scraper and transferred to 1.5 mL tubes. These lysates were then homogenized for FSR. Mixed protein fractions were then washed three times with 10% TCA solution by centrifugation to eliminate cytosolic amino acids. Proteins were then transferred in a 1.5 mL tube with 200 μ L of 6 M HCl and heated at 100 C to hydrolyze proteins into amino acids for 24 hours. An aliquot (50 μ L) of the hydrolysate was dried down and derivatized with same amount of 3:2:1 solution of methyl-8, methanol, and acetonitrile to determine 2H labeling of alanine on its methyl-8 derivative. The derivatized solution was then placed in a GC-MS capillary column (7890 A GC HP-5 ms capillary column, Agilent). 1 μ L of the solution was run on the GC-MS at a 20:1 split. A ratio of deuterated alanine over alanine was used to assess protein synthesis.

The detailed method for FSR calculation was described in the methods for Chapter III and elsewhere (81, 206).

iv. C2C12 RNA isolation, cDNA synthesis, and quantitative real-time PCR

After 72 hours of LCM intervention, the media was aspirated and washed with PBS. 1 mL of TRIzol reagent was added to each well in 6-well plate and cell lysates were then collected in a 1.5 mL microtube placed on ice. After 15-min at room temperature, 200 μ L of chloroform was added and samples were vortexed for 5-second and centrifuged for 25-min. After the centrifugation, the clear portion of the solution from the top was placed into a new 1.5 mL microtube. An equal amount of 70% of Diethyl Pyrocarbonate (DEPC) treated ethanol was added, and the samples were loaded into a RNeasy column. RNA isolation was then processed using an RNA isolation kit (K145002; Invitrogen, Carlsbad, CA, USA) per manufacturer protocol. A detailed RNA isolation processes and RT-qPCR assessment were described in the methods for Chapter III and prior study (206). Target TaqMan probes for *18s* (Mm03928990_g1), *IGF1* (Mm00439560_m1), *REDD1* (Mm00512504_g1), *DEPTOR* (Mm01195339_m1), *UBC* (Mm02525934_g1), *GADD45a* (Mm00432802_m1), *Atrogin1* (Mm00499523_m1), *Murf1* (Mm01185221_m1), *FOXO1* (Mm00490671_m1), *FOXO3* (Mm01185722_m1), *IL-6* (Mm00446190_m1), *TNF- α* (Mm00443258_m1), *NF-Kb1* (Mm00476361_m1), *NF-Kb2* (Mm00479807_m1), *LC3* (Mm00458724_m1), *p62* (Mm01700766_M1), *Cyclin-D1* (Mm00432359_m1), *Pax7* (Mm01354484_m1), *MyoD* (Mm01203489_g1), *Myogenin* (Mm00446194_m1), *PGC1- α 1* (Mm01208835_m1), *PPAR γ* (Mm01184322_m1), *NRF2* (Mm_00477784m1), and *DRP1* (Mm_00432881_m1) were purchased from Applied Biosystems (Life Technologies). Additional custom primer pairs specific for *ATG7*, *Beclin-1*, *Bnip3*, *PPAR α* , *TFAM*, *OPA1*, *MFN1*, *MFN2*, *MFF*, *FIS1*, and *OPA1* were used in which primer information has

been reported previously (12, 81, 184). All targets were normalized to the 18s Ct value, which did not differ between experimental groups.

II. Animal Interventions

Two separate sets of animal experiment were performed. 1) The first experiment was designed to test the efficacy of BGP-15 to target OPA1 protein using mice treated with daily administration of BGP-15 following tumor implantation, similar to *in vitro* experiments. 2) Second, to more specifically determine if OPA1 promotion attenuates cancer-induced cachectic phenotypes including muscle loss utilizing muscle OPA1 transgenic (TG) mice. By performing these paired experiments, we were able to assess the specific function of OPA1 while also providing whether pharmaceutical interventions with impacts on OPA1 may provide potential therapeutic efficacy. All animal methods were approved by the Institutional Animal Care and Use Committee of the University of Arkansas.

Experiment 1) 33 male C57BL/6J mice were purchased from Jackson Laboratory (000664, Bar Harbor, ME, USA) and divided into 4 different experimental groups (7-9 mice per group), (Con-PBS, Con-BGP-15, LLC-PBS, & LLC-BGP-15), (Con: control, PBS: phosphate-buffered saline, & LLC: Lewis lung carcinoma). Con-BGP-15 and LLC-BGP-15 animals were given a daily administration of BGP-15 (20mg/K BW) at 8 wks of age for 21 days while control animals were given a daily administration of PBS.

Experiment 2) 21 male (16 OPA1 TG and 5 WT) mice (C57BL/6J background) were divided into 4 groups (WT-PBS, WT-BGP-15, OPA1-PBS, & OPA1-BGP-15). OPA1 TG mice were developed by Dr. Luca Scorrano (U. Padova) and initial OPA1 TG breeders were provided by Dr. Thomas Sanderson (U. Michigan) via Dr. Luca Scorrano (U. Padova) and the breeding colony was maintained at our animal facility.

All experimental mice were kept on a 12:12-h light-dark cycle, housed at 72 degrees Fahrenheit, and given *ad libitum* access to normal rodent chow and water for the duration of the study. At 8 wks of age, experimental mice from both studies were subcutaneously given an injection of either LLC cells (1×10^5 /side) suspended in 100 μ L sterile (PBS) or an equal volume of sterile PBS as a sham control to both right and left hind flank. Tumors were allowed to develop for up to 3 to 4 wks. 5 muscle (soleus, plantaris, gastrocnemius, TA, and EDL) and 5 non-muscle tissues (heart, liver, spleen, tumor, and gonadal fat) were collected and tissue wet weight was measured. Plasma was separated from the blood by centrifugation. Tissue and plasma samples were then snap-frozen in liquid nitrogen and stored at -80°C for further analysis. All tissue weights were normalized to their initial bodyweight to account for different body mass prior to the LLC implantation.

i. Lewis Lung Carcinoma Cell Culture

LLC cells (CRL-1642, ATCC, Manassas, VA, USA) were plated in a 250 mL cell culture flask in 10% growth media with 1% penicillin/streptomycin and media was changed every 48 hours. Upon ~80% confluence, cells were trypsinized, suspended, and diluted in PBS prior to LLC implantation as described in the methods for Chapter III and prior study (12).

ii. Plasmid DNA Amplification and Electroporation

pMitoTimer plasmid were amplified and plasmid DNA were isolated using PureLink HiPure Plasmid Filter Maxiprep kit (K211017, Life Technologies) as per manufacturer protocol. At 6 wks of age, pMitoTimer plasmid were transfected into the right flexor digitorum brevis (FDB) muscle. More detailed protocols for pMitoTimer transfection were described in the methods for Chapter III and elsewhere (12, 204).

iii. In vivo Muscle Contractility Test

Approximately 48 hours prior to tissue collection, *in vivo* peak isometric torque, isometric torque frequencies, frequency at half maximum torque, 1/2 relaxation time, time to maximal contraction, and fatigability (susceptibility to fatigue) of the anterior crural (shin) muscles were performed as described (161). Briefly, while mice were anesthetized, the left hindlimb was shaved and an ethanol pad applied to clean the skin. The foot was placed in a footplate attached to a servomotor (Model 300B-LR, Aurora Scientific, Aurora, Ontario, Canada) using surgical tape while their body temperature was maintained at 37 °C using a heating pad. Two platinum electrodes (Model E2-12, Grass Technologies, RI, USA) were then inserted percutaneously on either side of the peroneal nerve. Muscle contractions were induced via electrical stimulator and stimulus isolation unit (Model S48 and SIU5, respectively; Grass Technologies). Torque and M-wave as a function of stimulation frequency were measured during 12 isometric contractions with the duration of 150 ms at various stimulation frequencies (10, 20, 30, 40, 60, 80, 100, 125, 150, 200, 250, and 300 Hz) to determine hindlimb motor unit recruitment based on two different physiological conditions: 1) hindlimb motor unit recruitments during normal movement, which occurs between 60 and 100 Hz(178). 2) During supra-maximal stimulation frequencies (i.e., >200 Hz) can reveal different contractile phenotypes such as low-frequency fatigue (179) followed by resting the hindlimb for 4-min. After measurement of submaximal and maximal isometric torques at 150 Hz, the anterior crural muscles underwent a fatigability test via applying 120 isometric contractions with duration of 150 ms per each stimulation at 40 Hz for a total protocol time of 2-min. During the recovery following the fatigability test, the normal movement of experimental mice was closely monitored to determine any injuries during the *in vivo* muscle force production and fatigability test.

iv. Fluorescence Microscopy for pMitoTimer

pMitoTimer was analyzed as previously described (12). Briefly, at the time of tissue harvesting, freshly collected FDB muscles were fixed with 4% paraformaldehyde (PFA) for 20-min followed by 5-min incubation with PBS at room temperature. Muscles were then spread out on a gelatin-coated glass slide using 2 forceps and mounted with a drop of 50% glycerol in PBS as mounting media. A coverslip was added on the top of the mounted sample and 4 drops of nail polish were applied at the corners to anchor the coverslip. pMitoTimer images were acquired at x100 magnification using the FITC (green; excitation/emission, 488/518 nm) and TRITC (red; excitation/emission, 543/572 nm) fluorescent channels on a Nikon Eclipse Ti-S inverted epifluorescent microscope (Nikon, Melville, NY, USA) with LED-based light source. Standardized acquisition parameters were established and followed for all imaging to match across samples. All assessments were performed in congruence with Laker et al. (163). A specially generated MATLAB program, a generous gift from Dr. Zhen Yan (U. Virginia), was used to analyze pMitoTimer red to green ratio (a mitochondrial oxidative stress marker) and pure red puncta number (a marker for completely degenerated mitochondria) (163).

v. Preparation of Separated and Permeabilized Muscle Fibers

During tissue harvesting, ~15 mg of fresh plantaris and gastrocnemius muscles were collected and placed in a petri dish containing ice-cold buffer X (60 mM K-MES, 35 mM KCl, 7.23 mM K₂EGTA, 2.77 mM CaK₂EGTA, 20 mM imidazole, 0.5 mM DTT, 20 mM taurine, 5.7 mM ATP, 15 mM phosphocreatine, and 6.56 mM MgCl₂ at pH 7.1). Connective tissues and blood clots were eliminated, and the fiber bundles were gently separated into a near-single fiber bundle to maximize their surface area under an upright stereoscopic microscope (Fisher Scientific, Waltham, MA, USA) using a pair of extra-sharp forceps (Fisher Scientific). The finely separated fiber bundles were then permeabilized in a tube with saponin (50 µg/mL) on a rotator for 30-min

at 4 °C. The permeabilized fiber bundles were washed in ice-cold buffer Z (110 mM K-MES, 35 mM KCl, 1 mM EGTA, 5 mM K₂HPO₄, 3 mM MgCl₂, 0.005 mM glutamate, 0.02 mM malate, and 0.5 mg/ml BSA at pH 7.1) for 5-min x 3 times as previously described (12, 181). The permeabilized fiber bundles were then used for mitochondrial RCR (12).

vi. Mitochondrial Respiratory Control Ratio (RCR)

Mitochondrial oxygen consumption was measured by polarography in a respiration chamber maintained at 37 °C (Oxygraph+, Hansatech Instruments, King's Lynn, UK) as described (12) and this method was adapted from Min et al (181). Briefly, permeabilized plantaris muscles were transferred to a respiratory chamber filled with 1 mL of respiration buffer Z containing creatine (20 mM) to saturate creatine kinase and allowed to equilibrate with the tissue for 5- to 10-min before adding any substrate. State 2 respiration was assessed by the addition of malate and pyruvate (5mM) using 10 µL 701RN Syringes (Hamilton, Reno, NV, USA) followed by maximal ADP-stimulated respiration (State 3) by adding ADP (0.25 Mm) and then basal mitochondrial respiration (State 4) by the addition of oligomycin (10 µg/mL) to inhibit ATP synthesis. The respiratory control ratio (RCR) was calculated by dividing State 3 by State 4 respiration.

vii. Statistics

For cell experiments, a two-way ANOVA was used as the global analysis for each dependent variable. Independent variables were Media condition (CCM versus LCM) and drug condition (dimethyl sulfoxide (DMSO) versus BGP-15). For animal experiments, a two-way ANOVA was utilized. Independent variables within each sex included genotype (WT vs. OPA1 TG) and injection type (LLC vs. PBS). When significant F ratios were found, statistical differences

among means were determined by Tukey's post hoc test. The comparison-wise error rate, α , was set at $P < 0.05$ for all statistical tests. All two-way ANOVA data and figures were analyzed using GraphPad Prism (La Jolla, CA). Data were expressed as means \pm standard error (SEM).

Footnote: All figures can be found at the end of chapter IV.

D. RESULTS

i. BGP-15 attenuates LCM-induced myotube atrophy.

To determine the efficacy of BGP-15 on myotube size during muscle cell atrophy in response to LCM, we treated myotubes with or without BGP-15. We found an interaction effect on myotube diameter. Specifically, myotubes treated with LCM-CON and LCM-BGP-15 were smaller in LCM-CON (~16%; $p < 0.001$) and LCM-BGP-15 (~9%; $p = 0.002$) compared to CCM-CON. Although LCM-CON myotubes were ~12% smaller than CCM-BGP-15 ($p < 0.001$), no statistical differences were found between CCM-BGP-15 and LCM-BGP-15. Myotubes treated with LCM-CON were ~7% smaller than LCM-BGP-15 ($p = 0.028$; **Figure 1A-B**).

To determine protein synthesis, we assessed FSR via 24 hrs of D₂O labeling. Although there was no main effect of LLC on FSR due to smaller sample size in LCM-CON, FSR was ~25% lower in myotubes treated with LLC (**Figure 1C**). FSR of LCM-CON was ~5.3-fold lower than LCM-BGP-15 (**Figure 1C**). To further assess regulation of the protein anabolic system, mRNA level of anabolic suppressors (DEPTOR and *REDD1*) and regulating factors (*Insulin like growth factor1 [IGF]*) were assessed. An interaction effect on *REDD1* was observed, where *REDD1* mRNA content was ~28% ($p = 0.041$) and ~53% ($p < 0.001$) higher in CCM-BGP-15 compared to LCM-CON and LCM-BGP-15, respectively (**Figure 1D**). There are no further statistical differences found in *DDPTOR* and *IGF1* mRNA level (**Figure 1E-F**).

ii. Suppressed autophagic-lysosomal pathway (ALP) and inflammatory cytokine mRNA in myotubes treated with BGP-15.

To determine alterations to protein degradation systems, we first examined mRNA content for ubiquitin-proteasome system (UPS). Although E3 ubiquitin ligases, *Atrogin*, and *MuRF* were unchanged among experimental groups, *Ubiquitin C (UBC)* revealed an interaction effect.

Specifically, *UBC* mRNA level was ~77% higher in CCM-BGP-15 compared with CCM-CON ($p=0.029$; **Figure 2A-C**). To further assess upstream targets for E3 ligases, we assessed *FOXO1* and *FOXO3*. While no changes were found in *FOXO1*, there was an interaction effect on *FOXO3* mRNA content, which was greater in CCM-BGP-15 (~51%; $p=0.011$) and LCM-CON (~44%; $p=0.031$) compared with CCM-CON (**Figure 2D-E**). As protein degradation was mainly driven by APS and ALP, we assessed mRNA content for ALP-related genes including *ATG7*, *p62*, *LC3*, and *Beclin*. A main effect of BGP-15 was noted on *ATG7*, with BGP-15 treated myotube exhibiting ~57% lower *ATG7* mRNA content compared with CON myotubes ($p=0.014$; **Figure 2F**). We found an interaction effect of *p62*. Specifically, *p62* mRNA level was ~37% greater in LLC-CON compared with CCM-CON ($p=0.028$) while this effect was absent between CCM-CON and LLC-BGP-15 (**Figure 2G**). There are no statistical differences in *LC3* and *Beclin*, although *Beclin* was ~49% higher in BGP-15 than CON ($p=0.066$; **Figure 2H-I**).

Since inflammatory cytokines play a crucial role in CC, we assessed mRNA content for pro-inflammatory cytokines (*IL-6* & *TNF- α*) and *NF- κ B*. We found a main effect of LCM on *IL-6*, where *IL-6* was ~7.7-fold greater in LCM-treated myotubes compared to CCM control ($p=0.002$; **Figure 2J**). A main effect of BGP-15 noted on *TNF- α* level that the BGP-15 group was ~73% lower in *TNF- α* compared with CON myotubes ($p=0.038$). We did not find any statistical differences in *NF- κ B2* mRNA content (**Figure 2L**).

iii. Greater OPA1 and compensatory regulation of mitochondrial quality control mRNA levels in response to BGP-15 treatment in myotubes.

Considering that BGP-15 is an upstream target for *OPA1*, which is a mitochondrial fusion protein, we sought to assess mitochondrial dynamics markers (mitochondrial fusion and fission) at the mRNA level. A main effect of LLC was noted on *mitochondrial fission 1 (FIS1)* that *FIS1* mRNA level was ~42% lower in both LCM treated myotubes compared to CCM treated ($p<0.001$;

Figure 3A). Although not statistically significant, *DRP1* was ~45% lower in LCM-BGP-15 compared with CCM-BGP-15 ($p=0.063$; **Figure 3B**). No statistical significance was found in *MFF*. A main effect of BGP-15 was noted on *OPA1*, with BGP-15 treated myotubes showing ~64% greater *OPA1* mRNA content compared with CON myotubes ($p=0.046$; **Figure 3D**). No significant difference was found in other mitochondrial fusion markers including *MFN1/2* (**Figure 3E-F**).

To determine mitochondrial biogenesis, we assessed mRNA content for *PGC1 α 1*, *PPAR γ* , *TFAM*, and *NRF2*. We found a main effect of LCM on *PGC1- α 1*, with LCM treated myotubes were ~84% higher in *PGC1- α 1* levels compared with CCM treated myotubes (**Figure 3G**). We did not find any statistical significance in other mitochondrial biogenesis markers including *PPAR γ* , *TFAM*, and *NRF2* (**Figure 3H-J**) *BNIP3* as a mitophagy marker revealed a main effect of LCM, with LCM treated myotubes were ~53% lower in *BNIP3* mRNA content compared with CCM myotubes (**Figure 3K**).

iv. Unchanged cell cycling and myogenic regulators in response to LCM or BGP-15 treated myotubes.

To determine changes in cell cycling and myogenic regulators in response do LCM with or without BGP-15, we assessed mRNA content for *Pax7*, *MyoD*, *Myogenin*, and *cyclin D1*. Although we did not find any statistical significance in those markers, the mean mRNA contents for *Pax7*, *MyoD*, and *Myogenin* were ~42%, ~51%, ~44% lower in BGP-15 treated myotubes compared with CON myotubes, respectively (**Figure 4A-D**).

v. Potential role of BGP-15 in CC in vivo.

Tissue weights from all animals are presented in **Figure 5**. Tissue weights for different skeletal muscles and non-skeletal muscles were measured to determine the efficacy of BGP-15

in response to LLC-induced tumor development. We found a main effect of LLC on tumor-free bodyweight that LLC mice were ~12% lower in tumor-free bodyweight compared with CON mice ($p=0.008$; **Figure 5A**). In skeletal muscle tissues, we found a main effect of LLC on soleus, plantaris, and gastrocnemius muscles. Specifically, muscle tissue weights of LLC mice were ~13% (soleus; $p=0.018$), ~9.7% (plantaris; $p=0.049$), and ~13% (Gastrocnemius; $p=0.023$) lower compared with CON mice, respectively (**Figure 5 A, B, & E**). An additional main effect of LLC was noted in non-skeletal muscle tissues, with LLC mice having ~13% lower heart ($p<0.001$), ~31% lower gonadal fat ($p=0.009$), and ~1.9-fold higher spleen tissue weights ($p<0.001$), respectively (**Figure 5H, I, & K**). There are no statistical differences in bodyweight, EDL, TA, liver, and tumor weights among experimental groups (**Figure 5**).

vi. Impaired muscle contractile function in LLC-induced tumor-bearing mice, but no protective effect with BGP-15 administration.

To determine muscle contractile function, we performed an *in vivo* electro-physiology test to assess torque frequencies, fatigability, peak torque force, time to maximal contraction, half-relaxation time, and Hz at 50% maximal contraction. We found an interaction effect on torque frequencies, with CON-PBS mice having ~45-57% greater torque at lower frequencies (from 30 to 60 Hz) compared with CON-BGP-15 and LLC-PBS mice ($p<0.05$; **Figure 6A**). There was a main effect of LLC on fatigability that the fatigability of LLC mice, where the fatigability of LLC mice was ~12-20% lower from 40 to 70 stimulations compared with CON animals ($p<0.05$; **Figure 6B**). We did not find statistical differences in peak torque, time to maximal contraction, half-relaxation time, and Hz at 50% maximal contraction among experimental groups (**Figure 6C-F**).

vii. Mitochondrial degeneration induced by LLC was attenuated by BGP-15 administration.

To determine mitochondrial network health, we assessed computational analysis of MitoTimer fluorescence. Although we did not find any statistical differences in MitoTimer red to green ratio (measurement for oxidative stress), we found a main effect of BGP-15 in pure red puncta (marker for complete mitochondrial degeneration due to mitophagy), with BGP-15 mice having ~71% lower pure red puncta level compared with PBS animals (**Figure 7A-C**).

viii. LLC induced muscle wasting was ameliorated by OPA1 overexpression in vivo (OPA1 TG).

Tissue weights from all animals are presented in **Figure 8**. At 8 wks of age, we found a significant difference in initial bodyweight (before the intervention) between WT and OPA1 TG animals, where OPA1 TG animals were ~5% lower compared to WT counterparts ($p=0.028$; **Figure 8L**). Therefore, tissue weight data were normalized to their initial BW prior to the LLC or PBS administration. We found a main effect of LLC with multiple tissues, with tumor-bearing mice having lower tumor-free body weight (~5%; $p=0.022$), gastrocnemius muscle (~7%; $p=0.009$), EDL muscle (~18%; $p=0.06$), and greater spleen tissue weight (~1.4-fold; $p=0.014$) compared with PBS animals (**Figure 8A, C, F, K**). A main effect of TG was found across multiple muscles, with OPA1 TG mice having higher soleus (~14%; $p=0.015$), gastrocnemius (~10%; $p=0.008$), plantaris (~%, $p=0.044$), EDL (~28%; $p=0.017$), and heart (~17%; $p=0.017$) weights relative to initial BW compared to WT animals (**Figure 8B-C, E-F, I**). There were no additional statistical differences in other tissue weights (TA, liver, fat, and tumor weight; **Figure 8D, G, H, J**).

ix. Unchanged muscle contractile function in OPA1 TG mice.

To further determine skeletal muscle contractile function mouse *in vivo* muscle electrophysiology was performed for torque frequency curve, peak isometric torque, fatigability, time to

maximal contraction, and time to half-relaxation. Although there were no statistical differences in torque frequencies and peak torque among experimental groups (**Figure 9A & C**), we found an interaction effect on multiple points of fatigability, with OPA1 TG-PBS animals showing ~6-26% greater torque at 10-40th stimulations compared to other animal groups ($p < 0.05$; **Figure 9B**). There was an interaction effect on time to maximal contraction, with WT-PBS mice having ~1.1-fold faster time to maximal contraction compared to other groups ($p = 0.013$, **Figure 9D**). No additional statistical differences were found in half-relaxation time and Hz at 50% maximal contraction (**Figure 9E-F**).

x. Unchanged mitochondrial network health & function in OPA1 TG mice.

Mitochondrial network health was assessed via computational analysis of MitoTimer fluorescence. We did not find any statistical differences in MitoTimer red to green ratio or pure red puncta although mean pure red puncta counts were ~53% higher in WT-LLC mice compared with OPA1-LLC (**Figure 10A-C**).

To determine mitochondrial respiratory capacity RCR was measured. We did not find any statistical differences on RCR among experimental groups (**Figure 10D-E**).

E. DISCUSSION

In the current study, we sought to determine if targeting OPA1 may attenuate cancer-induced muscle wasting by utilizing both pharmacological (both *in vivo* and *in vitro*) and a genetic overexpression model (*in vivo*). To our knowledge, this is one of the first studies to test the function of OPA1 in CC. We demonstrated both pharmacological and genetic overexpression of OPA1-induced a protective effect on muscle wasting. Our mRNA data from BGP-15 *in vitro* experiments revealed a protective effect on inflammatory and autophagy systems in myotubes treated with LCM plus BGP-15. This may suggest a potential mechanism of how OPA1 plays a role in cancer-induced muscle wasting. OPA1 TG *in vivo* experiments also resulted in an attenuation of muscle wasting in OPA1 overexpressed animals in response to LLC-induced cachexia. However, BGP-15 was largely ineffective as an *in vivo* approach to attenuate CC suggesting, therefore further experiments are necessary to identify translational therapeutic strategies that may target OPA1 to attenuate CC. Findings from BGP-15 *in vitro* and OPA1 TG *in vivo* experiments suggest OPA1 as a potential target to mitigate cancer-induced muscle wasting.

First, we set to test the efficacy of BGP-15, a pharmacological inducer of inducible HSP72, recently reported to promote OPA1 protein content (152), to alleviate cachexia *in vitro*. We treated differentiated myotubes with LCM to induce CC. LCM resulted in a smaller myotube diameter compared with the CCM control group, which was attenuated with BGP-15 intervention. This was partially supported by our protein synthesis data via FSR using 24 hrs of the D₂O labeling method. Lower protein synthesis in myotubes treated with LCM was normalized by BGP-15 although it did not reach a statistical significance. Previous studies reported 5 days of BGP-15 administration in a rodent intensive care unit (ICU) model resulted in attenuation of soleus muscle loss (203). Another study showed that 10 days of BGP-15 treatment after a muscle injury was able to ameliorate muscle atrophy (202). In addition, Campelj and coworkers (207) demonstrated that chemotherapy (irinotecan)-induced muscle atrophy was normalized by BGP-15 administration.

These prior investigations including the current study suggest BGP-15 may serve as a potential therapeutic target for various muscle atrophic conditions.

To further determine potential molecular mechanisms involved in muscle mass regulation in response to BGP-15 *in vitro*, we assessed various cellular signaling markers and pathways at the mRNA level via RT-qPCR. First, we found elevated mRNA content of *OPA1* in myotubes treated following BGP-15 intervention, indicating the BGP-15 treatment *in vitro* was sufficient to promote *OPA1* mRNA content. Our mRNA data shows that some of the cellular signaling markers including inflammation and autophagy associated targets along with *OPA1* appear to be involved in preventing muscle loss in LCM-mediated CC *in vitro*. Various pro-inflammatory cytokines such as tumor necrosis factor- α (TNF- α) and interleukin-6 (IL-6) have long been known to play an essential role in CC (9, 208, 209). These pro-inflammatory cytokines are often elevated in inflammation-mediated diseases including cancer, altering various cellular pathways associated with weight loss, especially skeletal muscle and adipose tissue weights via increasing protein degradation systems and lipolysis (9, 81). In line with the prior evidence, we found elevated *IL-6* and *TNF- α* mRNA content in LCM-induced myotubes. Interestingly, the *TNF- α* level remained low when myotubes were treated with BGP-15, suggesting BGP-15 might have an effect to inactivate *TNF- α* , thereby interfering protein degradation system in CC.

Protein degradation is mainly driven by two distinct mechanisms, the UPS and ALP, which are often activated during different forms of muscle atrophic conditions including cancer (12, 206) and disuse (10, 11). Our data revealed that UPS-associated mRNA markers such as ubiquitin E3 ligases (*Atrogin* and *MuRF*) and *FOXO1* remained unchanged. However, we found interesting changes in ALP-related markers. Specifically, autophagy-related 7 (*ATG7*), an important gene essential for autophagy and cytoplasmic to vacuole transport (210), remained low in BGP-15 treated myotubes. In addition, sequestosome-1 (*p62*), an autophagosome cargo protein that targets other proteins for selective autophagy (211), was higher in LCM treated myotubes

compared with CCM control, which was normalized by BGP-15 treatment. Taken together, these observations from our *in vitro* experiments suggest promotion of *OPA1* via BGP-15 overexpression appears to be associated with lowering inflammatory cytokine and ALP activities, thereby attenuating muscle loss in response to CC *in vitro*.

Activation of pro-inflammatory cytokines is one of the hallmarks of CC, which has been implicated with dysregulation of the mitochondrial quality control (MQC) system including mitochondrial biogenesis and dynamics (fusion and fission) (12, 18). *OPA1* regulates the fusion of the inner mitochondrial membrane and contributes to maintaining mitochondrial integrity (212). Previous studies demonstrated depletion of *OPA1* dysregulated genes associated with mitochondrial dynamics and biogenesis (212). Furthermore, Civiletto and coworkers (167) demonstrated that overexpression of *OPA1* ameliorated phenotypes of mitochondrial-associated diseases such as muscle wasting and impaired mitochondrial function in mice. In the current study, BGP-15 intervention *in vitro* induced greater *OPA1* mRNA content both in CCM and LCM treated myotubes. Although we did not find any main effect of BGP-15 in mitochondrial fission and biogenesis markers, we observed a compensatory main effect of LLC in mitochondrial fission and biogenesis. Specifically, we found upregulation of *PGC-1 α* and downregulation of *FIS1* and *BNIP3*. Previous investigations demonstrated that these three MQC-related markers are often dysregulated in response to CC in the opposite direction (downregulation of *PGC-1 α* and upregulation of *FIS1* and *BNIP3*) (12, 18, 44, 206) from what we observed in the current study. This might suggest a compensatory mechanism of mitochondrial fission and biogenesis in response to LCM-induced CC *in vitro*. Further investigations are warranted to determine protein content of these markers to determine more precise regulations of MQC in LCM-induced CC.

Based on observations from this *in vitro* study, we sought to test the function and role of *OPA1* in a mouse model of CC using both pharmacological (BGP-15 administration) and skeletal muscle-specific genetic overexpression of *OPA1*. In the current study, we used LLC-induced

tumor-bearing mice as an animal model of CC. This model has been well studied by our group (12, 81, 206) and others (194, 213, 214) and validated to induce cachectic phenotypes including marked muscle loss within 4 wks following tumor implantation (194, 206). In line with prior studies, both animal studies induced marked skeletal muscle loss in response to LLC allograft. For the BGP-15 *in vivo* experiments, mice administered with BGP-15 did not exhibit any protective effects on muscle tissue weights, which was not corresponding to previous studies utilizing BGP-15 treatment in atrophic rodents (202, 203, 207). The discrepancy between prior studies and the current study was that while we used an IP injection of BGP-15 (20mg/kg) for 21 days, others utilized either a higher dose (40mg/kg) (203) or a different method of delivery (oral gavage) (202). Most importantly, while others utilized a mechanically ventilated rat ICU (203) or chemotherapy-induced cachectic mouse model (207), we used a tumor-bearing mouse model. It is likely the tumor allograft presented with confounding effects of BGP-15 on the tumor which must be accounted for in pharmacologic approaches to treat CC. To our knowledge, we are the first to test the efficacy of BGP-15 in tumor-bearing mice.

In addition to a loss of muscle mass, impaired skeletal muscle function is prevalent in CC such as lower muscle contractility and accelerated muscle fatigue in both animals (68, 69) and humans (65). In the current study, tumor-bearing mice exhibited exacerbated muscle fatigability although BGP-15 treatment did not impact fatigability. Furthermore, lower torque frequencies were present in LLC-PBS mice compared with CON-PBS group, which appeared partially attenuated by BGP-15 treatment at low stimulation frequencies. Muscle contractility can be governed by various contractile units such as fiber type, motor unit, ATPase activity, and neuromuscular connection (67, 215). Since BGP-15 did not affect muscle mass in tumor-bearing mice, the partial correction of torque frequencies in LLC-BGP-15 mice may have been driven by preserved contractile units in the development of CC.

Since mitochondrial quality is often dysregulated in various models of muscle atrophy (12, 18, 206), we assessed computational analysis of MitoTimer fluorescence to determine mitochondrial network health. We found greater MitoTimer pure red puncta in the LLC-PBS group, which was normalized by LLC-BGP-15 treatment, indicating LLC-induced mitochondrial degeneration appears to be partially attenuated with BGP-15 administration. MitoTimer pure red puncta is considered as an indicator for mitochondria targeted for removal from the cell via mitophagy (163). We have previously reported elevation of MitoTimer pure red puncta and mitophagy level such as BNIP3 in tumor-bearing mice (12, 206). Therefore, it is plausible attenuation of pure red puncta level in LLC-BGP-15 mice was partially mediated by decreased mitophagy activity in CC although the underlying mechanism is still unclear. Hence, further studies are required to test the function of BGP-15 in the comprehensive aspects of mitochondrial degeneration in CC.

We originally hypothesized that BGP-15 would induce protective effects on muscle wasting via targeting OPA1 in tumor-bearing mice. However, muscle atrophy induced by tumor development was not attenuated with BGP-15 administration. These findings were not matched with our BGP-15 *in vitro* data, which suggests BGP-15 action *in vivo* might be confounded by tumor presence. Accordingly, to more specifically test the role of OPA1 in CC, we utilized skeletal muscle-specific overexpression of *OPA1* in tumor-bearing mice. Interestingly, LLC-induced muscle wasting including gastrocnemius and EDL was attenuated with *OPA1* overexpression while the tumor mass was unchanged compared with WT-LLC mice. A prior study showed that COX15 deficient mice (mitochondrial disease model) exhibited smaller muscle cross-sectional area (CSA) and impaired mitochondrial function, however, these negative effects were normalized by *OPA1* overexpression (167). Evidence from the current study and others therefore suggests *OPA1* may play an essential role in regulating different forms of muscle atrophy.

To further determine if OPA1 overexpression can induce protective effects on common cachectic phenotypes including impaired muscle contractile function and mitochondrial network health in response to tumor development, we applied the same assessments performed for the BGP-15 *in vivo* experiments. We did not find any changes in muscle torque frequency or peak isometric torque among the experimental groups. In fatigability measurement, however, we found greater fatigability in OPA1-PBS mice than in other groups while this effect was absent in OPA1-LLC group. Furthermore, mean torque frequency was slightly lower in OPA1-LLC mice compared with other groups. It is worth mentioning one of the limitations of this study that the number of mice in OPA1 TG groups was 2 to 3 per group, while WT animals were 7 to 8 per group. There was relatively high variability between two mice in that OPA1-LLC group, resulting in a lower mean torque frequency with relatively higher SEM. Since this study is still ongoing, these muscle contractility data might be different from the current data once we have sufficient power for these assessments. At the end of the current OPA1 TG project, we are expected to have 10-12 mice per each group.

In conclusion, we sought to determine the function of OPA1 utilizing both a pharmacological induction (both *in vitro* and *in vivo*) and genetic overexpression of OPA1 method (*in vivo*). Both BGP-15 *in vitro* and OPA1 TG *in vivo* experiments resulted in attenuation of muscle loss in response to LLC and LCM intervention, suggesting the potential efficacy of targeting OPA1 in CC. However, *in vivo* data with treatment by BGP-15 do not suggest a likely use of BGP-15 as a viable therapeutic for CC and thus a need remains to discover viable options to target OPA1 during CC. BGP-15 *in vitro* mRNA data suggests that a protective effect on muscle wasting via BGP-15 treatment appears to be associated with lower inflammatory cytokine as well as ALP activities potentially mediated by *OPA1* upregulation. Although the OPA1 TG *in vivo* experiment is still ongoing, the current data provides a promising therapeutic potential for cancer-induced muscle wasting.

F. FIGURES

Figure 1.

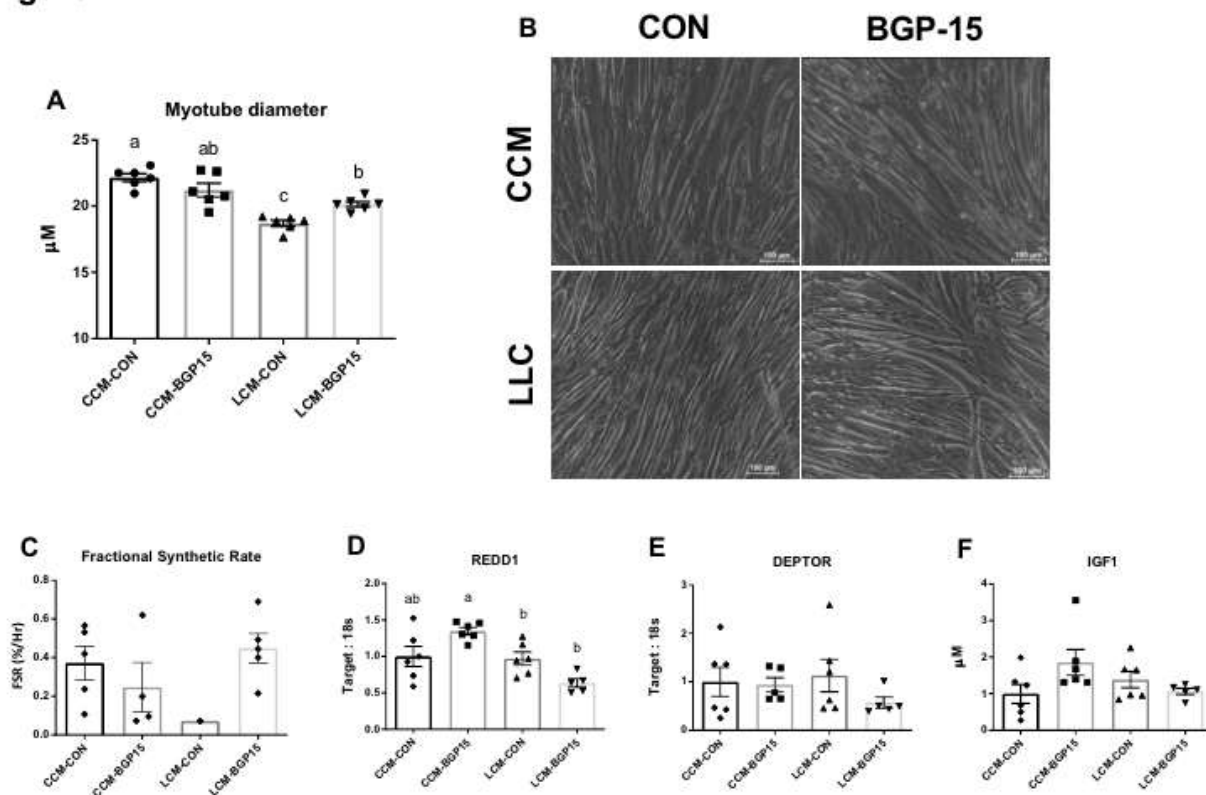


Figure 1. BGP-15 attenuates LCM-induced myotube atrophy

(A-B) Measurement and representative images of myotube diameter in response to LCM/CCM with or without BGP-15. (C) Protein synthesis rate via FSR using 24 hours of D₂O incorporation. (D-E) mRNA abundance of protein anabolic suppressors (*DEPTOR* and *REDD1*) and (F) anabolic regulating factor; *Insulin like growth factor1 (IGF1)*. An N of 5-6 replicates (wells) per condition was used and each condition were tested in two independent experiments (3 replicates per each experiment). Only one sample was detectable for FSR in LCM-CON group due to a low FSR abundance in panel C.

Figure 2.

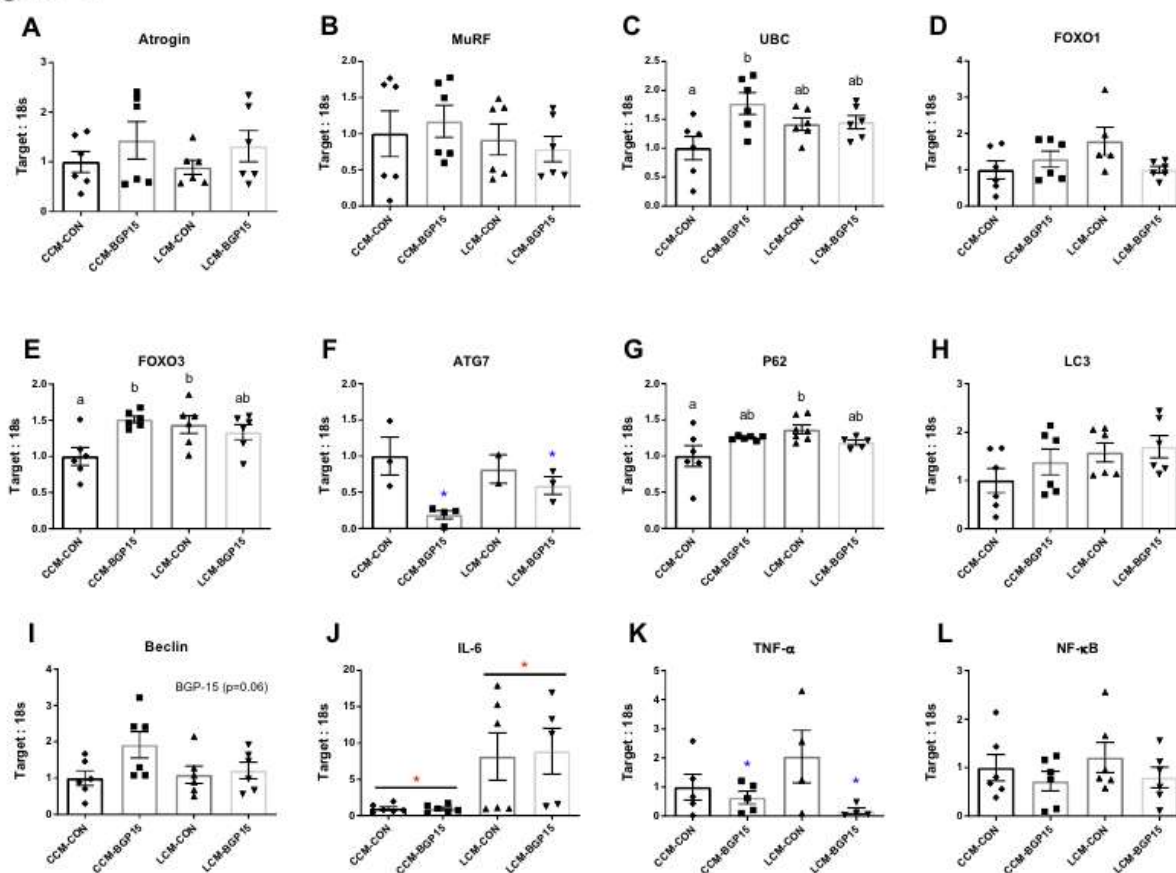


Figure 2. Suppressed APL and inflammatory cytokine mRNA in myotubes treated with BGP-15.

(A-E) mRNA abundance of UPS related markers; *Atrogin*, *MuRF*, *UBC*, *FOXO1*, & *FOXO3*. (F-I) mRNA abundance of APL related markers; *ATG7*, *p62*, *LC3*, *Beclin*. (J-L) mRNA abundance of inflammatory cytokines; *IL-6*, *TNF- α* , & *NF- κ B*. Data described as mean \pm SE. Statistical significance identified by denoting as * for main effect of LLC or BGP-15, and as “different letters” for an interaction effect with alpha value set at $p < 0.05$. ME: Main effect. An N of 5-6 replicates (wells) per condition was used and each condition were tested in two independent experiments (3 replicates per each experiment).

Figure 3.

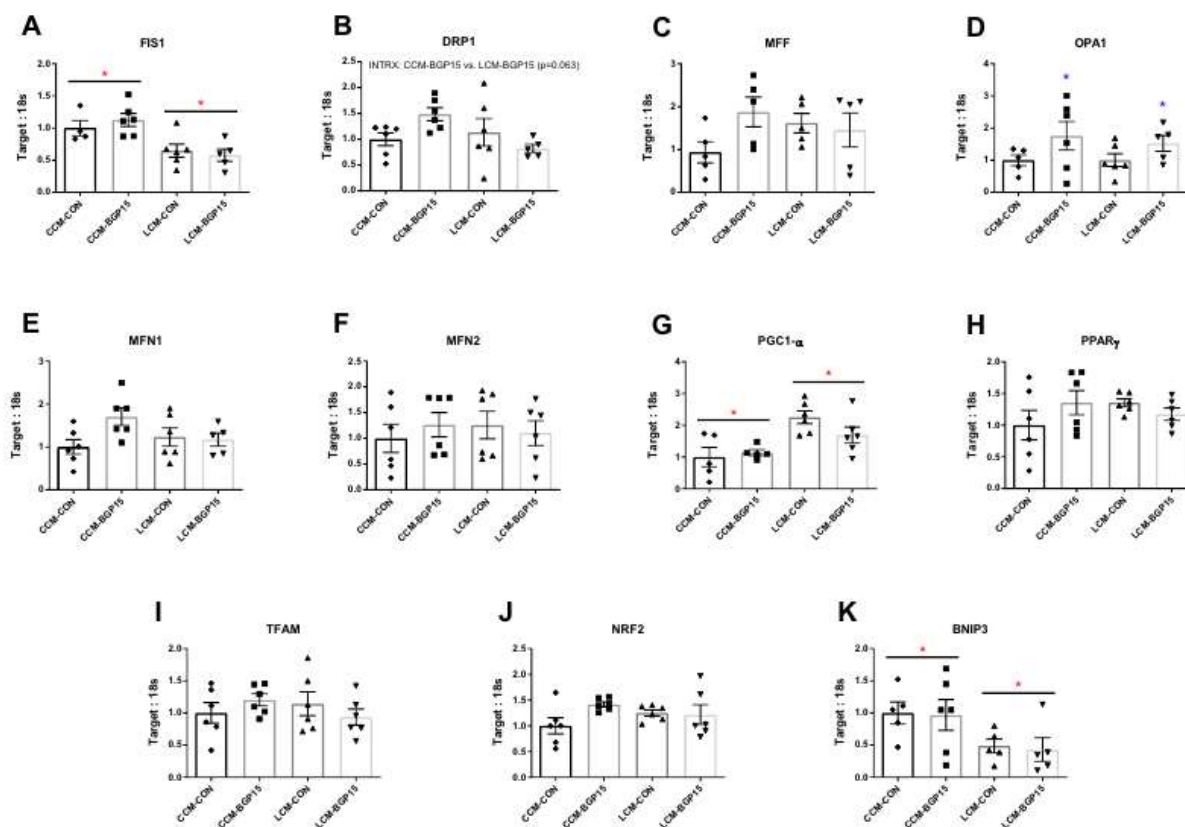


Figure 3. Greater *OPA1* and compensatory regulation of mitochondrial quality control mRNA levels in response to BGP-15 treatment in myotubes.

(A-B) mRNA abundance of mitochondrial fission markers; *FIS1* & *DRP1*. (C-F) mRNA abundance of mitochondrial fusion markers; *MFF*, *OPA1*, *MFN1*, & *MFN2*. (G-J) mRNA abundance of mitochondrial biogenesis markers; *PGC-1 α* , *PPAR γ* , *TFAM*, & *NRF2*. (K) mRNA abundance of mitochondrial autophagy marker; *BNIP3*. Data described as mean \pm SE. Statistical significance identified by denoting as * for main effect of LLC or BGP-15 with alpha value set at $p < 0.05$. ME: Main effect. An N of 5-6 replicates (wells) per condition was used and each condition were tested in two independent experiments (3 replicates per each experiment).

Figure 4.

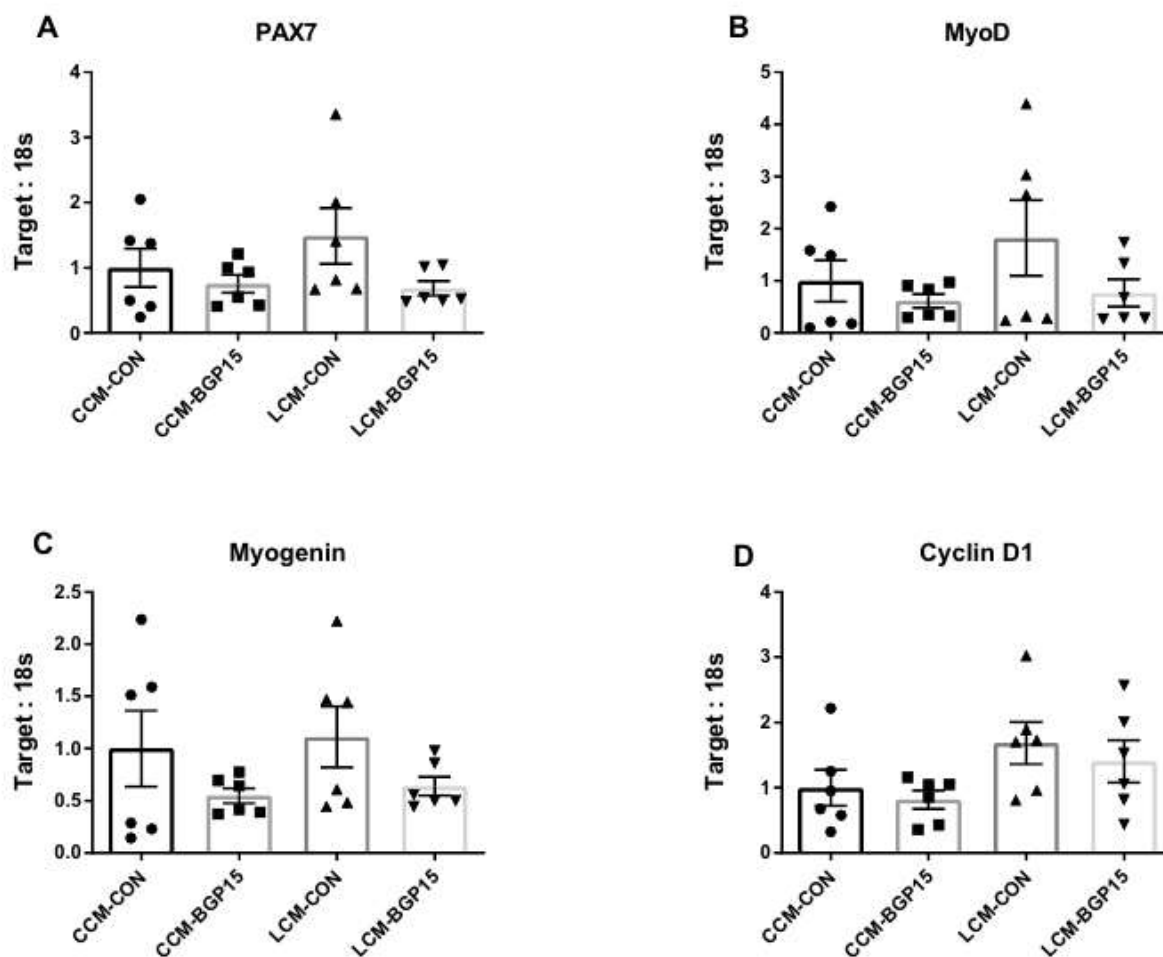


Figure 4. Unchanged cell cycling and myogenic regulators in response to LCM or BGP-15 treated myotubes.

(A-C) mRNA abundance of myogenic regulating factors; *PAX7*, *MYOD*, & *Myogenin*. (D) mRNA abundance of cell cycling marker; *Cyclin D1*. An N of 5-6 replicates (wells) per condition was used and each condition were tested in two independent experiments (3 replicates per each experiment).

Figure 5.

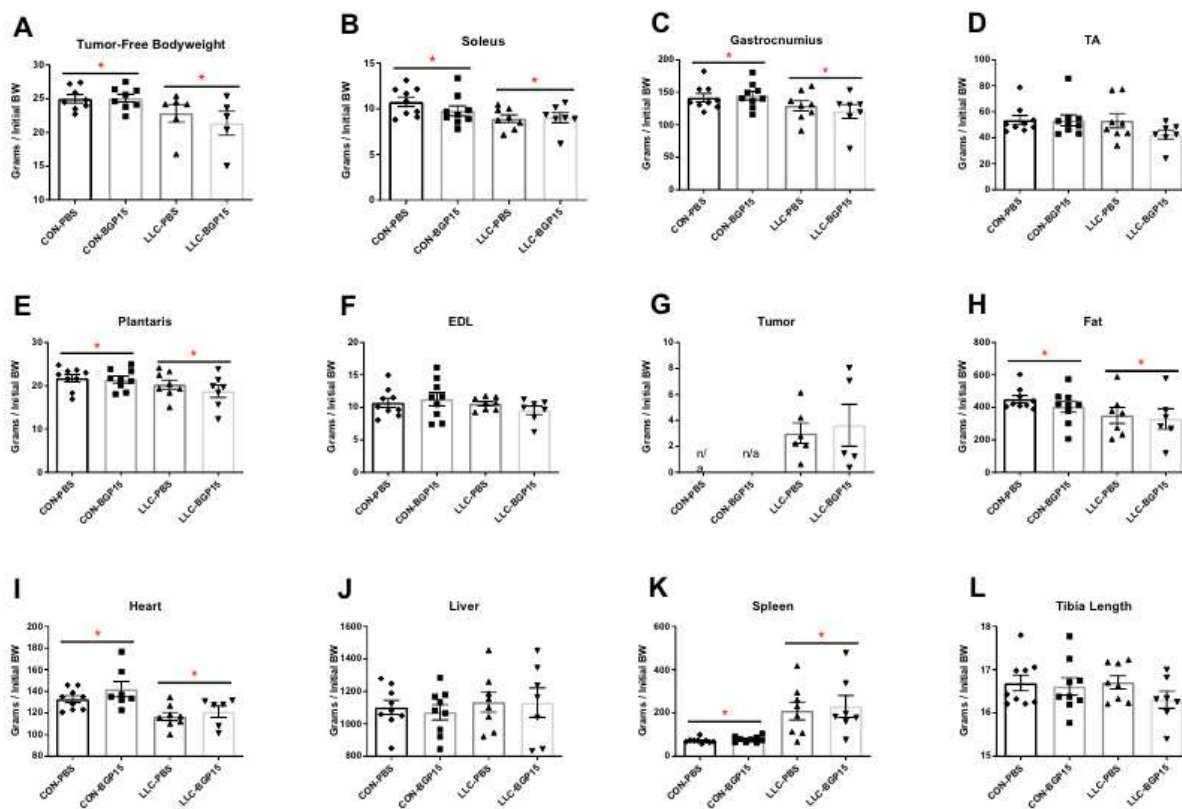


Figure 5. Potential role of BGP-15 in CC in vivo.

(A) Tissue weight measurement for tumor-free bodyweight. (B-F) Tissue weight measurement for lower limb muscles; Soleus, Gastrocnemius, TA, Plantaris, and EDL. (G-K) Tissue weight measurement for non-muscle tissues; tumor, gonadal fat, heart, liver, and spleen. (L) Tibia length measurement. Data described as mean \pm SE. Statistical significance identified by denoting as * for main effect of LLC or BGP-15 with alpha value set at $p < 0.05$. ME: Main effect. An N of 5-9 animals per group was used.

Figure 6.

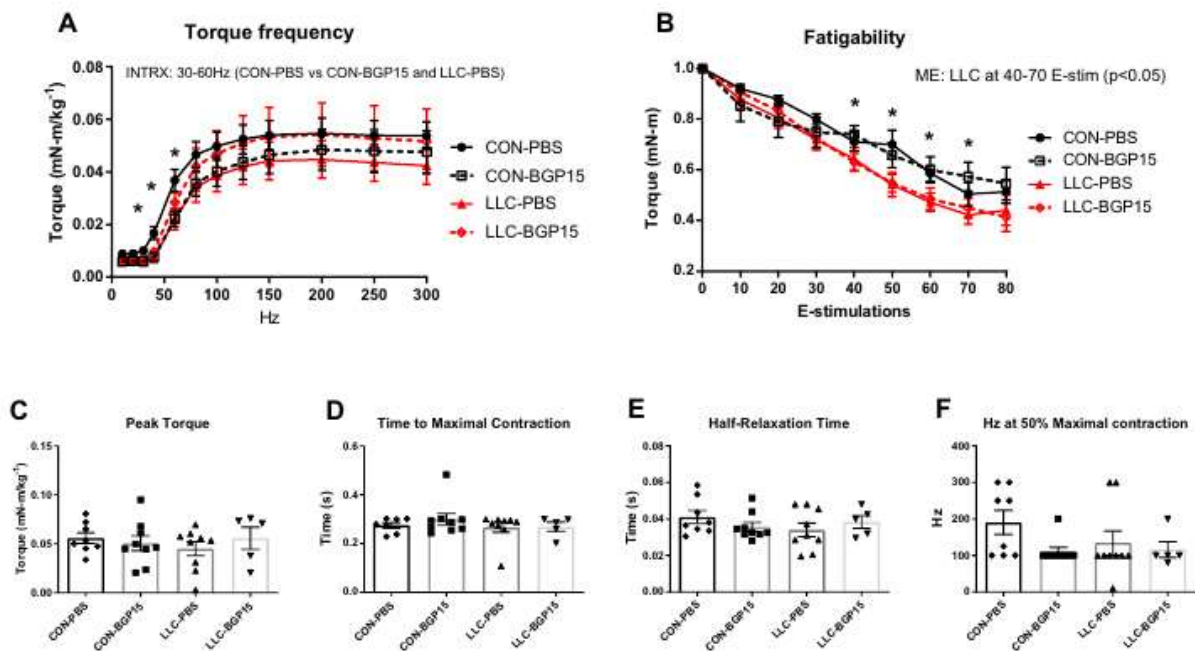


Figure 6. Impaired muscle contractile function in LLC-induced tumor-bearing mice, but no protective effect with BGP-15 administration.

(A) Torque frequency curve measured in $\text{mN}\cdot\text{m}$. (B) Fatigability measurement shows percent decrease in peak torque ($\text{mN}\cdot\text{m}$) following 120 E-simulations in 120 seconds at 40 Hz. (C) Peak isometric torque ($\text{mN}\cdot\text{m}$) (D) Time to maximal contraction. (E) Half relaxation time (F) Hz at half maximal contraction. Data described as mean \pm SE. Statistical significance identified by denoting as * for main effect of LLC or BGP-15, and an interaction effect with alpha value set at $p < 0.05$. ME: Main effect. An N of 5-9 animals per group was used.

Figure 7.

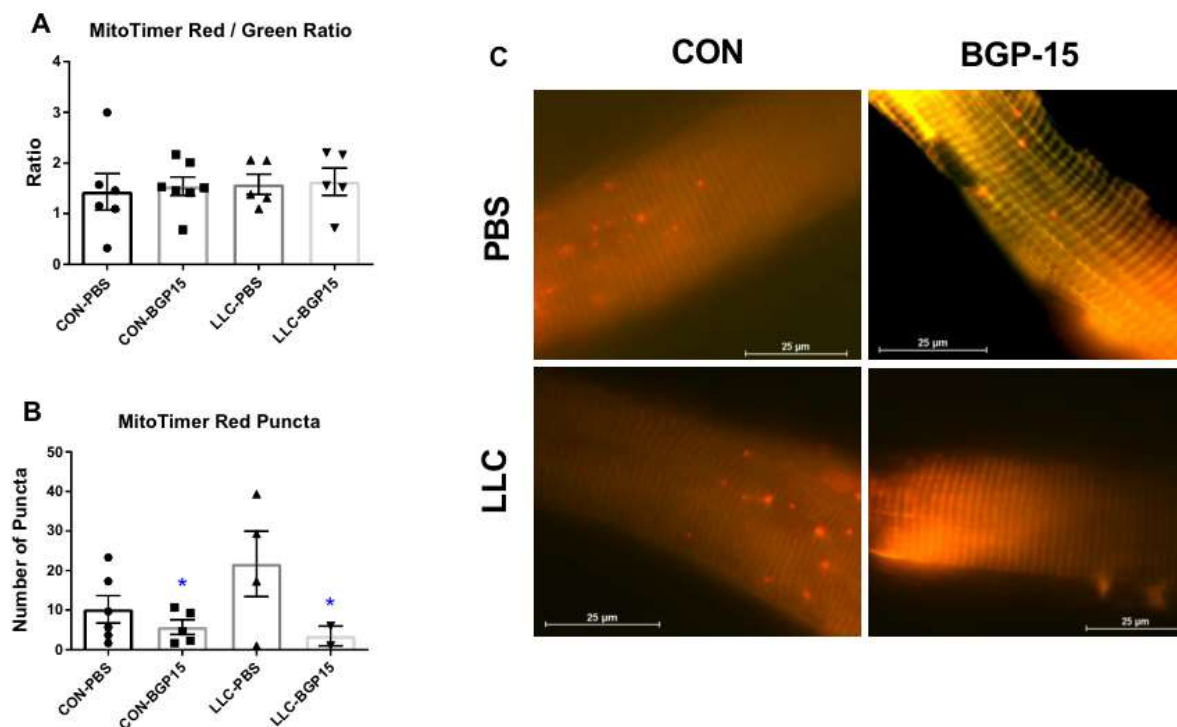


Figure 7. Mitochondrial degeneration induced by LLC was attenuated by BGP-15 administration.

(A) MitoTimer Red to Green Ratio (B) MitoTimer Pure Red Puncta counts. (C) Representative images of MitoTimer in single muscle fiber. Data described as mean \pm SE. Statistical significance identified by denoting as * for main effect of BGP-15 with alpha value set at $p < 0.05$. ME: Main effect. An N of 2-7 animals per group was used.

Figure 8.

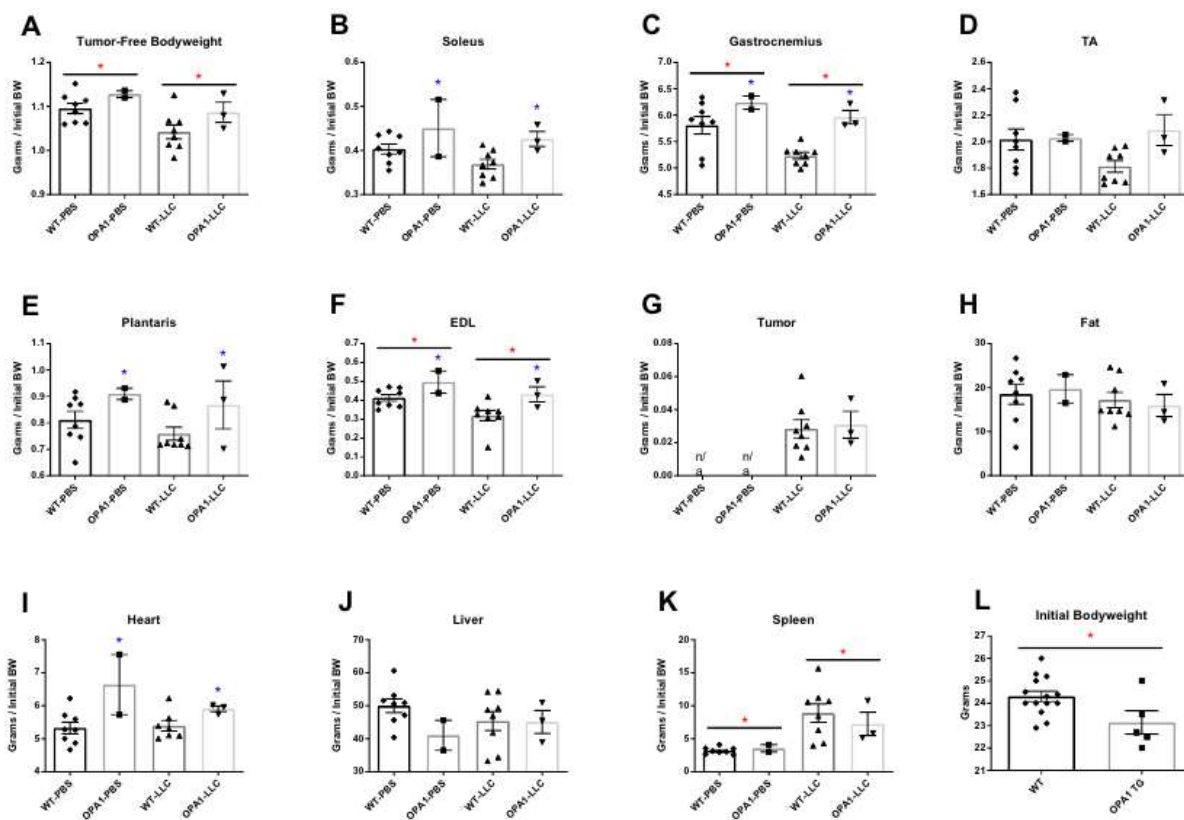


Figure 8. LLC induced muscle wasting was ameliorated by OPA1 overexpression in vivo (OPA1 TG).

(A) Tissue weight measurement for tumor-free bodyweight. (B-F) Tissue weight measurement for lower limb muscles; Soleus, Gastrocnemius, TA, Plantaris, and EDL. (G-K) Tissue weight measurement for non-muscle tissues; tumor, gonadal fat, heart, liver, and spleen. (L) Tissue weight measurement for initial bodyweight. All tissue weight data were normalized to their initial bodyweight to account different body mass prior to the experimental intervention. Data described as mean \pm SE. Statistical significance identified by denoting as * for main effect of LLC or BGP-15 with alpha value set at $p < 0.05$. ME: Main effect. An N of 2-8 animals per group was used.

Figure 9.

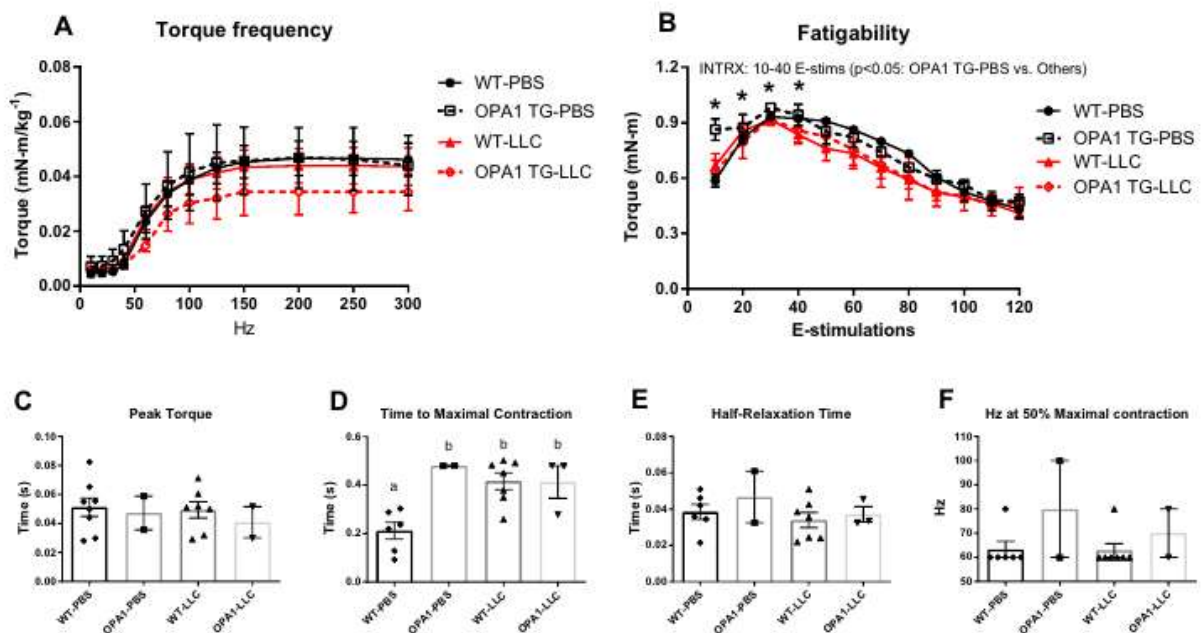


Figure 9. Unchanged mitochondrial network health & function in OPA1 TG mice.

(A) Torque frequency curve measured in mN-m. (B) Fatigability measurement shows percent decrease in peak torque (mN-m) following 120 E-stimulations in 120 seconds at 40 Hz. (C) Peak isometric torque (mN-m) (D) Time to maximal contraction. (E) Half relaxation time (F) Hz at half maximal contraction. Data described as mean \pm SE. Statistical significance identified by denoting as * for an interaction effect with alpha value set at $p < 0.05$. An N of 2-8 animals per group was used.

Figure 10.

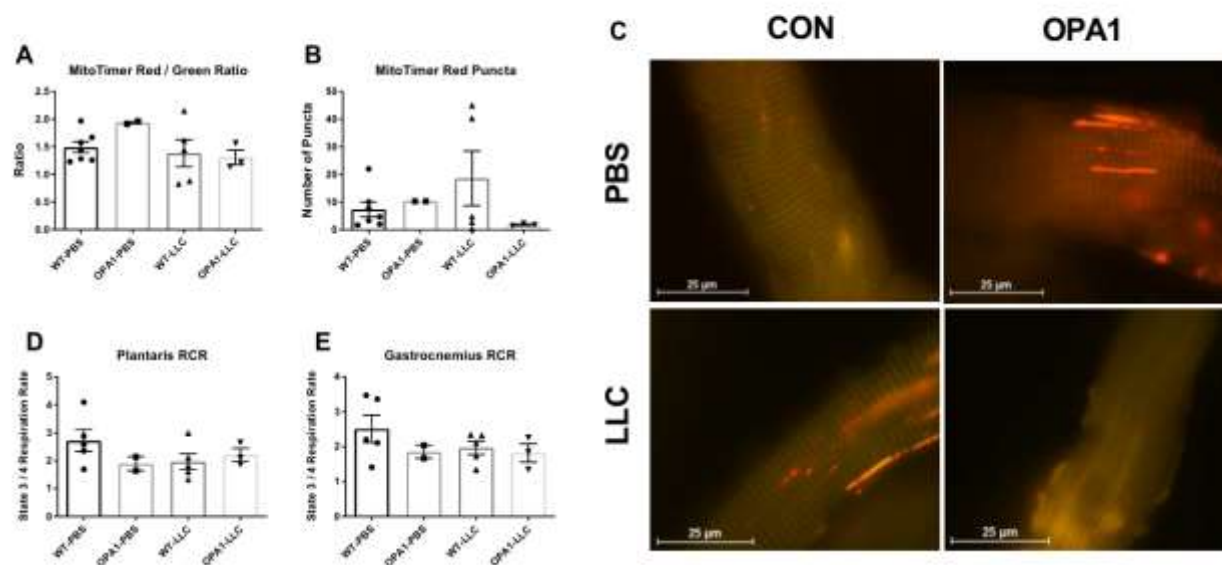


Figure 10. Unchanged mitochondrial network health & function in OPA1 TG mice.

(A) MitoTimer Red to Green Ratio (B) MitoTimer Pure Red Puncta counts. (C) Representative images of MitoTimer in single muscle fiber. (D) Plantaris mitochondrial respiratory capacity via RCR. (E) Gastrocnemius mitochondrial respiratory capacity via RCR. An N of 2-7 animals per group was used.

I. CONCLUSION

- A. CHAPTER 3: Development of metabolic and contractile alterations in development of cancer cachexia in female tumor-bearing mice.

In this study, we set to investigate alterations in the skeletal muscle during the development of CC focused on tissue weights, protein turnover, mitochondrial quality, and muscle contraction. We found various metabolic and contractile impairments with tumor development. However, these alterations are relatively minor and protected compared with previously reported male studies. The current study imply that females exhibit an enhanced capacity of mitigate aberrations associated with the onset of CC in the initial stages of tumor development. Further works are necessary to delineate these specific protections in female mice to provide precise mechanisms.

- B. CHAPTER 4: Targeting OPA1 for prevention of cancer-induced muscle loss.

In the second study, we set to test the function of OPA1 utilizing both BGP-15 administration (*in vivo* & *in vitro*) and genetic overexpression of OPA1 (*in vivo*) in CC. Both BGP-15 *in vitro* and OPA1 TG *in vivo* studies resulted in protective effects on muscle wasting in response to LCM and LLC-induced CC. BGP-15 *in vitro* data further suggests that the protective effect on muscle loss in CC appears to be associated with decreased inflammation and ALP activity. Further works are required to fully understand the efficacy of OPA1 in CC.

- C. Overall Conclusion.

This dissertation tested two independent but related research hypotheses. First, we investigated molecular alterations in the skeletal muscle during the development of CC in females.

These data demonstrated impaired metabolic and contractile function as tumor develops. However, these metabolic and contractile dysregulations are relatively modest compared to that of males from previous studies (12, 81), suggesting a distinct biological sex differences in the development of CC. Second, targeting OPA1 via both *in vivo* and *in vitro* resulted in protective effects on muscle wasting and regulations of both inflammation and ALP appear to be involved in muscle mass regulation during CC, suggesting OPA1 could be potential therapeutic target for cancer-induced muscle wasting.

Overall, my dissertation studies suggest both biological sex and mitochondrial health are crucial aspects when it comes to cancer-induced muscle atrophy. Especially, OPA1 plays a crucial role in mitochondrial homeostasis and females have a greater protective effect on mitochondria degeneration than males in response to CC, it would be invaluable to investigate the role of OPA1 in females during the development of CC. These two major findings from the current dissertation studies would provide as invaluable information in the field of cancer research and can help to advance the therapeutic potential for clinical cancer patients.

D. Limitations and Delimitations

i. Limitations

There are a few limitations inherent to these studies. Limitations of Aim 1 (Chapter III) were relatively minimal compared to Aim 2 (Chapter IV) in that Aim 1 was completed and successfully published in *Journal of Applied Physiology* on January 5th, 2022. During the submission process, I was able to minimize limitations and improve the quality of article. However, there were a few limitations for Aim 1. Specifically, our tumor allograft method was utilized in relatively young mice (8 to 12 wks old). These mice were considered as young adult compared to human development. However, according to National Cancer Institute's Surveillance, Epidemiology, and End Results (SEER) from 2013-2017, the median age of human cancer diagnosis is 66 years old, which is considered as older adults. For that reason, our animal model of CC may not accurately represent that of human cancers. Thus, future studies should consider utilization of more aged animals to better represent the nature of human cancer patients. In addition, we used LLC allograft as an animal clinical model of CC. Although these carcinomas were derived from the lung, the tumors do not arise in the tumor tissue of origin. This might be another limitation of the current study in that this off-site tumor development may not properly represent the type of tumor. Therefore, future works are warranted to utilize more transplantable models to better represent the type of cancer/tumor.

Regarding limitations for Aim 2, there were a few limitations that are worth mentioning. For the OPA1 TG study, data presented in the current dissertation is not complete. Here, we have used 21 male mice which is nearly half of the final animal numbers in males. Therefore, we could not process tissue samples for more analysis such as protein and mRNA signaling, immunohistochemistry, and mitochondrial reactive oxygen species emission rate by the time of my dissertation defense. In addition, I was going to have both males and females to investigate biological sex differences with OPA1 *in vivo* experiments. However, due to the lack of numbers

per each group in females (one mouse in both WT-PBS and WT-LLC group) by the time of dissertation defense, elected not present female data in the current dissertation as current data are insufficient to draw conclusion. Therefore, data from OPA1 TG experiments to date are more representative of pilot data.

ii. Delimitations

For Aim 1 study, we elected to investigate alterations in the skeletal muscle of females to determine potential biological sex differences in CC. Although this may limit the nature of biological sex investigation without including males in the current study, the study design was matched to our prior male CC studies (12, 81) to more directly compared alterations between males and females. We opted to utilize LLC allograft as a pre-clinical model of CC for both Aim 1 and 2 studies. However, the interpretations may be limited when we deliver general messages from the current studies in that our LLC model is derived from lung tissue, which represents lung cancer. Accordingly, our findings may or may not well represent other types of cancer. However, the current study was specifically designed to follow and investigate further finding from previous works (12, 81). In this case, our study design and model would provide more strength of this study.

For Aim 2 study, we had to opt to use a transgenic animal model of OPA1 study to test the efficacy of OPA1 instead of a AAV-induced intra-muscular gene transfer method that I proposed originally. OPA1 study was strengthened by utilizing more direct approach to test the function of OPA1. Although AAV model have a high efficiency rate of gene transfer, transgenic models will have more strength in this study in that this system induces overexpression of OPA1 gene in the skeletal muscle more efficiently.

E. Final Thoughts

My dissertation data provides two novel research outcomes that 1) biological sex as an important variable in the development of CC & 2) Mitochondrial fusion protein OPA1 as a potential therapeutic target for cancer-induced muscle degenerations. More detailed mechanisms of how females are protected during the development of CC and more precise roles of OPA1 in CC are warranted to advance cancer therapy, thereby improving cancer outcomes.

F. REFERENCES

1. **Sung H, Ferlay J, Siegel RL, Laversanne M, Soerjomataram I, Jemal A, and Bray F.** Global cancer statistics 2020: GLOBOCAN estimates of incidence and mortality worldwide for 36 cancers in 185 countries. *CA: a cancer journal for clinicians* 71: 209-249, 2021.
2. **Fearon K, Strasser F, Anker SD, Bosaeus I, Bruera E, Fainsinger RL, Jatoi A, Loprinzi C, MacDonald N, and Mantovani G.** Definition and classification of cancer cachexia: an international consensus. *The lancet oncology* 12: 489-495, 2011.
3. **Matsunaga T, Satio H, Miyauchi W, Shishido Y, Miyatani K, Murakami Y, Hanaki T, Kihara K, Yamamoto M, and Tokuyasu N.** Impact of skeletal muscle mass in patients with recurrent gastric cancer. *World journal of surgical oncology* 19: 1-10, 2021.
4. **Brown JL, Rosa-Caldwell ME, Lee DE, Blackwell TA, Brown LA, Perry RA, Haynie WS, Hardee JP, Carson JA, and Wiggs MP.** Mitochondrial degeneration precedes the development of muscle atrophy in progression of cancer cachexia in tumour-bearing mice. *Journal of cachexia, sarcopenia and muscle* 8: 926-938, 2017.
5. **Brown JL, Lee DE, Rosa-Caldwell ME, Brown LA, Perry RA, Haynie WS, Huseman K, Sataranatarajan K, Van Remmen H, Washington TA, Wiggs MP, and Greene NP.** Protein imbalance in the development of skeletal muscle wasting in tumour-bearing mice. *J Cachexia Sarcopenia Muscle* 9: 987-1002, 2018.
6. **VanderVeen BN, Fix DK, and Carson JA.** Disrupted skeletal muscle mitochondrial dynamics, mitophagy, and biogenesis during cancer cachexia: a role for inflammation. *Oxidative medicine and cellular longevity* 2017: 2017.
7. **VanderVeen BN, Hardee JP, Fix DK, and Carson JA.** Skeletal muscle function during the progression of cancer cachexia in the male ApcMin/+ mouse. *Journal of Applied Physiology* 124: 684-695, 2018.
8. **Boland ML, Chourasia AH, and Macleod KF.** Mitochondrial dysfunction in cancer. *Frontiers in oncology* 3: 292, 2013.
9. **Yan Z, Lira VA, and Greene NP.** Exercise training-induced regulation of mitochondrial quality. *Exercise and sport sciences reviews* 40: 159, 2012.
10. **Greene NP, Lee DE, Brown JL, Rosa ME, Brown LA, Perry RA, Henry JN, and Washington TA.** Mitochondrial quality control, promoted by PGC-1 α , is dysregulated by Western diet-induced obesity and partially restored by moderate physical activity in mice. *Physiological reports* 3: e12470, 2015.

11. **Hurtley SM.** Mitochondrial quality control. *Science* 350: 1052-1053, 2015.
12. **White JP, Puppa MJ, Sato S, Gao S, Price RL, Baynes JW, Kostek MC, Matesic LE, and Carson JA.** IL-6 regulation on skeletal muscle mitochondrial remodeling during cancer cachexia in the Apc Min/+ mouse. *Skeletal muscle* 2: 1-16, 2012.
13. **Giacomello M, Pyakurel A, Glytsou C, and Scorrano L.** The cell biology of mitochondrial membrane dynamics. *Nature reviews Molecular cell biology* 21: 204-224, 2020.
14. **Santarelli R, Rossi R, Scimemi P, Cama E, Valentino ML, La Morgia C, Caporali L, Liguori R, Magnavita V, and Monteleone A.** OPA1-related auditory neuropathy: site of lesion and outcome of cochlear implantation. *Brain* 138: 563-576, 2015.
15. **Patten DA, Wong J, Khacho M, Soubannier V, Mailloux RJ, Pilon-Larose K, MacLaurin JG, Park DS, McBride HM, and Trinkle-Mulcahy L.** OPA1-dependent cristae modulation is essential for cellular adaptation to metabolic demand. *The EMBO journal* 33: 2676-2691, 2014.
16. **Anand R, Wai T, Baker MJ, Kladt N, Schauss AC, Rugarli E, and Langer T.** The i-AAA protease YME1L and OMA1 cleave OPA1 to balance mitochondrial fusion and fission. *Journal of Cell Biology* 204: 919-929, 2014.
17. **Tezze C, Romanello V, Desbats MA, Fadini GP, Albiero M, Favaro G, Ciciliot S, Soriano ME, Morbidoni V, and Cerqua C.** Age-associated loss of OPA1 in muscle impacts muscle mass, metabolic homeostasis, systemic inflammation, and epithelial senescence. *Cell metabolism* 25: 1374-1389, 2017.
18. **Civiletto G, Varanita T, Cerutti R, Gorletta T, Barbaro S, Marchet S, Lamperti C, Viscomi C, Scorrano L, and Zeviani M.** Opa1 overexpression ameliorates the phenotype of two mitochondrial disease mouse models. *Cell metabolism* 21: 845-854, 2015.
19. **Literáti-Nagy Z, Tory K, Literáti-Nagy B, Kolonics A, Török Z, Gombos I, Balogh G, Vígh L, Horváth I, and Mandl J.** The HSP co-inducer BGP-15 can prevent the metabolic side effects of the atypical antipsychotics. *Cell Stress and Chaperones* 17: 517-521, 2012.
20. **Szabo A, Sumegi K, Fekete K, Hocsak E, Debreceni B, Setalo Jr G, Kovacs K, Deres L, Kengyel A, and Kovacs D.** Activation of mitochondrial fusion provides a new treatment for mitochondria-related diseases. *Biochemical pharmacology* 150: 86-96, 2018.
21. **Nascimento TL, Silva MT, and Miyabara EH.** BGP-15 improves contractile function of regenerating soleus muscle. *Journal of muscle research and cell motility* 39: 25-34, 2018.

22. **Cacciani N, Salah H, Li M, Akkad H, Backeus A, Hedstrom Y, Jena BP, Bergquist J, and Larsson L.** Chaperone co-inducer BGP-15 mitigates early contractile dysfunction of the soleus muscle in a rat ICU model. *Acta Physiologica* 229: e13425, 2020.
23. **Lim S, Deaver JW, Rosa-Caldwell ME, Lee DE, Morena Da Silva F, Cabrera AR, Schrems ER, Saling LW, Washington TA, and Fluckey JD.** Muscle miR-16 deletion results in impaired insulin sensitivity and contractile function in a sex-dependent manner. *American Journal of Physiology-Endocrinology and Metabolism* 2022.
24. **Zhang G, Jin B, and Li YP.** C/EBP β mediates tumour-induced ubiquitin ligase atrogin1/MAFbx upregulation and muscle wasting. *The EMBO journal* 30: 4323-4335, 2011.
25. **Lim S, Deaver JW, Rosa-Caldwell ME, Haynie WS, Morena da Silva F, Cabrera AR, Schrems ER, Saling LW, Jansen LT, and Dunlap KR.** Development of metabolic and contractile alterations in development of cancer cachexia in female tumor-bearing mice. *Journal of Applied Physiology* 132: 58-72, 2022.
26. **Call JA, McKeehen JN, Novotny SA, and Lowe DA.** Progressive resistance voluntary wheel running in the mdx mouse. *Muscle & nerve* 42: 871-880, 2010.
27. **Gorassini M, Eken T, Bennett DJ, Kiehn O, and Hultborn H.** Activity of hindlimb motor units during locomotion in the conscious rat. *Journal of neurophysiology* 83: 2002-2011, 2000.
28. **Jones LA, and Hunter IW.** Force sensation in isometric contractions: a relative force effect. *Brain research* 244: 186-189, 1982.
29. **Laker RC, Xu P, Ryall KA, Sujkowski A, Kenwood BM, Chain KH, Zhang M, Royal MA, Hoehn KL, Driscoll M, Adler PN, Wessells RJ, Saucerman JJ, and Yan Z.** A novel MitoTimer reporter gene for mitochondrial content, structure, stress, and damage in vivo. *J Biol Chem* 289: 12005-12015, 2014.
30. **Min K, Smuder AJ, Kwon O-s, Kavazis AN, Szeto HH, and Powers SK.** Mitochondrial-targeted antioxidants protect skeletal muscle against immobilization-induced muscle atrophy. *Journal of applied physiology* 111: 1459-1466, 2011.
31. **Campelj DG, Timpani CA, Petersen AC, Hayes A, Goodman CA, and Rybalka E.** The paradoxical effect of PARP inhibitor BGP-15 on irinotecan-induced cachexia and skeletal muscle dysfunction. *Cancers* 12: 3810, 2020.
32. **Narsale AA, and Carson JA.** Role of IL-6 in cachexia—therapeutic implications. *Current opinion in supportive and palliative care* 8: 321, 2014.

33. **White JP, Puppa MJ, Gao S, Sato S, Welle SL, and Carson JA.** Muscle mTORC1 suppression by IL-6 during cancer cachexia: a role for AMPK. *American Journal of Physiology-Endocrinology and Metabolism* 304: E1042-E1052, 2013.

34. **Patel HJ, and Patel BM.** TNF- α and cancer cachexia: Molecular insights and clinical implications. *Life sciences* 170: 56-63, 2017.

35. **Rosa-Caldwell ME, Lim S, Haynie WA, Brown JL, Deaver JW, Morena Da Silva F, Jansen LT, Lee DE, Wiggs MP, and Washington TA.** Female mice may have exacerbated catabolic signalling response compared to male mice during development and progression of disuse atrophy. *Journal of Cachexia, Sarcopenia and Muscle* 2021.

36. **Rosa-Caldwell ME, Lim S, Haynie WS, Brown JL, Lee DE, Dunlap KR, Jansen LT, Washington TA, Wiggs MP, and Greene NP.** Mitochondrial aberrations during the progression of disuse atrophy differentially affect male and female mice. *Journal of Cachexia, Sarcopenia and Muscle* 2021.

37. **Zhang P, Ling L, Zheng Z, Zhang Y, Wang R, Wu M, Zhang N, Hu M, and Yang X.** ATG7-dependent and independent autophagy determine the type of treatment in lung cancer. *Pharmacological Research* 163: 105324, 2021.

38. **Moscat J, and Diaz-Meco MT.** p62 at the crossroads of autophagy, apoptosis, and cancer. *Cell* 137: 1001-1004, 2009.

39. **Rahn JJ, Stackley KD, and Chan SSL.** Opa1 is required for proper mitochondrial metabolism in early development. *PLoS One* 8: e59218, 2013.

40. **Puppa MJ, Gao S, Narsale AA, and Carson JA.** Skeletal muscle glycoprotein 130's role in Lewis lung carcinoma-induced cachexia. *The FASEB Journal* 28: 998-1009, 2014.

41. **Busquets S, Toledo M, Orpí M, Massa D, Porta M, Capdevila E, Padilla N, Frailis V, López-Soriano FJ, and Han HQ.** Myostatin blockage using actRIIB antagonism in mice bearing the Lewis lung carcinoma results in the improvement of muscle wasting and physical performance. *Journal of cachexia, sarcopenia and muscle* 3: 37-43, 2012.

42. **Argilés JM, Figueras M, Ametller E, Fuster G, Olivan M, de Oliveira CCF, López-Soriano FJ, Isfort RJ, and Busquets S.** Effects of CRF2R agonist on tumor growth and cachexia in mice implanted with Lewis lung carcinoma cells. *Muscle & Nerve: Official Journal of the American Association of Electromyography and Clinical Neurophysiology* 37: 190-195, 2008.

43. **Murphy KT, Chee A, Trieu J, Naim T, and Lynch GS.** Importance of functional and metabolic impairments in the characterization of the C-26 murine model of cancer cachexia. *Disease models & mechanisms* 5: 533-545, 2012.

44. **Kilgour RD, Vigano A, Trutschnigg B, Lucar E, Borod M, and Morais JA.** Handgrip strength predicts survival and is associated with markers of clinical and functional outcomes in advanced cancer patients. *Supportive Care in Cancer* 21: 3261-3270, 2013.

45. **Close RI.** Dynamic properties of mammalian skeletal muscles. *Physiological reviews* 52: 129-197, 1972.

46. **Van Eijden T, and Turkawski SJJ.** Morphology and physiology of masticatory muscle motor units. *Critical reviews in oral biology & medicine* 12: 76-91, 2001.

III. APPENDICES

A. AUP/IBC Approval letters

i. Appendix 1



Office of Research Compliance

June 8, 2018

MEMORANDUM

TO: Dr. Nicholas Greene

FROM: Ines Pinto, Biosafety Committee Chair

RE: Protocol Renewal

PROTOCOL #: 15025

PROTOCOL TITLE: Mitochondrial Degeneration in the Onset of Cancer-Cachexia Induced Muscle Atrophy

APPROVED PROJECT PERIOD: **Start Date** July 9, 2015 **Expiration Date** July 8, 2021

The Institutional Biosafety Committee (IBC) has approved your request, dated May 24, 2018, to renew IBC # 15025, "Mitochondrial Degeneration in the Onset of Cancer-Cachexia Induced Muscle Atrophy".

The IBC appreciates your assistance and cooperation in complying with University and Federal guidelines for research involving hazardous biological materials.

1424 W. Martin Luther King, Jr. • Fayetteville, AR 72701
Voice (479) 575-4572 • Fax (479) 575-6527

The University of Arkansas is an equal opportunity/affirmative action institution.

ii. Appendix 2

UNIVERSITY OF
ARKANSAS

Office of Research Compliance

To: Nicholas Greene
From: Jeff Wolchok
Date: November 25, 2019
Subject: IACUC Approval
Expiration Date: November 24, 2022

The Institutional Animal Care and Use Committee (IACUC) has APPROVED your protocol #20045, *Aim 2.1, Targeting Opa1 in Cancer-Cachexia*.

In granting its approval, the IACUC has approved only the information provided. Should there be any further changes to the protocol during the research, please notify the IACUC in writing (via the Modification form) prior to initiating the changes. If the study period is expected to extend beyond November 24, 2022 you may submit a modification to extend the project up to three years, or submit a new protocol. The IACUC may not approve a study for more than three years at a time.

The following individuals are approved to work on this study: Nicholas Greene, Tyrone Washington, Seongkyun Lim, Christopher Nelson, and Wesley Haynie. Please submit personnel additions to this protocol via the modification form prior to their starting work.

The IACUC appreciates your cooperation in complying with University and federal guidelines involving the care and use of animals.

JCW/jgr

1424 W. Martin Luther King, Jr. • Fayetteville, AR 72701
Voice (479) 575-4572 • Fax (479) 575-6527

The University of Arkansas is an equal opportunity/affirmative action institution.

iii. Appendix 3

Office of Research Compliance

November 15, 2019

MEMORANDUM

TO: Dr. Nicholas P. Greene

FROM: Ines Pinto, Biosafety Committee Chair

RE: New Protocol

PROTOCOL #: 20009

PROTOCOL TITLE: Development of Targeted Approaches in Prevention of Cancer-Cachexia

APPROVED PROJECT PERIOD: **Start Date** November 14, 2019 **Expiration Date** November 13, 2022

The Institutional Biosafety Committee (IBC) has approved Protocol 20009, "Development of Targeted Approaches in Prevention of Cancer-Cachexia". You may begin your study.

If modifications are made to the protocol during the study, please submit a written request to the IBC for review and approval before initiating any changes.

The IBC appreciates your assistance and cooperation in complying with University and Federal guidelines for research involving hazardous biological materials.

1424 W. Martin Luther King, Jr. • Fayetteville, AR 72701
Voice (479) 575-4572 • Fax (479) 575-6527

The University of Arkansas is an equal opportunity/affirmative action institution.

iv. Appendix 4

4/12/2018

vpredweb.uark.edu/iacuc-webapp/mods/letter.php?ID=1251&PROTOCOL=18111



Office of Research Compliance

To: Nicholas Greene
Fr: Craig Coon
Date: April 12th, 2018
Subject: IACUC Approval
Expiration Date: April 5th, 2021

The Institutional Animal Care and Use Committee (IACUC) has APPROVED your protocol # **18111**: *Mitochondrial degeneration in the development of cancer-induced muscle loss in female mice*.

In granting its approval, the IACUC has approved only the information provided. Should there be any further changes to the protocol during the research, please notify the IACUC in writing (via the Modification form) prior to initiating the changes. If the study period is expected to extend beyond April 5th, 2021 you must submit a newly drafted protocol prior to that date to avoid any interruption. By policy the IACUC cannot approve a study for more than 3 years at a time.

The following individuals are approved to work on this study: Nicholas Greene, Tyrone Washington, Megan Rosa, and Wesley Haynie. Please submit personnel additions to this protocol via the modification form prior to their start of work.

The IACUC appreciates your cooperation in complying with University and Federal guidelines involving animal subjects.

CNC/tmp

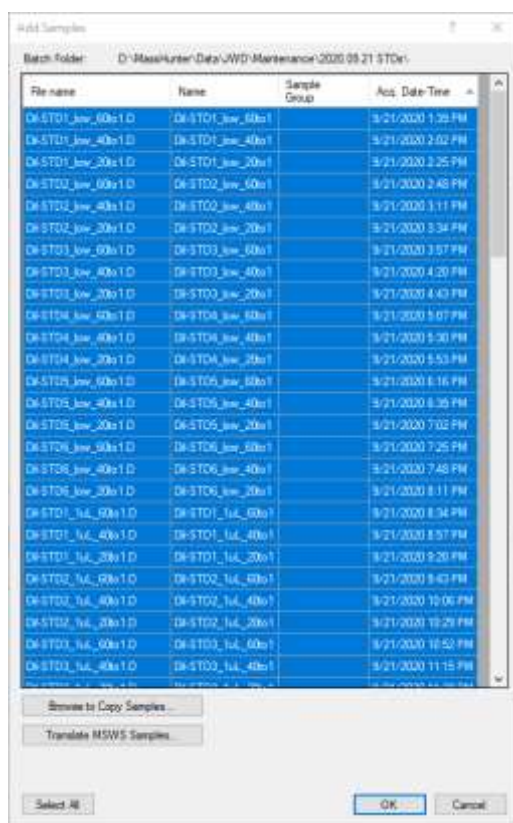
B. Protocols

I. Cachexia Research Laboratory – Analysis of protein synthesis via FSR in vitro.

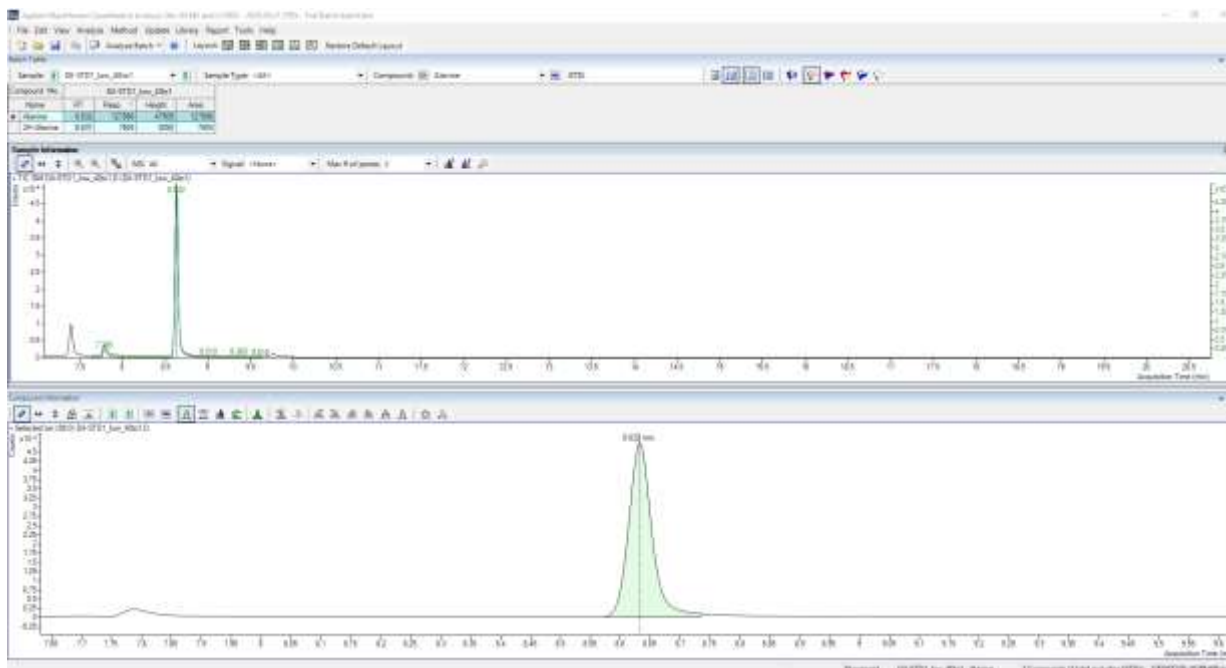
A detailed method was described in the methods for Chapter III and IV and this section will be committed for the analysis of FSR using muscle samples from *in vitro*. After the completion of FSR measurement, it is required to assess both plasma and tissue calculated enrichment to determine the final FSR value.

i. Sample analysis (for both plasma and tissue)

1. Open the MS Quantitative Analysis software from the desktop.
2. File > New Batch (Or open batch for existing batch) > Select Samples/Standards to be included in batch processing.



3. Selecting OK will load all selected samples/standards into the batch processing screen.





4. Method > Open > Open and Apply from Existing File.
5. Select ^2H -Acetone or ^2H -Alanine in the C:\GCMS\inch\daMethods directory.
6. Analyze the entire batch by selecting Analyze > Analyze Batch. Or by pressing F5.
7. Every sample/standard will be listed in a drop-down box.

Batch Table

Sample: Dil-STD1_low_40to1 Sample

Compound Me...		Dil-STD1_low_40to1			
Name	RT	Resp. ▾	Height	Area	
▶ Alanine	8.632	127886	47505	127886	
2H-Alanine	8.631	7804	3058	7804	

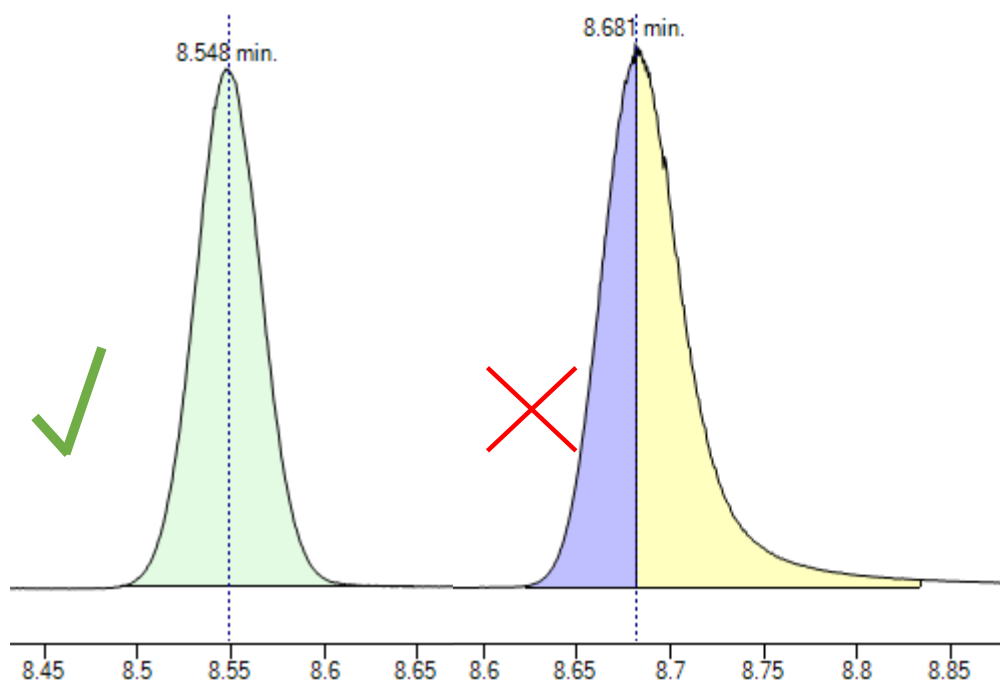
- 8.
9. The samples can be navigated by selecting a sample from the drop-down box, or by pressing the green arrows to the left or right of the drop-down box.
10. Each sample reports the retention time (RT), Response, Height, and Area (Response and Area are the same) for all isotopes measured by the GCMS method that was used during data acquisition. For ^2H -Alanine, this is m/z 99 and 100. For ^2H -Acetone, this is m/z 58 and 59. For each, the heavier isotope corresponds to deuterium enrichment. Each isotope can be selected by clicking on the appropriate name in the table. For the purposes of this protocol, each parent ion (99 and 58) will be referred to as m+0, and each labeled molecule (100 and 59) will be referred to as m+1.

Batch Table				
Sample:  Dil-STD1_low_40to1		Sample 		
Compound Me..	Dil-STD1_low_40to1			
Name	RT	Resp. ▾	Height	Area
▶ Alanine	8.632	127886	47505	127886
2H-Alanine	8.631	7804	3058	7804

11. Below this window there are two larger windows:

- Sample Information: shows the extracted chromatogram for each isotope being measured).
- Compound Information: shows a focused chromatogram for the isotope selected in step 9.

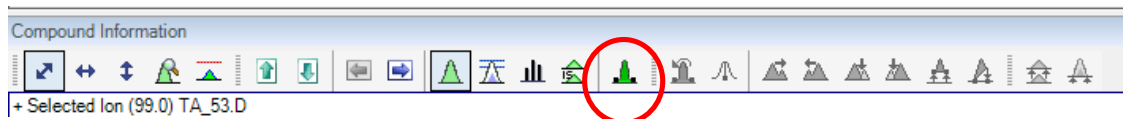
12. The analysis software has attempted to measure the peak height and area under the curve using various algorithms. Visually inspect each chromatographic peak for appropriate software integration and adjust where appropriate. See end of document for examples of inappropriate peak shapes and their common causes and possible solutions.



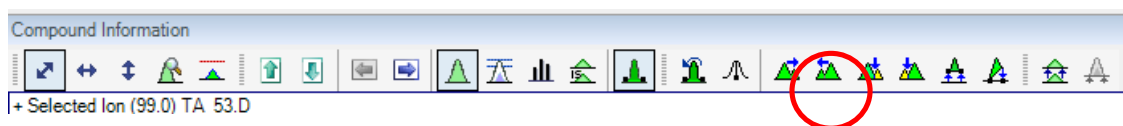
13. Errors in automatic peak integration are indicated with various colors that correspond to various problems. The above picture on the right is an example of bad peak integration. This is due to the jagged nature of the peak causing the software to be unsure if this is a

single peak, or two almost overlapping peaks. In this case, manual integration must be performed to fix the problem.

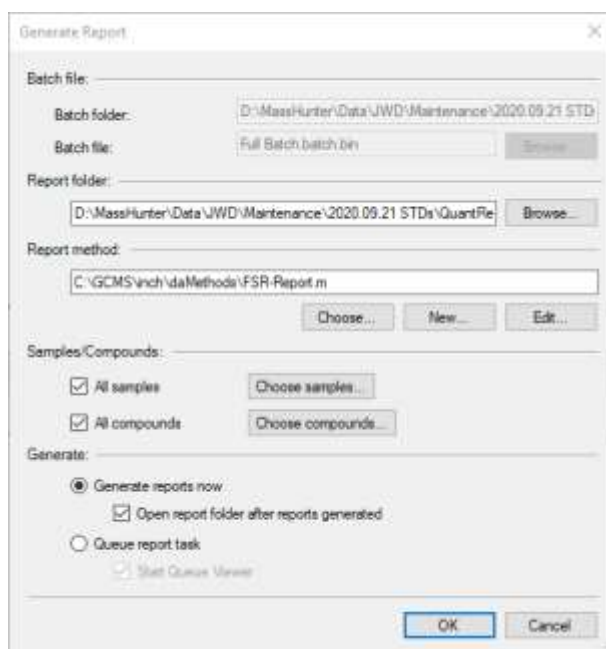
14. Begin manual integration by selection the manual integration icon in the “Compound Information” window.



Then, for this particular integration problem, select “Merge Right Peak.” The resulting peak should now be integrated properly and appear similar to other peaks.



15. Once all peaks for each isotope have appropriate integrations, it will be necessary to re-analyze the batch by selecting “Analyze > Analyze Batch” or by pressing F5.
16. To export all data, select “Report > Generate” from the toolbar. The following menu will appear.



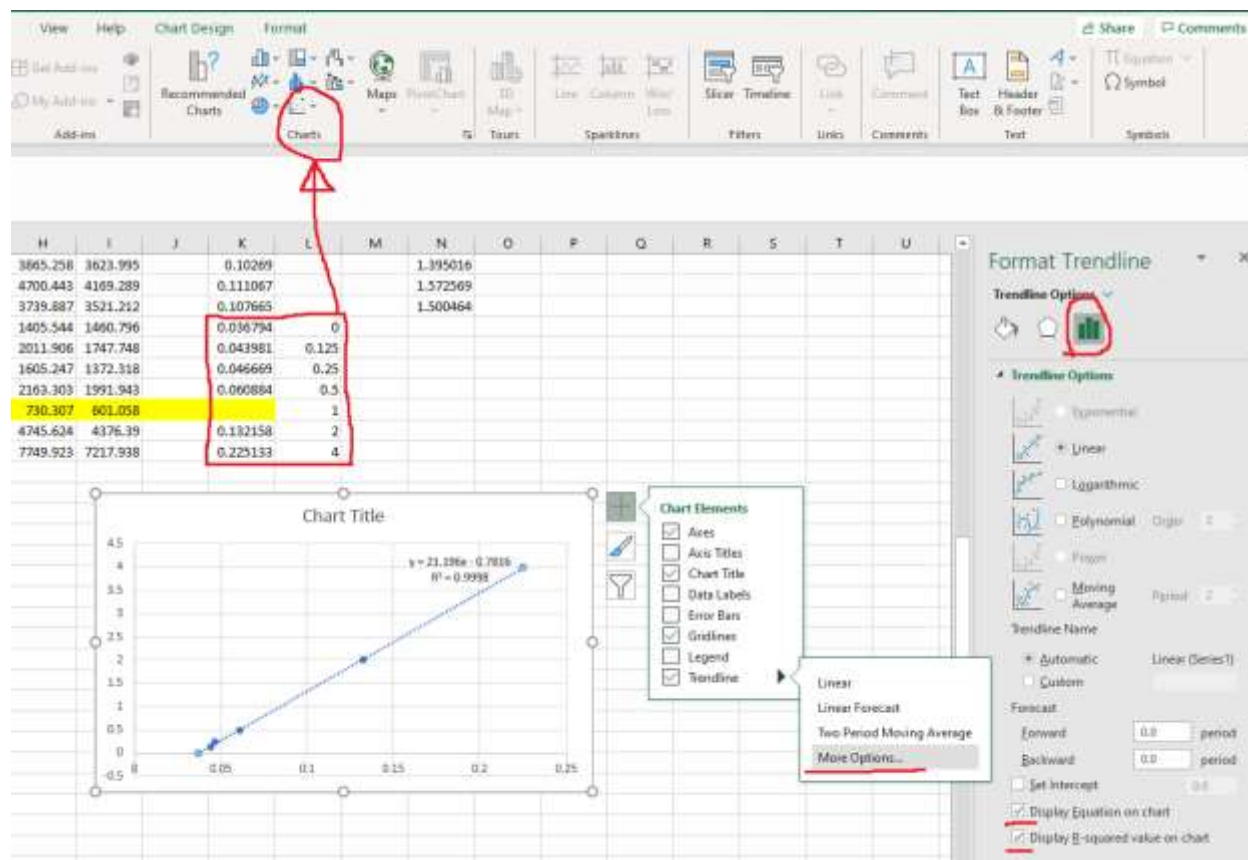
The default path to save the report is the same folder where the samples are saved. The report method for both ^2H -Alanine and ^2H -Acetone is FSR-Report. Clicking “OK” will begin generating a data output report in a new excel spreadsheet. The folder containing this new

spreadsheet will open automatically when the report is generated. This can take a few seconds, to a few minutes depending on how many samples are included in the batch report.

- 17.** This Excel spreadsheet will contain a list of samples with their retention times, peak height, and area under the curve for each isotope measured.
- 18.** By taking the ratio of $m+1/m+0$ area under the curve for each sample, we can then compare them to a standard curve linear equation.

ii. Plasma calculated enrichment.

1. For plasma samples, graph the response of plasma standards using a scatter plot with percent enrichment on the y-axis and the m+1/m+0 ratio on the x-axis. Calculate a best-fit line equation and R^2 . The R^2 should be above 0.99 if done correctly. Apply each plasma sample to the best fit line as the x variable, and y will be plasma enrichment for that sample.



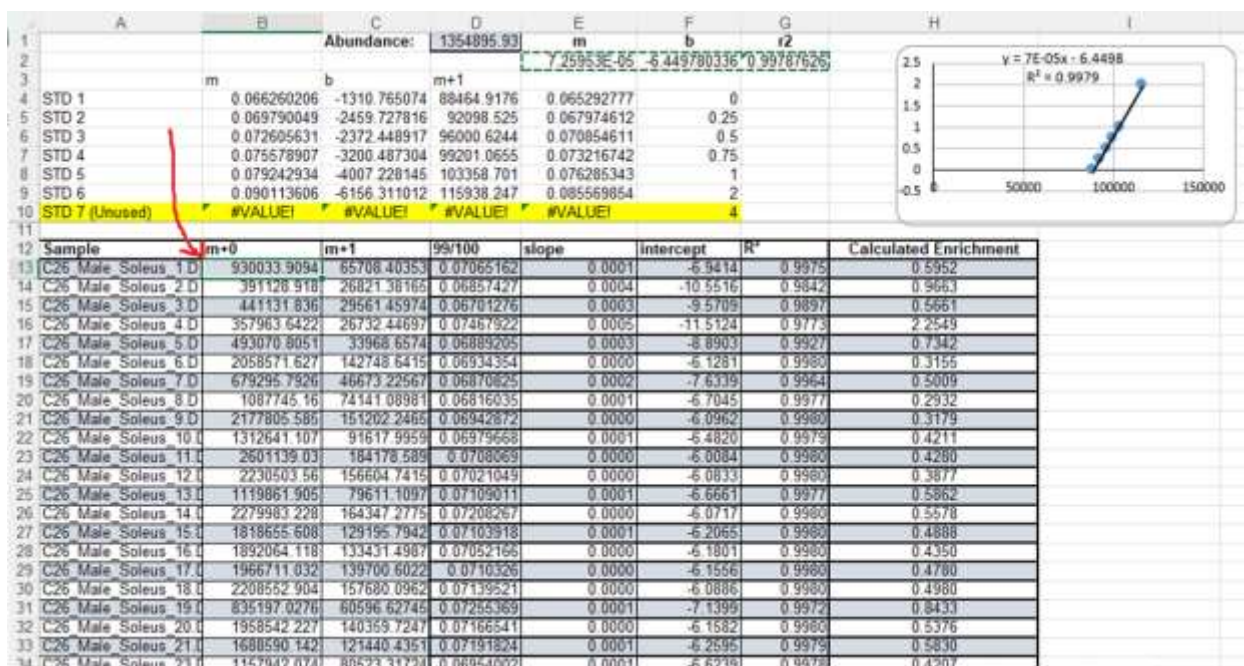
2. Apply equation from the scatter plot e.g., $= (21.196 * K63) - 0.7816$ to 58/59 value = final plasma enrichment.

iii. Muscle tissue calculated enrichment.

1. For tissue samples, we use the separate excel spreadsheet found in the “GCMS Standards” folder on the GCMS computer. Follow the instructions within the spreadsheet on the worksheet titled “STD 1-6 Linear”.

	A	B	C	D	E	F	G	H	I	J	K	L
1	Data File	Type	RT		Height	Area		Height	Area		99/100	
2	Batch Data: D:\MassHunter\Data\C26\Females\C26 Female Gastroc (final)\QuantResults\batch1.batch.bin											
3	Analysis T: ##### Analyst N: DESKTOP- Report Ge DESKTOP-1IQPN4R\imml											
4	Calibration		1/1/0001	Analyze Q	10.1	Report Qu	10.2					
5	2H-Alanine				2H-Alanine (99)			alanine (100)				
6	Data File	Type	RT		Height	Area		Height	Area		99/100	
7	C26_Femz	Sample	8.69		76264.66	254768.7		1112909	3605440		0.070662	
8	C26_Femz	Sample	8.691		57037.19	200923.3		829882.5	2912334		0.06899	
9	C26_Femz	Sample	8.72		16470.59	88350.04		240061.2	1327627		0.066547	
10	C26_Femz	Sample	8.732		12766.99	74338.88		186838.5	1137195		0.06537	
11	C26_Femz	Sample	8.724		13206.41	74795.03		189377.7	1117989		0.066901	
12	C26_Femz	Sample	8.718		18824.19	100056.9		271061	1503124		0.066566	
13	C26_Femz	Sample	8.715		18614.89	95091.24		270914.9	1493882		0.063654	
14	C26_Femz	Sample	8.713		18358.74	99926.87		263723.3	1447452		0.069036	
15												
16	C26_Femz	Sample	8.697		58535.83	207508.5		828503.3	3017494		0.068768	
17	C26_Femz	Sample	8.699		39316.56	151758.2		555955.6	2145901		0.07072	
18	C26_Femz	Sample	8.696		38120.92	139516.9		544438.3	2077697		0.06715	
19	C26_Femz	Sample	8.69		63013.96	224812.5		898467.2	3171529		0.070885	
20	C26_Femz	Sample	8.692		58986.17	204391.8		856167.7	2959691		0.069058	
21	C26_Femz	Sample	8.691		56236.61	195016.5		818871.8	2836619		0.06875	
22	C26_Femz	Sample	8.688		67595.11	228326.9		973806.9	3265396		0.069923	
23	C26_Femz	Sample	8.688		61326.73	204698.6		904925.9	3048980		0.067137	
	55189.26	186922.6	804133.7	2707604	0.069036	C26 Female Gastroc B C	0.997967			0.264193576		

2. When it is exported to excel, get ratio of 99/100 area value “see red circled”. Open an excel file “STD 2020 Corr Area” and go to a tab named as “STD 1-6 Linear”



- Copy and paste your m+0, m+1, and 99/100 values from your working excel to "STD 1-6 Linear" tab. locate your mouse cursor at first sample under "m+0" (in the example, it is cell "B13"). Then hit "control + Y" This will automatically get you R² and calculated enrichment (CE) values. Copy R² and CE values and transfer back to your working excel sheet.

K	L	M	N	O	Q
99/100		Data File	R2	Calculated Enrichment (CE)	CE Average
0.071726		C26_Female_Gastroc_10_	0.997917	0.463044507	0.33719
0.069417		C26_Female_Gastroc_10_	0.997969	0.322321145	
0.068368		C26_Female_Gastroc_10_	0.997968	0.226203369	
0.070193		C26_Female_Gastroc_11_	0.997946	0.346605473	0.335619
0.069501		C26_Female_Gastroc_11_	0.997971	0.315662817	
0.069779		C26_Female_Gastroc_11_	0.997971	0.344589687	
0.069096		C26_Female_Gastroc_12_	0.997946	0.249928058	0.315286
0.071641		C26_Female_Gastroc_12_	0.997951	0.479715497	
0.068652		C26_Female_Gastroc_12_	0.997954	0.216212979	
0.070453		C26_Female_Gastroc_14_	0.99796	0.432232215	0.418848
0.070267		C26_Female_Gastroc_14_	0.997951	0.422674644	
0.069988		C26_Female_Gastroc_14_	0.997944	0.401636822	
0.069851		C26_Female_Gastroc_15_	0.997946	0.316722877	0.28244
0.069852		C26_Female_Gastroc_15_	0.997952	0.321300868	
0.068552		C26_Female_Gastroc_15_	0.997957	0.209296223	
0.069707		C26_Female_Gastroc_16_	0.997936	0.297539361	0.243349
0.068883		C26_Female_Gastroc_16_	0.997962	0.244187994	
0.068236		C26_Female_Gastroc_16_	0.997965	0.188320479	

4. Copy R2 and CE values and transfer back to your original excel file. Get a mean of each sample (each sample was triplicated) (see red circled). **Note:** you can exclude one of your triplicates if one values is too lower or higher than the other two.

	S	T	U	V	W	X	AA	AB
Animal info		group	CE Average		Plasma CE	FINAL (Gastroc CE/ Plasma CE)		
C26_Female_TA1_A	10D		0.32333		1.534090795	0.210764		
C26_Female_TA2_A	10D		0.159209		1.626775215	0.097868		
C26_Female_TA3_A	10D		0.330072		1.558519079	0.211786		
C26_Female_TA31	10D		0.150336		-0.623802644			
C26_Female_TA32	10D		0.246797		1.763254749	0.139967		
C26_Female_TA33	10D		0.134826		1.503911265	0.08965		
C26_Female_TA34	10D		0.218923		1.313062967	0.166727		
C26_Female_TA35	10D		0.209278		1.556313088	0.134471		
C26_Female_TA36	10D		0.28023		1.530041988	0.183152		
C26_Female_TA4_A	10D		0.335887		1.518315716	0.221223		
C26_Female_TA5_A	10D		0.304989		1.565726939	0.194791		
C26_Female_TA6_A	10D		0.253767					
C26_Female_TA10	15D		0.33719		1.633587228	0.206411		
C26_Female_TA11	15D		0.335619		1.625459504	0.206477		
C26_Female_TA12	15D		0.315286		1.58052506	0.199482		

5. Reorganize based on animal group and number. Normalize your tissue CE to Plasma CE value to get a final FSR value. Note: You should have plasma CE data in different excel file at this point. Transfer plasma CE to here for the final FSR value.